

UC Riverside

UC Riverside Electronic Theses and Dissertations

Title

Selective Chemistry of Metal Oxide Atomic Layer Deposition on Si Based Substrate Surfaces

Permalink

<https://escholarship.org/uc/item/55t058st>

Author

Guo, Lei

Publication Date

2015

Peer reviewed|Thesis/dissertation

UNIVERSITY OF CALIFORNIA
RIVERSIDE

Selective Chemistry of Metal Oxide Atomic Layer Deposition on Si Based Substrate
Surfaces

A Dissertation submitted in partial satisfaction
of the requirements for the degree of

Doctor of Philosophy

in

Materials Science and Engineering

by

Lei Guo

March 2015

Dissertation Committee:

Dr. Francisco Zaera, Chairperson

Dr. Pingyun Feng

Dr. David Kisailus

Copyright by
Lei Guo
2015

The Dissertation of Lei Guo is approved:

Committee Chairperson

University of California, Riverside

ACKNOWLEDGEMENTS

I would like to extend my profoundest gratitude to my Ph.D. advisor, Prof. Francisco Zaera, for providing me this incredible opportunity to do research in his lab and supporting me during the past four and half years. He is a great scientist and chemist. I am so proud to be his student. His instructions can always inspire me and bring me to a higher level of thinking. He also provides me very insightful discussions about the research. What I learned from him is not only how to do research, but also how to view this world from a new perspective.

I want to thank Prof. Pingyun Feng and Prof. David Kisailus for serving on my advancement and doctoral committees. I want to extend my gratitude to Professor Valentine Vullev and Professor Umar Mohideen for lending me the experimental instruments from their groups.

I want to express my thanks to Dr. Ilkuen Lee, Dr. Xiangdong Qin and Dr. Zihuan Weng and other people from Prof. Zaera's group. Dr. Lee helped me a lot in sample characterization. I learned many useful techniques and skills from these senior group members.

At last, I want to thank my dear friends, Lanlan Zhong, Na Li, Lin Liu, Hailu Chen, Mingsheng Wang and Jun Xu, for their help and support during the past years during my stay in University of California, Riverside.

COPYRIGHT ACKNOWLEDGEMENTS

The text of this dissertation, in part or in full, is a reprint of the material as it appears in the publications below. Dr. Francisco Zaera directed and supervised the research which forms the basis for this dissertation. Dr. Xiangdong Qin helped me in set up the equipment and supervised me in the first year.

[1]Van Delft, J.A., D. Garcia-Alonso, and W.M.M. Kessels, Atomic layer deposition for photovoltaics: applications and prospects for solar cell manufacturing. *Semiconductor Science and Technology*, 2012. **27**(7).

[2]Guo, L. and Zaera, F., Spatial Resolution in Thin Film Deposition on Silicon Surfaces by Combining Silylation and UV/Ozonolysis, *Nanotechnology*, **2014**, 25(50).

DEDICATION

To my parents

Nanxin Guo and Minyan Xu

For their endless love

To my husband

Dong Gui

For his love and support

ABSTRACT OF THE DISSERTATION

Selective Chemistry of Metal Oxide Atomic Layer Deposition on Si Based Substrate Surfaces

by

Lei Guo

Doctor of Philosophy, Graduate Program in Materials Science and Engineering

University of California, Riverside, March 2015

Dr. Francisco Zaera, Chairperson

A versatile home-made atomic layer deposition (ALD) reactor was designed and built in our lab. This reactor can be used to deposit metal oxides on both wafer substrates and porous inorganic particles. Also, a simple procedure for selective ALD has been developed for the processing of silicon wafers in order to facilitate the spatially resolved growth of thin solid films on their surfaces. Specifically, a combination of silylation and UV/ozonolysis was tested as a way to control the concentration of the surface hydroxo groups required for subsequent atomic layer deposition (ALD) of metals or oxides. Water contact angle measurements were used

to evaluate the hydrophilicity/hydrophobicity of the surface, a proxy for OH surface coverage, and to optimize the UV/ozonolysis treatment. Silylation with silanes was found to be an efficient way to block the hydroxo sites and to passivate the underlying surface, and UV/O₃ treatments were shown to effectively remove the silylation layer and to regain the surface reactivity. Both O₃ and 185 nm UV radiation were determined necessary for the removal of the silylation layer, and additional 254 nm radiation was found to enhance the process. Attenuated total reflection-infrared absorption spectroscopy was employed to assess the success of the silylation and UV/O₃ removal steps, and atomic force microscopy data provided evidence for the retention of the original smoothness of the surface. Selective growth of HfO₂ films via TDMAHf+ H₂O ALD was seen only on the UV/O₃ treated surfaces; total inhibition of the deposition was observed on the untreated silylated surfaces. We believe that the silylation-UV/O₃ procedure advanced here could be easily implemented for the patterning of surfaces in many microelectronic applications.

TABLE OF CONTENTS

| | |
|--|----|
| CHAPTER 1. INTRODUCTION AND OVERVIEW | 1 |
| 1.1 ATOMIC LAYER DEPOSITION | 1 |
| 1.2 VARIATIONS OF ALD REACTORS | 7 |
| 1.3 ALD APPLICATIONS..... | 10 |
| 1.4 SELECTIVE ALD | 12 |
| CHAPTER 2. ALD REACTOR DESIGN AND BUILDING | 14 |
| 2.1 ASSEMBLY OF THE ALD REACTOR | 14 |
| 2.2 APPLICATION OF THE HOME-MADE ALD REACTOR..... | 19 |
| CHAPTER 3. SELECTIVE ALD ON SILICON SURFACE BY COMBINING SILYLATION AND UV/OZONOLYSIS | 21 |
| 3.1 SILANES AND SURFACE MODIFICATION | 21 |
| 3.1.1 Introduction..... | 21 |
| 3.1.2 SAMs on metal and oxide | 22 |
| 3.1.3 Hydrophobicity, hydrophilicity and contact angle | 25 |
| 3.1.4 Surface modification by silanes | 26 |
| 3.1.5 Different methods of SAM fabrication | 27 |
| 3.2 UV/OZONE TREATMENT..... | 29 |
| 3.2.1 Introductions | 29 |
| 3.2.2 Mechanism..... | 30 |
| 3.2.3 Application of UV/Ozone cleaning..... | 31 |
| 3.3 SELECTIVE ALD PROCESS | 32 |
| 3.4 EXPERIMENTS AND DETAILS | 34 |
| 3.4.1 Sample preparation | 34 |
| 3.4.2 Characterization | 35 |
| 3.5 <i>Results and discussion</i> | 39 |
| 3.6 CONCLUSION..... | 65 |
| CHAPTER 4. SELECTIVE ALD ON IBM WAFERS SURFACE BY COMBINING SILYLATION AND UV/OZONOLYSIS..... | 69 |
| 4.1 INTRODUCTION | 69 |
| 4.2 EXPERIMENT DETAILS | 70 |
| 4.2.1 Sample preparation | 70 |
| 4.2.2 Characterization | 71 |
| 4.3 RESULTS AND DATA ANALYSIS | 72 |
| 4.4 CONCLUSION..... | 93 |
| REFERENCE..... | 95 |

LIST OF FIGURES

| | |
|---|----|
| FIGURE 1.1 Schematic drawing for ALD process----- | 2 |
| FIGURE 1.2 Illustration of the self-limiting nature of ALD process----- | 4 |
| FIGURE 1.3 ALD growth rate in the function of precursor dose----- | 5 |
| FIGURE 1.4 Typical precursors used in ALD process----- | 7 |
| FIGURE 1.5 Schematic drawing of closed system ALD chamber ----- | 8 |
| FIGURE 1.6 Different types of ALD reactor used in industries----- | 9 |
| FIGURE 2.1 Solid works model of the home built ALD----- | 15 |
| FIGURE 2.2 Vertical View of the solidworks model of the ALD chamber----- | 17 |
| FIGURE 2.3 Overview of the reactor----- | 18 |
| FIGURE 2.4 Sample holder of the ALD reactor ----- | 19 |
| FIGURE 2.5 N ₂ adsorption on Al ₂ O ₃ -x-SBA-15 after ALD ----- | 20 |
| FIGURE 3.1 Examples of the types of molecular structures used to make SAMs on Au for electronic applications----- | 23 |
| FIGURE 3.2 Examples of molecular structures used for self-assembly on oxide surfaces----- | 24 |
| FIGURE 3.3 Illustration of contact angle ----- | 25 |
| FIGURE 3.4 Schematic for UV/Ozone treatment on solid surface----- | 31 |
| FIGURE 3.5 Selective atomic layer deposition (ALD) scheme developed----- | 34 |
| FIGURE 3.6 Al mold used in the UV/Ozonolysis for patterning Substrate ----- | 37 |
| FIGURE 3.8 Pictures of water droplets on Si(100) surfaces silylated with either HMDS (left) or trichloro(octadecyl)silane (ODTS, right) as a function of time | |

of exposure to our UV/O₃ treatment-----46

FIGURE 3.9 Summary of contact angle data obtained as a function of UV/O₃ exposure time for the original Si(100) (right panel) substrate and for Si(100) surfaces silylated with TMCS (trimethylchlorosilane, also right panel) and with HMDS and ODTS (left panel)-----46

FIGURE 3.10 Pictures of water droplets on Si(100) surfaces silylated with HMDS before (left) and after (right) 35-min UV/O₃ treatments-----48

FIGURE 3.11 Hf 4f X-ray photoelectron spectra (XPS) from HMDS-silylated Si(100) surfaces after the growth of HfO₂ films -----51

FIGURE 3.12 Hf 4f XPS from ODTS-silylated Si(100) surfaces after the growth of HfO₂ films via TDMAHf + H₂O ALD at 110 °C-----53

FIGURE 3.13 Average thickness of HfO₂ films grown on Si(100) via ALD as a function of the number of ALD cycles-----55

FIGURE 3.14 (a) Scanning electron microscopy image (SEM, top) and (b) energy dispersive X-ray microanalysis data (EDX, bottom) line-scan profile from a Si(100) surface silylated with HMDS, processed using a UV/O₃ treatment, and exposed to 100 cycles of HfO₂ ALD-----57

FIGURE 3.15 SEM and EDX data from a Si(100) surface silylated with HMDS, processed using a UV/O₃ treatment, and exposed to 30 cycles of HfO₂ ALD -----59

FIGURE 3.16 Scanning electron microscopy image (SEM) from a Si(100) surface silylated with HMDS, processed using a UV/O₃ treatment, and exposed to 200 cycles of HfO₂ ALD -----63

FIGURE 3.17 SEM (a) and energy dispersive X-ray microanalysis data (b,c and d) from a Si(100) surface silylated with HMDS, processed using a UV/O₃ treatment by a mask, and exposed to 200 cycles of HfO₂ ALD -----64

FIGURE 3.19 EDX line-profiles from the photomask -----68

FIGURE 3.20 Schematic of selective ALD process -----71

FIGURE 4.1 ATR trace for native IBM 1, 2, 3 and 4 wafers -----73

FIGURE 4.2 Pictures of water droplets on as a function of time of exposure to our UV/O₃ treatment -----75

FIGURE 4.3 AFM image of IBM wafers surfaces as a function of time of exposure to our UV/O₃ treatment -----76

FIGURE 4.4 Pictures of water droplets on native IBM 3(left) and HMDS silylated IBM 4 (right) as a function of time of exposure to our UV/O₃ treatment -----78

FIGURE 4.5 AFM image of (a) native IBM 3, (b)native IBM 4, (c) HMDS / IBM 4, (d) UV exposed IBM 3, (e) UV exposed HMDS / IBM4, (f) Covered HMDS/ IBM 4 surfaces-----79

FIGURE 4.6 Summary of contact angle data obtained as a function of UV/O₃ exposure time for the original native IBM 1 (left panel) and 3(right panel) substrate and for IBM 2(left panel) and 4(right panel) surfaces silylated with HMDS -----80

FIGURE 4.7 Summary of contact angle data obtained as a function of UV/O₃ exposure time for the IBM 2 and 4 surfaces silylated with ODTS -----81

FIGURE 4.8 AFM image of (a) ODTS IBM 2, (b) UV exposed ODTS IBM 2, (c) Covered ODTS IBM 2, (d) ODTS IBM 4, (e) UV exposed OTDS/IBM4, (f)

| | |
|---|----|
| Covered ODTS/ IBM 4 surfaces----- | 82 |
| FIGURE 4.9 Hf 4f X-ray photoelectron spectra (XPS) from IBM 1 surfaces after the growth of HfO ₂ films via TDMAHf + H ₂ O ALD at 110 °C ----- | 84 |
| FIGURE 4.10 Hf 4f XPS from HMDS/IBM 2 surfaces after ALD----- | 86 |
| FIGURE 4.11 Hf 4f XPS from IBM 3 surfaces after the growth of HfO ₂ films via TDMAHf + H ₂ O ALD at 110 °C ----- | 88 |
| FIGURE 4.12 Hf 4f XPS from HMDS silylated IBM 4 surfaces after the growth of HfO ₂ films via TDMAHf + H ₂ O ALD at 110 °C ----- | 90 |
| FIGURE 4.13 Average thicknesses of HfO ₂ films grown on the IBM 1 to 4 ----- | 92 |

LIST OF TABLES

| | |
|--|----|
| Table 3.1 Data from water contact angle measurements on the Si(100) surface after different cleaning and silylation steps. ----- | 44 |
| Table 3.2 Atomic force microscopy root-mean-square (AFM rms) roughness data from Si(100) surfaces after different cleaning, silylation, and UV/O ₃ treatments.----- | 52 |
| Table 3.3 Average film thicknesses in Å for Si(100) surfaces right after silylation with HMDS, UV/O ₃ treatment, and a 20 cycle HfO ₂ ALD.----- | 61 |
| Table 3.4 Average film thicknesses in Å for Si(100) surfaces right after silylation with ODTs, UV/O ₃ treatment, and a 20 cycle HfO ₂ ALD.----- | 61 |
| Table 4.1 Information of the wafers offered by IBM. ----- | 69 |
| Table 4.2 Surface roughness of the IBM 1 and 3 samples before and after silane, and UV/Ozone treatments, respectively. ----- | 83 |

Introduction and Overview

1.1 Atomic Layer Deposition

Atomic layer deposition (ALD) is an important thin film deposition technique used in microelectronic device fabrication for a variety of applications. ALD was first invented in 1977 to deposit zinc sulfide films, which was used in electroluminescent devices. It is now being exploited in the production of advanced microelectronics for high-k dielectric and metal films in transistor gate stacks and capacitors, Cu barrier/seed films, and a variety of gap layers and diffusion barriers for thin-film, magnetic head and non-volatile memory applications[1-4].

ALD has several advantages over other traditional methods such as (metal organic) chemical vapor deposition ((MO) CVD) and physical vapor deposition (PVD). ALD processes have precise thin film thickness control at an atomic scale (Angstrom and monolayer), excellent step coverage (as high as 100:1) and conformal deposition on high aspect ratio structures.5-8 ALD processes also keep with the industry trend to move to lower thermal processing as most processes operate well below 400 °C. The ALD temperatures are typically much lower to those of conventional CVD processes, which are typically above 500 °C [9-11].

A scheme showing the reactions involved during ALD is displayed in Figure 1.1. The deposition process is conducted on a substrate with reactive surface moieties. The first precursor is introduced into the chamber and allowed to chemisorb on the substrate until the surface reaches saturation, and then the excess precursor is purged from the system. The second precursor is then introduced into the chamber and made to react with the adsorbed species on the substrate surface. Reaction byproducts and excess precursor are again removed from the chamber by using a purging gas (inert gas). At this time, the substrate surface is covered with a monolayer of the desired compound, and this represents one cycle in the ALD process. With these binary reactions repeated, thin films can be deposited and atomic-level thickness can be controlled.

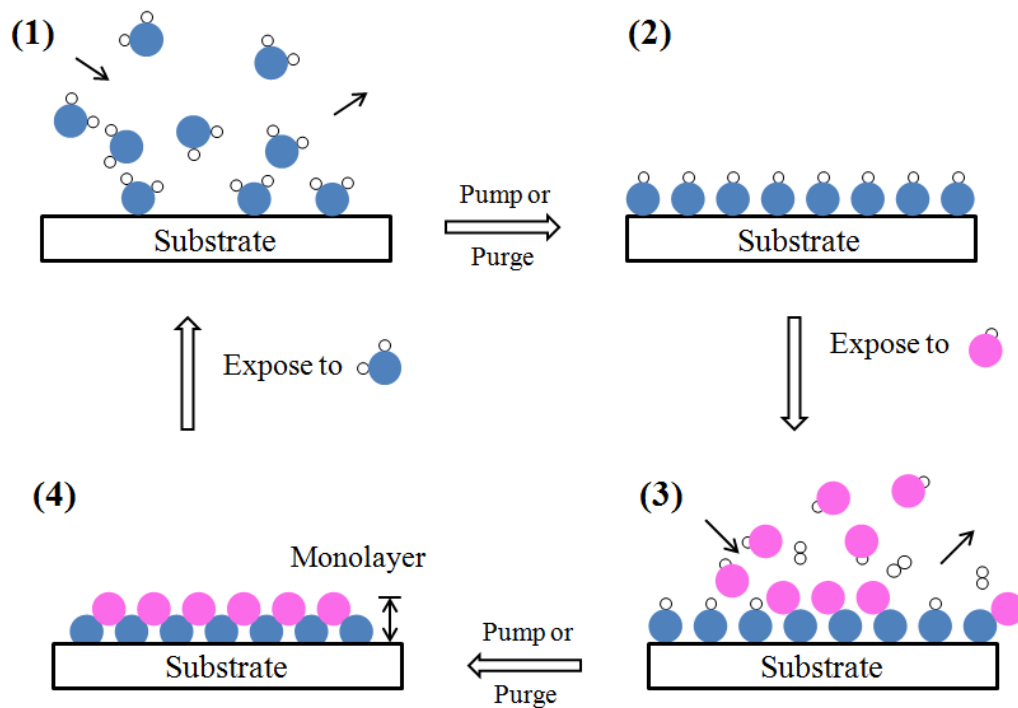


FIGURE 1.1 Schematic drawing for ALD process

The surface reaction mechanism requires ALD parameters (like temperature and reactor pressure) to be optimized to realize accurate thickness control and superior conformity. The reactor temperature is a very important parameter to control surface saturation. It determines the ALD reactions in two aspects: (1) provides the activation energy for the ALD reaction, and (2) helps desorb the excess reactants and by-products after the reaction. The optimal ALD process temperature window for monolayer coverage is defined in Figure 1.2. The ALD window is related to precursor dose and purging time. A sufficient dose of a thermally stable precursor is needed to achieve whole surface coverage. It should not decompose at the reactor temperature when it is delivered to the substrate surface. Usually ALD needs an overdose of the precursor to achieve full surface saturation. Control of the dose can be achieved by controlling the following parameters of the precursor: precursor flows, temperature and partial pressure, and the total reactor chamber pressure.

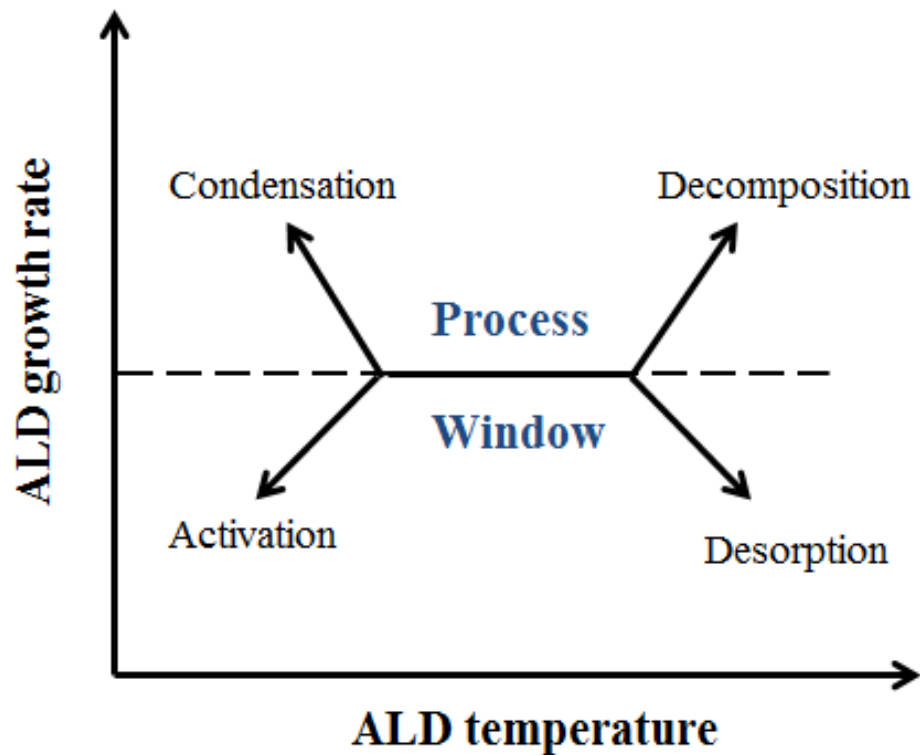


FIGURE 1.2 Illustration of the self-limiting nature of ALD process

Figure 1.3 shows the ALD growth rate as a function of precursor pulse time. The ALD growth rate first increases linearly with precursor pulse time, but levels off after reaching saturation. In comparison, CVD, or PVD show a constant growth rate with increasing dosing time. Hence, saturation curves can be used to determine if the process is self-limiting and confirm if it is an ALD process.

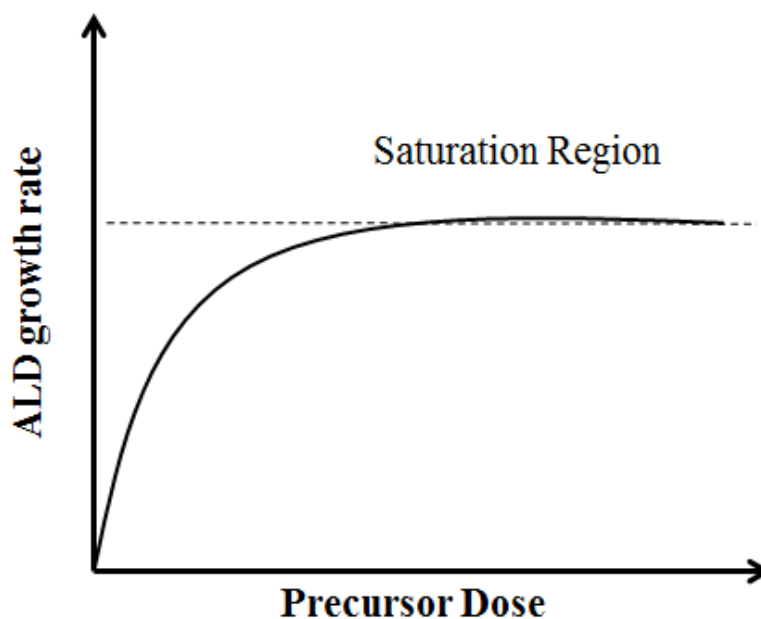


FIGURE 1.3 ALD growth rate in the function of precursor dose

Besides temperature, the precursor selection is also a very important parameter to the whole ALD process. There are several properties an ALD precursor should have: (1) volatility but thermally stability so that it does not decompose during vaporization and deposition, (2) preferable solubility in an inert solvent or liquid at room temperature, (3) high reactivity to the other complementary reagents, (4) preferential reactivity towards the substrate and the growing film, (5) self-limiting reactivity with the substrate and the film surface, (6) ability to create volatile reaction byproducts and have optimal ligand size. It is essential that precursors are volatile but thermally stable so that they do not decompose during vaporization, and it is also preferable that they are soluble in an inert solvent in an inert solvent or liquid at room temperature. Furthermore, they must have preferential reactivity towards the substrate and the growing film.[1, 2] It is also

important that ALD precursors have self-limiting reactivity with the substrate and the film surface. The trend in precursor selection is now moving toward liquid organometallics, because they are easy to use and produce less harmful byproducts. Furthermore, ALD has a very high precursor utilization efficiency that often offsets the high cost of novel precursors. Typical precursor types used in ALD are shown in Figure 1.4. With these precursors, many materials can be deposited by ALD process, such as (1) oxides, including dielectrics (Al_2O_3 , TiO_2 , HfO_2 , ZrO_2 and etc.), transparent conductors (In_2O_3 , SnO_2), semiconductors (ZnO , WO_3 , MnO_x), superconductors ($YBa_2Cu_3O_{7-x}$), and ternary oxides ($LaNiO_3$ and $LaMnO_3$); (2) nitrides, including semiconductors and dielectrics (AlN , GaN , InN and SiN_x) and metallic nitrides (TiN , $Ti-Si-N$, TaN , W_2N and etc.); (3) II-VI compounds (ZnS , $ZnSe$, CaS , CdS and etc.) (4) III-V compounds ($GaAs$, $AlAs$, GaP and etc.); (5) fluorides (CaF_2 , SrF_2 and ZnF_2); and (6) elements (Si , Ge , Cu , Ni , Mo , Ta , Ru and etc.)

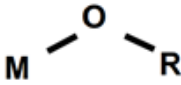
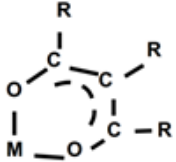
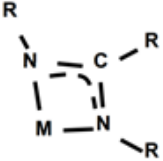
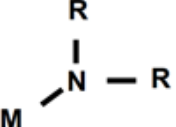

| | | | |
|--|--|--|--|
| $\text{M} - \text{R}$ <p>Alkyls</p> |  <p>Alkoxides</p> |  <p>β - diketonates</p> | |
| $\text{M} - \text{X}$ <p>Halides, where X= Cl, Br, I</p> |  <p>Amidinate</p> |  <p>Alkylamides</p> |  <p>Cyclopentadienyls</p> |
| <p>The R's represent alkyl groups consisting of carbon and hydrogen, such as methyl (CH₃) or ethyl (C₂H₅)</p> | | | |

FIGURE 1.4 Typical precursors used in ALD process

1.2 Variations of ALD reactors

There have been different types of ALD reactors developed since the technique has been invented. There are four main types: closed system chambers, open system chambers, semi-closed system chambers, and semi-open system chambers. And among the four kinds, the closed system chambers (Figure 1.5) are most commonly used[3, 4].

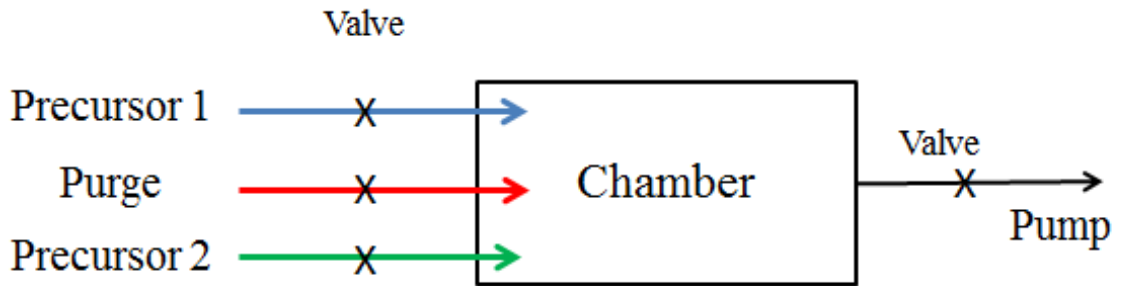


FIGURE 1.5 Schematic drawing of closed system ALD chamber

Many research labs build their own home-made ALD reactors (closed system chambers in most cases), but there are also some types used in industries, including (Figure 1.6): (a) Showerhead-type single wafer ALD reactor; (b) batch ALD reactor; (c) in-line spatial ALD reactor (designed by SoLayTec); (d) in-line spatial ALD reactor (designed by Levitech); (e) roll-to-roll ALD reactor (designed by Lotus Applied Technology); (f) roll-to-roll ALD reactor (designed by Beneq)[5].

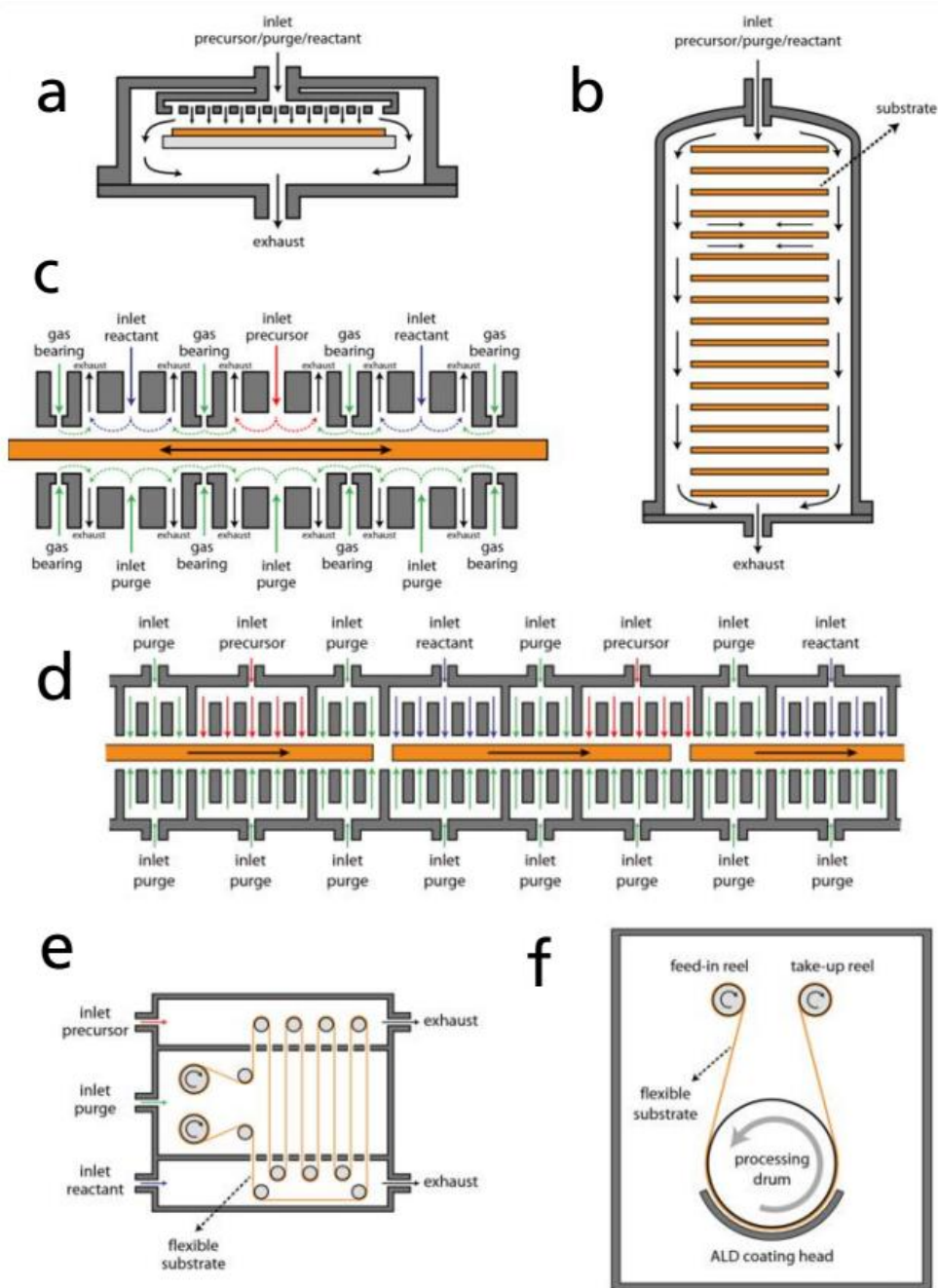


FIGURE 1.6 Different types of ALD reactor used in industries (a-f) (This figure is reproduced/adapted with permission from Ref. 5, Copyright 2012, Semiconductor Science and Technology, IOPscience)

1.3 ALD Applications

Based on the advantages discussed above, atomic layer deposition technique has been widely used for microelectronics, photovoltaics, and biomedical applications [6, 7].

In microelectronics, ALD has been used to deposit high-k gate oxides, high-k dielectrics, ferroelectrics, and metal or nitride interconnects. In high-k gate oxides and high-k dielectrics, it is essential to control the ultrathin film growth. The most commonly seen high-k oxides are Al_2O_3 , ZrO_2 , and HfO_2 . The motivation for the choice of these oxides comes from the tunneling problem of high current through the commonly used SiO_2 gate dielectrics in metal-oxide-semiconductor field-effect transistors (MOSFETs) when they are downscaled to a thickness of 1.0 nm and below [8, 9]. With high-k oxides, a thicker gate dielectric can be deposited for the required capacitance density, thus the tunneling current can be reduced through the structure. In ferroelectrics, ALD are used to deposit the ferroelectric layers in the metal-ferroelectric-insulator-silicon (MFIS) structure of ferroelectric memory field effect transistors (FEMFETs), using materials that include $\text{SrBi}_2\text{Ta}_2\text{O}_9$ (SBT) [10, 11] and $\text{Bi}_{3.25}\text{La}_{0.75}\text{Ti}_3\text{O}_{12}$ (BLT) [12, 13]. They are used to replace lead-zirconate-titanate (PZT) as the ferroelectric layer in the MFIS structure, since it is difficult to apply sufficient voltage to the PZT layer because its dielectric constant is much higher than that of SiO_2 . With metals and nitrides, the use of ALD includes: (1) noble metals for ferroelectric random access memory (FRAM) and DRAM capacitor electrodes [14, 15]; (2) Cu interconnects and/or Cu seed layers for Cu electrodeposition and tungsten seeds for tungsten CVD [16-19]; (3) metal nitrides, used as metal barriers

and as gate metals (e.g. titanium nitride, tantalum nitride, tungsten nitride)[20, 21]. Metal barriers are used in Cu-based chips to avoid Cu diffusion into the surrounding materials such as insulators and the silicon substrate. Also, these barriers prevent Cu from contamination by elements diffusing from the insulators. The metal barriers have strict demands: they are supposed to be pure, dense, conductive, conformal, thin, and to have good adhesion towards metals and insulators.

In photovoltaics, ALD is used in depositing surface passivation layers for c-Si solar cells[22], buffer layers for CI(G)S solar cells[23], encapsulation of CIGS and OPV solar cells[24, 25], barrier layers for dye-sensitized solar cells (DSSCs) [26-29], and nanostructured solar cells[30, 31]. In the c-Si solar cell industry, reducing the cell thickness and improving its efficiency are two approaches to achieve the reduction of the cost per watt peak. It is very important to reduce the electronic losses at the c-Si surface. This can be achieved by using effective surface passivation layers, deposited by ALD, in both front and backside of the solar cells. In CIGS solar cells, the buffer layers, which ensure good interfacial properties between CIGS absorber and ZnO window layer, are usually less than 100 nm thick. ALD can achieve a precise thickness control of this layer needed to prevent the solar cell from a low open circuit voltage and poor efficiency, due to the negative conduction band offset at the CIGS and ZnO interface[23]. In encapsulation of flexible CIGS and OPV solar cells, robust, transparent and flexible materials are needed. ALD can produce pinhole-free flexible films at low temperatures, and have many advantages compared to traditional encapsulating material-glasses. In

DSSCs, a barrier layer deposited by ALD can suppress the recombination of charge carriers at the interface of the photoanode and the dye or electrolyte.

In biomedical application, ALD applications include modifying nanoporous particles and membranes, and fabricating thin biocompatible coatings. Due to the low-temperature deposition advantage, ALD is also a possible manufacturing process for flexible organic field-effect transistors (OFETs).[32] ALD has been used to modify the surface of nanoporous materials, which are emerging throughout the biomedical industry in drug delivery and tissue engineering. TiO_2 ALD has been used to fabricate the materials used in optical waveguide sensors as diagnostic tools.[33] Also, unlike many other methods, the saturation and self-limiting nature of the ALD reactions means that even deeply embedded surfaces and interfaces are coated with a uniform film. Nanoporous surfaces can have their pore size reduced further in the ALD process because the conformal coating completely coats the inside of the pores and decreases the pore diameter by increasing ALD cycles. This accurate pore size controllability can be used in many applications.[34]

1.4 Selective ALD

With all the advantages mentioned above, ALD is able to meet the needs of industry in many applications. Hence, ALD has wide applications in semiconductor industry, including depositing high dielectric constant gate oxides in MOSFET structures and for metal diffusion barriers in backend processes. In addition, ALD has met the challenging requirement of miniaturization in the semiconductor industry, which needs atomic level

scale fabrication methods with high aspect structures. It also has been used for low electron leakage dielectrics for magnetic read/write heads and for diffusion barrier coatings with low gas permeability.

Many ALD processes are very sensitive to substrate surface conditions. As a result, functional groups on substrate surfaces can be manipulated before the ALD process, and with that, selective film deposition can be achieved on specific areas of devices. Area-selective ALD is an additive process, compared to other conventional subtractive-patterning strategies. This is because in area-selective ALD, the targeted material is deposited only where needed. Many substrate surfaces (SiO_2 or Si, for example) have little selectivity toward most ALD precursors, hence the need to utilize modifiers such as silanes to achieve surface modification for selective deposition. Organic monolayers provide the ability to tune the reactivity between ALD precursors and the surface by changing key functional groups. The organic monolayers can block the active sites (-OH, etc.) at the underlying substrate, or can create more nucleation sites (-OH, etc) on surfaces as activator (multiplier). Structures achieved by selective ALD are not determined by the resolution of the lithography, but by a difference in chemistry of the precursor as a function of the surface of the substrate.

ALD reactor design and building

2.1 Assembly of the ALD reactor

We built a home-made ALD reactor in our laboratory to achieve specific requirements for our applications. Figure 2.1 shows the overview of the main structure of the ALD reactor. The chamber of the ALD reactor consists of a six-way cross. The up-face is connected to a viewport which affords the viewing of the inside the chamber during experiments. The bottom face of the six-way cross is connect to a cross male union, of which one end is connected to a molecular sieve trap and then to a mechanical pump; the other two ends are connected to other faces of the chamber for gas delivering. The front face of the chamber is connected with a sample holder. The back face of the chamber is connected to a pressure gauge and then to a pressure meter, which can detect the pressure inside the chamber. Under vacuum, the chamber could reach background a pressure of approximately 0 mTorr. All of these components may be seen more clearly in vertical view of the chamber model in Figure 2.2.

Nitrogen gas is introduced from the top through a gas line and then diverged into two lines, each one on one side of the chamber. On each side of the chamber, the gas line diverges into two parts again: one going through Valves 1 and 5 for purging the chamber with nitrogen gas flow, and the other directed through Valve 3 and 7 for bubbling of the metalorganic precursor.

During experiments, heating tapes are wrapped all over the chamber and the gas line to make this ALD chamber a warm-wall reactor. The sample holder is also heated, to

135 °C, up by using a heating wire in the feedthrough. All the heating tapes are controlled by one thermal controller and one variable transformer; and the heating system built in the sample holder is controlled by another thermal and variable transformer.

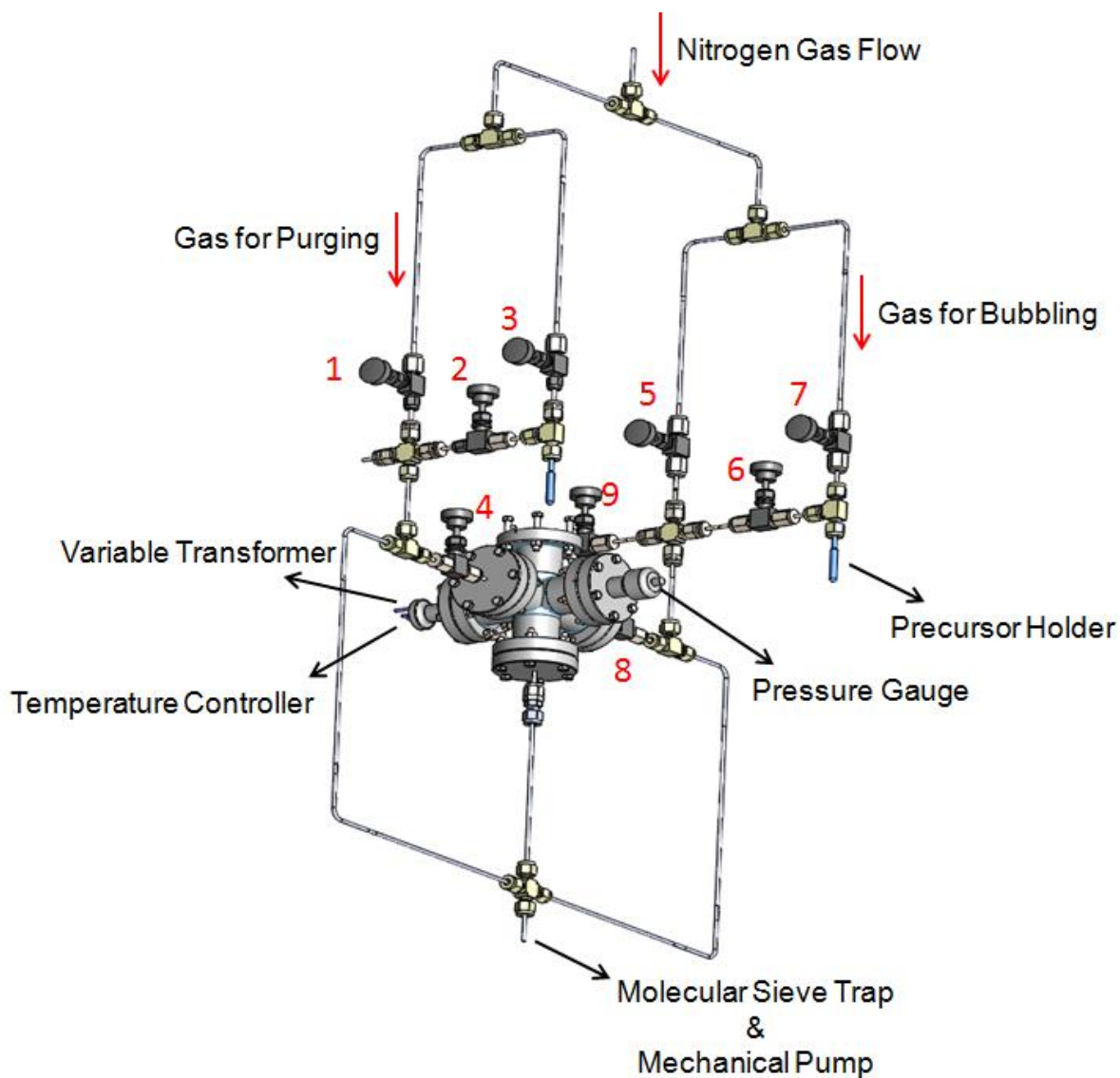


FIGURE 2.1 SolidWorks model of the home built ALD

One cycle of the ALD process is operated as follows (Al_2O_3 ALD deposition is discussed here as an example):

(1) Tetramethyl aluminum (TMA), the precursor used for Al_2O_3 ALD, is loaded in a glass tube and connected to Valve 3. Valve 4 is turned open, and then Valve 3 is opened as well. Then Valve 2 is opened gradually until reaching a pressure at 150 mTorr in the chamber, and that pressure is then held constant for 120 seconds. At this point the TMA precursor is bubbled into the chamber. Then, Valve 2, then Valve 3, are closed.

(2) Valve 1 is gradually open to make the chamber pressure reach 1000 mtorr, and that pressure is kept for 5 minutes. Then Valves 1 and 4 are closed. This step is performed to purge the chamber and gas line with pure nitrogen gas to get rid of any excess precursor vapor in the system.

(3) Deionized water (DI water, the second reactant) is loaded on the glass tube connected to Valve 7. Valve 8, then Valve 7, is opened. Valve 6 is then opened gradually to reach a gas pressure of 200 mtorr for 120 seconds. Valve 6 is closed first, and then Valve 7. This step is performed to bubble water vapor, used as the second reactant, into the chamber.

(4) Valve 5 is opened gradually to make the chamber pressure reach 1000 mtorr, and then that pressure is held for 10 minutes. Valves 5 and 8 are closed. This step is designed to purge the chamber and gas line with pure nitrogen gas to get rid of any excess water vapor in the system.

These ALD cycles can be repeated by repeating the procedure (1) to (4) listed above.

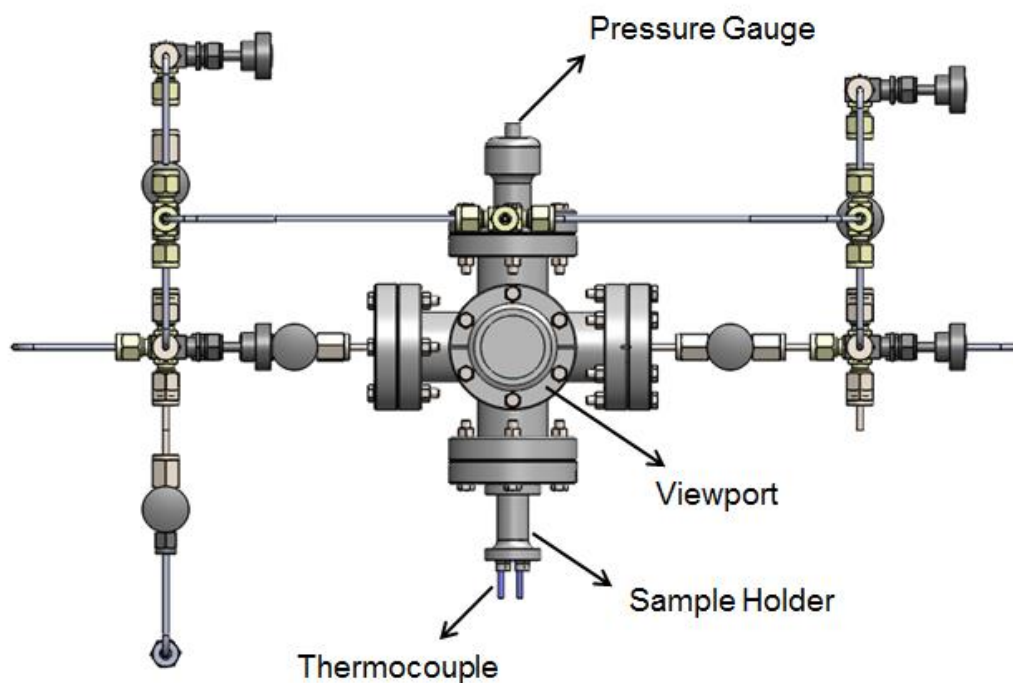


FIGURE 2.2 Vertical View of the ALD chamber

Figure 2.3 The ALD reactor in our laboratory. During experiments, all the lines for gas and precursor delivery are wrapped with heating tape and foil to keep the delivering lines warm to avoid condensation. This is a warm-wall reactor design.



FIGURE 2.3 Overview of the reactor

Figure 2.4 provides an image of the sample holder, which is based on the use of a commercial electrical feedthrough. One end of the feedthrough is a solid flange, in the center of which there are two electrode and two thermocouple connectors. The thermocouple has wires welded under the sample holder for the detection of the

temperature of the sample holder (the same as the temperature of the sample during experiments). The two electrical electrodes are connected to the variable transformer to provide current for resistive heating of the sample holder.



FIGURE 2.4 Sample holder of the ALD reactor

2.2 Application of the home-made ALD reactor

This ALD reactor has been used by several colleagues in our group to perform ALD on mesoporous silica for pore size controlling. It has been used in several projects, including one for tuning selectivity of catalysts via regulation of pore size in porous silica (by Dr. Zhihuan Weng), and another to control drug release via pore size control (by Dr. Zhihui Chen). Figure 2.5 shows data from Dr. Zhihuan Weng experiments. The left figure displays the N_2 adsorption on ALD- Al_2O_3 - x -SBA-15 samples, obtained after different ALD cycles x , from 0 to 5. The right panel of the figure shows the pore diameter of the SBA-15 calculated from the raw adsorption data. It can be seen that the pore diameter decreased with increasing number of ALD cycles. This

data indicate that our ALD reactor has successful in controlling the pore size of mesoporous materials.

N₂ adsorption on ALD-Al₂O₃-x-SBA-15

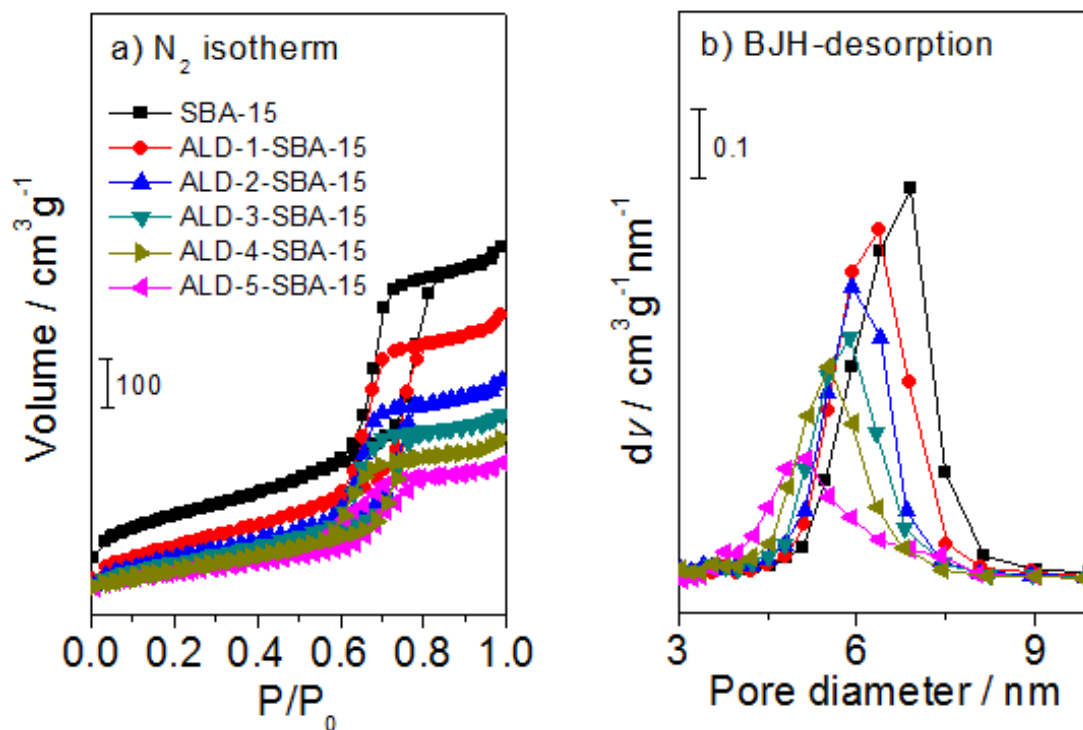


FIGURE 2.5 N₂ adsorption on ALD-Al₂O₃-x-SBA-15 after x=0 to 5 ALD cycles (left); Right panel: Pore diameter calculated from the raw adsorption shown on the left left. (Reproduced from work by Dr. Zhihuan Weng)

Selective ALD on silicon surfaces by combining silylation and UV/Ozonolysis

3.1 surface modification with silanes

3.1.1 Introduction

Silanes are silicon compounds that react with inorganic solid substrates such as glass, silicon oxide or germanium, and are used to change the surface properties of those solids. After reaction, they form stable covalent bonds and lead to an organic substitution that changes the physical properties of the treated solid substrate, including: hydrophobicity/hydrophilicity, dielectric constant, absorption, and charge conduction. The silanes used for these purposes are different from those used as coupling agents in adhesive applications. All the silanes mentioned here are non-functional silanes, that is, they can modify the surface without imparting reactivity. The applications of these silanes include uses for: water-repellents, anti-stiction coatings for MEMs, fillers for composites, pigment dispersants, dielectric and anti-fog coatings, self-assembled monolayers, nanoparticle synthesis, and mineral surface treatments. In the next section, more information on hydrophobic and hydrophilic silanes will be introduced.

3.1.2 Self-assembled monolayers (SAMs) on metal and oxide surfaces

Silanes can form organic monolayers on solid substrates, and these layers can provide the ability to tune the reactivity between ALD precursors and the surface by changing key functional groups on surface. People usually refer to silane monolayers on substrate surfaces as “Self-assembled monolayers (SAMs)”. Although this may not be entirely appropriate, we will nevertheless describe those layers as “SAMs” here for convenience. There are two main types of SAMs on solids, on metals and on oxides[35].

For SAMs on metals, the most extensively investigated types are alkanethiols on platinum[36], gold[37, 38] and copper[39, 40]. It is easy to deposit thin SAMs films on Au as well, and to pattern those with chemical etchants or conventional lithographic tools; hence this is perhaps the most commonly used procedure for patterning. Also, Au is inert to oxidation. The most commonly used method for SAMs formation is to immerse the substrate in a dilute solution of the target thiol for over 12 hours at the room temperature. Long immersion times are required because of the slow reorganization processes that take place during film growth [41]. It is very important to choose appropriate conditions such as solvent, solution concentration, temperature, and immersion time to optimize the structure of resulting SAMs [42, 43]. Alkane thiol and dithiol molecular structures are used on Au for electronic applications (Figure 3.1) because they form dense-pack and well-ordered domains. Other thiols based on oligophenylenes (OPs), oligo(phenyleneethynylenes) (OPEs), and oligo(phenylenevinylenes) (OPVs) are also used on Au. The labile thiocarbonate or disulfide

functional groups are sometimes used for substrate chemisorption instead of the R-SH group. SAMs formed from these tools have different functionalities, including terthiophenes,[44-46] tetracyanoquinodi-methane,[47] and azo-groups.[48, 49]

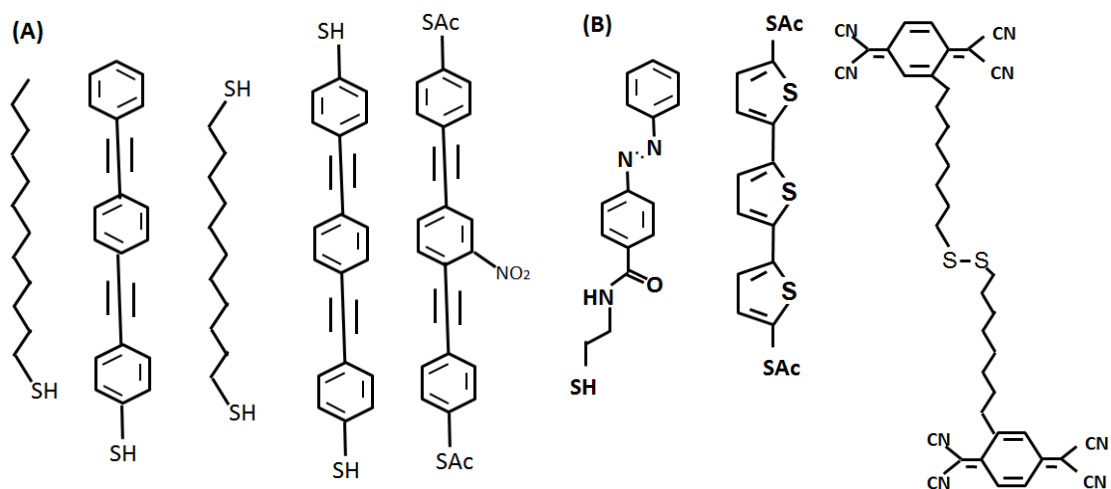


FIGURE 3.1 Examples of the types of molecular structures used to make SAMs on Au for electronic applications. A) Mono(di)thiols, and molecular wires (OPE). (B) Molecular wires from azo compounds. (This figure is adapted with permission from Ref. 35, Copyright 2009, Advanced Materials, Wiley)

For SAMs on oxides, organosilane precursors (RSiX_3 , $\text{X} = \text{Cl}$, OMe and OEt) are used. Those need hydroxylated surface (oxide surface) to start the deposition reaction. With SiO_2 surfaces, for example, the driving force for self-assembly is the in situ formation of siloxanes, which connects the silane to the surface silanol groups (such as $-\text{Si-OH}$) via very strong Si-O-Si bonds. The underlying siloxane network as well as interchain interactions and reaction temperature determine the order and packing of the chemisorbed silanes, because of the amorphous substrate surface[50]. In particular, silanes like hexamethyldisilazane (HMDS) can be deposited on surfaces by exposure to the silane vapor at room temperature, or by heating or under vacuum[51]. Usually, this

type of silanes has short chain lengths and high vapor pressures. Figure 3.2 shows the structures of silane precursors used commonly for the formation of SAMs on oxides. They include simple alkane chains such as octyltrichlorosilane (OTS) and octadecyltrichlorosilane (ODTS), hexamethyldisilazane (HMDS), and other types of functionalized molecules. There are also other types of materials like n-alkanoic acids (carboxylic end groups) and phosphonic acids that can bind to a variety of oxides surfaces and form similar SAMs as thioils on Au[52].

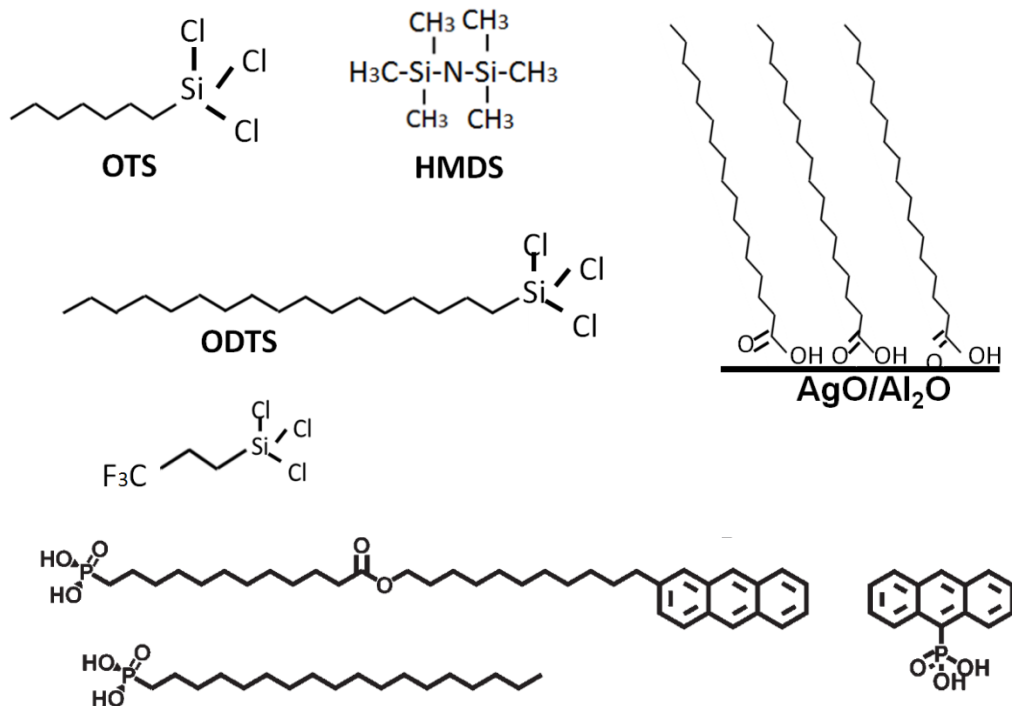


FIGURE 3.2 Examples of molecular structures used for self-assembly on oxide surfaces: silanes and carboxylic acids and phosphonic acids. (This figure is adapted with permission from Ref. 35, Copyright 2009, Advanced Materials, Wiley)

3.1.3 Hydrophobicity, hydrophilicity, and contact angle

Hydrophobicity and hydrophilicity are used to describe the interaction of water with surfaces. Hydrophilicity means that a surface tends to adsorb water or easily get wetted without forming a droplet on the surface. It indicates that the forces between water and the surface are stronger than the forces within the solid and the liquid water. Hydrophobicity, by contrast, refers to the case where the surface behaves in the opposite way. Both hydrophilicity and hydrophobicity are determined by the interaction of the boundary layer of a solid phase with a liquid and vapor phase. Contact angles are usually used to quantify the wettability of a solid surface by a liquid, and quantified via the Young equation. Figure 3.3 shows the contact angle Θ formed in the interphase between vapor, liquid and solid phases. Water forms a standing droplet on a hydrophobic surface and the contact angle increases with surface hydrophobicity. If the contact angle is larger than 80° , the surface is considered as hydrophobic, whereas if the contact angle of the droplet is less than 30° , the surface is considered as hydrophilic.

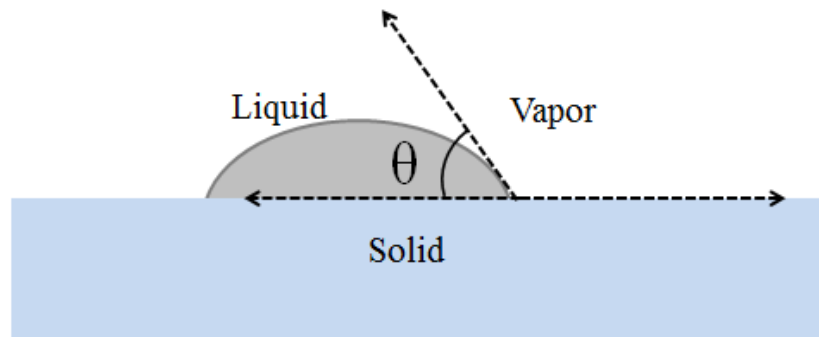


FIGURE 3.3 Illustration of the contact angle formed at the interphase of among liquid, vapor and solid phases. (Acknowledgement: This figure is drawn by Lei Guo, however adapted from the figure in Wikipedia: http://en.wikipedia.org/wiki/Contact_angle)

3.1.4 Surface modification by silanes

As shown above, most organosilanes have one organic substituent and three hydrolysable substituents. The alkoxy groups of the trialkoxysilanes are hydrolyzed to form silanol-containing species in most surface treatment applications. There are four main steps in the silane reactions. The first step is the hydrolysis of the three labile groups. The following process is condensation to form oligomers. Then, oligomers hydrogen-bond with OH groups on the substrate, and finally, the substrate surface forms a covalent linkage, with a concomitant loss of water. Here all the steps are described sequentially, but these reactions can take place simultaneously after the first hydrolysis step. There is usually only one bond from by each silicon atom of the organic silane to the substrate surface at the interface, and the two remaining silane groups are present either in condensed or free form. The R group of the silane remains available for covalent reaction or physical interaction with other phases.

There are several factors contributing to the ability of an organic silane to form a hydrophobic surface, including the extent of surface coverage, the organic substitution, residual unreacted groups, and the distribution of the silanes on the surface. Their hydrophobic entities of silanes, including aliphatic hydrocarbon substituents or fluorinated hydrocarbon substituents, enable them to induce surface hydrophobicity. The organic substitution of the silane must be non-polar in order to generate a hydrophobic surface. The free energy of transfer of hydrocarbon molecules from an aqueous phase to a homogeneous hydrocarbon phase can be related to the hydrophobic effect of the

organic substitution. Van der Waals interactions are predominant factors in interactions with water for non-polar entities. Such interactions compete with hydrogen bonding in the ordering of water molecules. Van der Waals interactions in solid surfaces are primarily related to the instantaneous polarizability of the solid, and are proportional to the dielectric constant or permittivity at the primary UV absorption frequency and the refractive index of the solid. Entities with sterically closed structures that minimize van der Waals contact are more hydrophobic than open structures that allow van der Waals contact. Hence, polypropylene and polytetrafluoroethylene are more hydrophobic than polyethylene. Similarly, methyl-substituted alkylsilanes and fluorinated alkylsilanes provide better hydrophobic surface treatments than linear alkyl silanes.

3.1.5 Different methods for SAMs fabrication

SAMs can be applied to substrates by a variety of methods, such as bulk solution deposition, microcontact printing, and vapor phase deposition.

Bulk solution deposition is one of the most common SAMs deposition methods. It is also one of the cheapest methods, as it does not depend on expensive equipment and it can be employed for large area batch processing or continuous deposition. It can yield stable, adherent, uniform and hard films with good reproducibility. The growth of SAMs strongly depends on growth conditions, such as the duration of the deposition, the silane percentage in the toluene solution, the temperature of the solution, and the chemical nature of the substrate.

Microcontact printing (or μ CP) has been utilized to fabricate SAMs in a dry glove box to control humidity [53-56]. Microcontact printing is a form of soft lithography that uses the relief patterns on a master polydimethylsiloxane (PDMS) stamp to form SAMs patterns of ink on the surface of a substrate through conformal contact as in the case of nanotransfer printing (nTP). Several advantages derive from this method, including: (1) it creates patterns with micro-scale features simply and easily; (2) multiple stamps can be created from a single master; (3) it is performed in a glove box, without the need for constant use of a cleanroom (a cleanroom is only needed for master fabrication) (4) it is cheap and uses less energy than conventional techniques. However, the cost is somewhat higher than the bulk phase solution method. The contact angles of SAMs fabricated by this method are almost the same of those obtained by the solution phase method[57].

In addition, SAMs can also be fabricated by vapor phase deposition [58-62]. Vapor phase processes have advantages over other SAMs fabrication method, including less precursor consumption and reduction of the aggregation of the precursor molecules before deposition on the substrate surface [63, 64]. It is so interesting that vapor-phase-developed SAMs show similar behavior as the solution-prepared SAMs, with the same properties in terms of contact angle and ALD blocking efficiency[65]. A sample made by dilute solution of a ODTS precursor in a toluene solvent at room temperature with the liquid phase method displayed the same properties as another made by the vapor

method carried out in the absence of solvent at significantly higher substrate and gas temperatures, 170 °C[57].

In this dissertation, the bulk solution deposition method is utilized for SAMs formation on silicon (100) and other related semiconductor substrates.

3.2 UV/Ozone treatment

3.2.1 Introduction

With microelectronic manufacturing technology developing in recent decades, conventional surface cleaning methods cannot meet the industrial requirement. Hence, several new cleaning methods have been developed. There are two main types of cleaning techniques used currently: dry and wet. Wet cleaning usually refers to processes involving hydrofluoric acid solutions. Dry cleaning includes (1) plasma cleaning; (2) laser and X-ray cleaning, via thermal action; (3) ion milling cleaning, via surface etching; and (4) ultraviolet (UV)/ozone treatments.

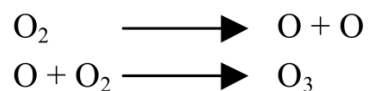
In general, contaminants are classified into two types: organic and inorganic. Organic contaminants include vacuum-pump oil, machine oil, human sebum, and carbon thin films formed by vacuum deposition.

The ability of ultraviolet light to decompose organic molecules has been known for a long time. However, it is only during past decades that people have started to explore UV cleaning of solid surfaces. The light absorbed can only be effective in producing

photochemical changes, so the wavelengths emitted by the UV sources are a very important variable parameter in this process.

3.2.2 Mechanism

The mechanism of UV/ozone cleaning is presented below (and also in Figure 3.4 Figure 10). Usually, low-pressure mercury UV light tubes generate light at two main wavelengths, 184.9 and 253.7 nm [66]. The 184.9nm wavelength is important because oxygen adsorbs this UV light to produce single oxygen atoms, and those recombine with oxygen molecules to form ozone (O₃).



253.7 nm UV light irradiated on ozone lead it to decompose. Atomic oxygen, formed during the formation and decomposition of ozone, is a strong oxidant. If organic contaminants are also irradiated by ultraviolet, that causes photolysis and generates by product in the forms of ions, free radicals, excited molecules, or neutral molecules.

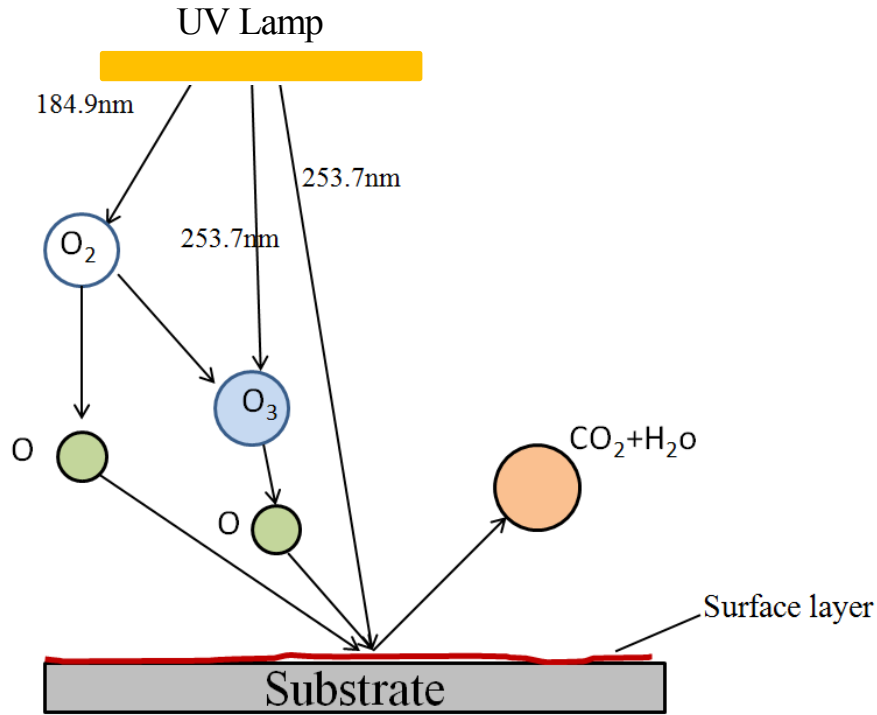


FIGURE 3.4 Schematic for the UV/ozone treatments on solid surfaces.

3.2.3 Application of UV/ozone cleaning

In the manufacturing of crystal oscillators, UV/ozone cleaning is popular as a way to remove the surface contamination that affects the performance of the oscillators. The adsorption and desorption of monolayer contamination on surfaces cause an increase in frequency; therefore, contaminants at one or less than monolayer need to be removed. And UV/ozone cleaning satisfies this requirement.

UV/ozone has also been employed to clean oxide metal films of metals such as Zr, Hf and Al. Metal oxides such as zirconia and hafnia are being investigated as new materials for applications as gate dielectrics in future complementary metal-oxide-semiconductor devices. In this research, it has been found that the oxidation kinetics of the metals increases significantly in the presence of UV light[67].

In addition, cleaning has high effectiveness in removing organic contaminations from gold surfaces. It can significantly decrease the temperature dependency of thermo-compression wire bonding. Therefore, this cleaning method is used in improving the reliability of wire bonding at low temperatures. UV/ozone cleaning may also be used in surface treatments prior to coating, plating or vaporization, in the modification of polymer surfaces, and in the peeling and etching of photoresist thin films.

3.3 Selective ALD Processes

In this chapter, a new selective ALD approach is introduced to pattern silicon surfaces for thin film deposition [68]. This method combines an initial surface passivation step by silylation of the substrate surface with UV/ozonolysis for the selective removal of the silane agent. Both silylation and UV/ozonolysis are individually well known processes. Silylation is used for surface passivation or activation [69-72], the addition of hydrophobicity or hydrophilicity [73, 74], or in general for surface derivatization [75, 76]. UV/ozonolysis is used for activation of organic layers [77, 78], surface cleaning [79-82], CVD or ALD precursors [83-85] and surface oxidation[86]. However, to the best of our knowledge, the combination of the two steps in the way described here for selective ALD has not been discussed in past literature.

Our selective ALD procedure consists of three steps, as shown in Figure 3.5. The first is the introduction of hydrophobicity to oxide-terminated silicon substrates to block all hydroxide surface groups by silylation. These hydroxide surface groups are believed to

provide reaction sites for most ALD processes [87-89]. The second step is the spatially resolved removal of the silylation agent selectively by a combination of UV radiation and ozonolysis. This step is designed to re-expose the hydroxide surface groups. The final step is an ALD process to build up the desirable thin films, with spatial resolution given by the differential in reactivity between the silylated and UV/ozone-reactivated areas of the surface. The main parameters to tune and optimize this procedure are identified below, and the effectiveness of our protocol is evaluated for the selective thin film growth by ALD.

Selective ALD via Silylation + UV/Ozonolysis

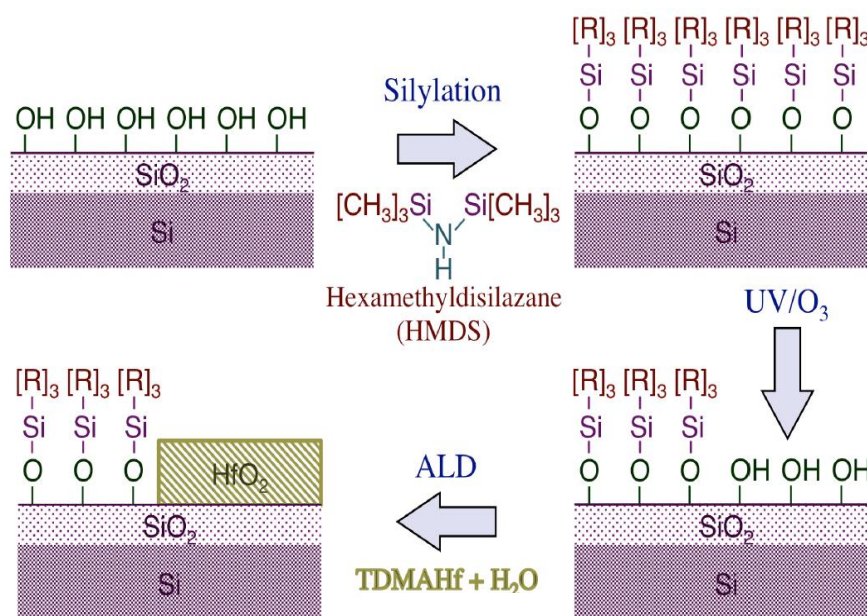


FIGURE 3.5 Selective atomic layer deposition (ALD) scheme developed in this chapter. The Si (100) substrate is first silylated with hydrophobic silanes to block all surface OH functional groups. The following step is the selective removal of the resulting organic layer using a combination of UV radiation and ozonolysis. Subsequent ALD occurs preferentially at the surfaces treated with the UV-ozonolysis procedure. (This figure is reproduced with permission from Ref. 68, Copyright 2014, Nanotechnology, IOPscience)

3.4 Experimental details

3.4.1 Sample preparation

The Si(100) wafers (Si-Tech) were cut into 1 x 1 cm² pieces and treated following a RCA cleaning before silylation.

RCA cleaning[90] involves the following steps:

- (1) Nanostripper (NS) treatment with a mixture of sulfuric acid (H₂SO₄) (EMD Milipore, 98%): hydrogen peroxide (H₂O₂) (Fisher Scientific, Certified ACS, 30% in water) = 3:1 (by volume) solution for 10 min (or 1 min in some of the experiments in Figure x), followed by washing with Milli-Q water for 15 mins;
- (2) Oxide removal with a mixture of hydrofluoric acid (EMD Milipore, 48% in water) (HF):H₂O = 1:20 solution (by volume) for 1 min, followed by washing with water for 5 mins;
- (3) Special cleaning 1 (SC1) treatment with a mixture made out of 20 ml Milli-Q water, 5 ml H₂O₂, and 5 ml 30 wt% NaOH solution, T = 80 °C, 10 min; followed by washing with water for 5 mins;
- (4) Special cleaning 2 (SC2) treatment with a mixture made out of 20 ml Milli-Q water, 5 ml H₂O₂, and 5 ml 12% HCl solution (Fisher Scientific, 37w/w% in water), T = 80 °C, 10 min; followed by washing with water for 5 mins;
- (5) Rinsing with Milli-Q water and drying in N₂ flow.

Then, the Si(100) samples were soaked in different silylation solutions with different silylation conditions, as listed below:

- (1) Hexamethyldisilazane (HMDS, Sigma-Aldrich, 99.9% purity) silylation: immersion in pure HMDS, dry N₂ environment, T = 112 °C, 24 hours;
- (2) Trichloro(octadecyl)silane (ODTS, Sigma-Aldrich, ≥90%) silylation: immersion in 10 mM ODTS solution in toluene (Macron Chemicals, HPLC grade, 99.5%), dry N₂ environment, room temperature, 48 hours;
- (3) Trimethylchlorosilane (TMCS, Aldrich-Sigma, ≥99%) silylation: immersion in 5 vol% TMCS solution in toluene, dry N₂ environment, room temperature, 24 hours.

After silylation, Si samples were taken out and rinsed with toluene and acetone (Sigma-Aldrich, 99.5%) separately and dry with N₂ flow.

UV/ozonolysis: This step was designed to make a half-half pattern of the silane on the Si surface. The instrument used for the UV radiation was a Spectrolinker XL-1500 UV crosslinker equipped with both its original λ (wavelength) = 254 nm lamp and an additional λ = 185 nm source. The UV power was set to 10,000 $\mu\text{W}/\text{cm}^2$, and UV/O₃ exposures of 900s and 1500 s were used for HMDS and ODTS silylated samples, respectively. A homemade Al mold was used to cover half of the the Si wafers in order to directly compare the behavior of samples exposed to ozone alone versus ozone plus UV radiation. Figure 3.6 shows the details of the Al mold and how the silylated Si wafers were made into pattern with the Al mold. The grey rectangular block in that diagram stands for the Al mold and the black one for the Si wafers. The wafer thickness was 0.55 mm, and the height of the inside mold was 0.56 mm. This means that our mold was placed close to the wafer surface without touching it. The UV radiation was blocked

by this mold; however the ozone produced could still disperse into the space between the mold and the covered substrate wafer.

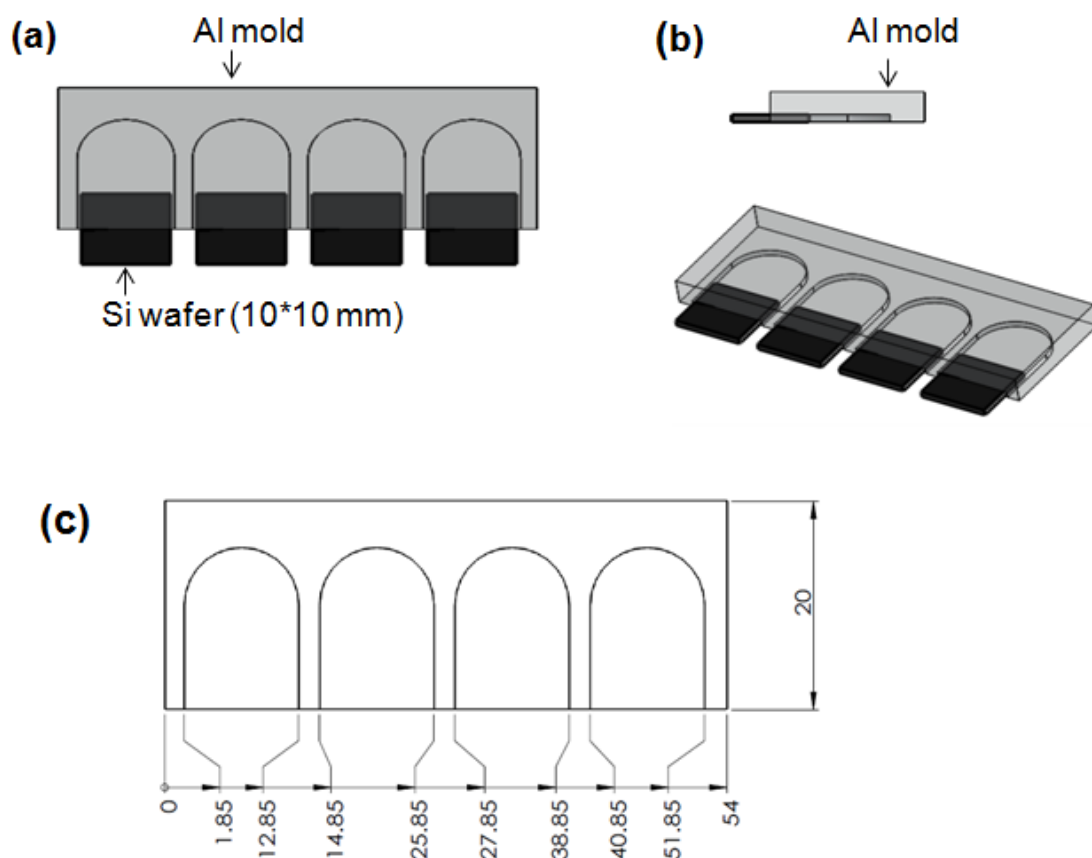


FIGURE 3.6 Al mold used in the UV/ozonolysis procedure for patterning the substrate surfaces. (a) is the vertical view of the UV/ozonolysis arrangement. The silane-covered Si wafer was half inserted underneath the Al mold, which means that half of the silane-covered Si wafer was exposed in UV radiation while the other was protected by the Al mold. (b) Side view. (c) Technical drawing of the Al mold. All the sizes reported here are in mm.

HfO₂ ALD: Atomic layer depositions (ALD) of HfO₂ thin films were carried out by using a commercial Savannah, Ultratech/Cambridge Nanotech instrument. The ALD

cycles were set for sequential exposures to the TDMAHf (TDMAHf, $[(\text{CH}_3)_2\text{N}]_4\text{Hf}$, Sigma-Aldrich, 99%) and water precursors, with dry N_2 purging in between. The time sequence of the exposure to the TDMAHf precursor and nitrogen gas purging is: TDMAHf/ N_2 / H_2O / N_2 =0.25s/25s/0.025s/25s. The chamber temperature was set to 110 ° and 250 ° C. The TDMAHf precursor was kept at 75 °C and delivered using a bubbler (the gas lines were kept at 115 °C to avoid condensation), and N_2 was used as a continuous carrier gas, at a rate of 20 sccm. The sample was loaded in the center of the chamber.

3.4.2 Characterization

ATR-IR Absorption Spectroscopy: Attenuated total reflection (ATR) infrared absorption spectra were acquired by using a Tensor 27 Bruker FTIR spectrometer with a deuterated triglycine sulfate (DTGS) detector and a commercial Harrick Scientific horizontal reflection Ge attenuated total reflection semispherical accessory (GATR, 65 ° incidence angle). All spectra were taken by averaging 1024 scans taken at 4 cm^{-1} . The spectra of the treated Si(100) samples were reference to similar spectra obtained for the clean, non-derivatized, Si(100) surface.

Water Contact Angles: A Kruss Easy Drop instrument was used to measure the contact angle of the water droplets on the top of the surface of the samples. Contact angles were calculated with an accuracy of 0.1 ° by the instrument's software. However, an overall measurement error of ± 3 ° was estimated by averaging six to twelve measurements with

different samples. These samples were prepared from the starting Si(100) wafers to include any errors introduced in the preparation procedure.

XPS: X-ray photoelectron spectroscopy (XPS) was used to monitor the deposition of HfO₂. A Kratos analytical AXIS instrument was used, equipped with a 165-mm mean radius semihemispherical electron energy analyzer and a 120-element delay line detector. A monochromatized Al-anode X-ray gun was used as the excitation source. An electron flood source was used as needed to compensate for sample charging. The Hf 4f and Si 2p data were acquired using spectrometer constant pass energy of 20 eV, 0.1 eV energy steps, and a 200 ms dwell time. Film thicknesses were estimated by using a homogeneous layer model and exponential signal decay versus film thickness, using reported electron inelastic mean free paths.

AFM: Surface roughness was estimated by using atomic force microscopy (AFM). A Nanoscope IIIa Digital Instrument was employed for the measurement. The measurement was carried out in tapping mode, using n-type silicon tips. Scanning was carried out at a rate of 1 Hz, typically over an area of 5 x 5 μm² but also over smaller 1 x 1 μm² when higher magnification was required. Surface roughness was estimated by calculating the root-mean-square (RMS) variation in height over the entire area scanned.

Ellipsometry: Film thicknesses were also estimated by using a commercial Horiba Jobin Yvon Uvisel M200 instrument equipped with a 75 W Xenon lamp, with a 120 - 2200 nm spectral range.

SEM: Scanning electron microscopy (SEM) was employed to carry out further surface characterization. A Nova NanoSEM450 instrument with an in-lens SE/BSE detector (TLD) was used. The measurement was operated at electron energy of 5 kV. Atomic composition was determined by using an integrated energy dispersive X-ray microanalysis (EDX) system from Oxford Instruments, which was attached to the SEM chamber.

3.5 Results and discussion

Infrared absorption spectroscopy was employed to follow the evolution of the surface of the Si(100) wafers after the silylation and O₃/UV ozonolysis steps. Figure 3.7 shows key ATR-IR traces. They were obtained after each of those steps for the case of surface derivatization using HMDS. After the HMDS treatment, silylation becomes evident by the development of a peak at 1257 cm⁻¹. This is due to the symmetric deformation of the methyl group in the newly formed Si-CH₃ surface species (blue trace, second from bottom).⁵⁹ This feature is obviously identifiable by its clear broadening and shift upon silylation, though it does overlap with the SiO₂ LO mode at 1251 cm⁻¹.^[91] In addition, the reaction of the HMDS with the surface is indicated by the disappearance of the peaks at 945 and 1184 cm⁻¹, due to the

symmetric Si–N–Si stretching and N–H deformation modes of that molecule, respectively.^{59,61} The former feature is replaced by a broad peak at 1120 cm^{-1} , which is associated with the Si–O–CH₃ moiety.

The methyl groups in the silylated surface layer remain intact upon exposure to ozone, in the half covered with the Al, as the IR trace for the sample exposed to O₃ but not to UV radiation (purple, second from top) is quite similar to that recorded for the surface before treatment. The main features there, namely, the broad feature at 1120 cm^{-1} from the Si–O–CH₃ moiety and the two 1251 and 1257 cm^{-1} peaks from the SiO₂ LO and CH₃ deformation modes, respectively, remain the same. On the other hand, the spectrum from the sample treated with both O₃ and UV radiation (red, top trace) only retains the sharp peak from the SiO₂ substrate at 1251 cm^{-1} ; the features at 1257 and 1120 cm^{-1} associated with the surface methyl groups are no longer visible. All of these observations indicate that the organic matter has been removed from the surface.

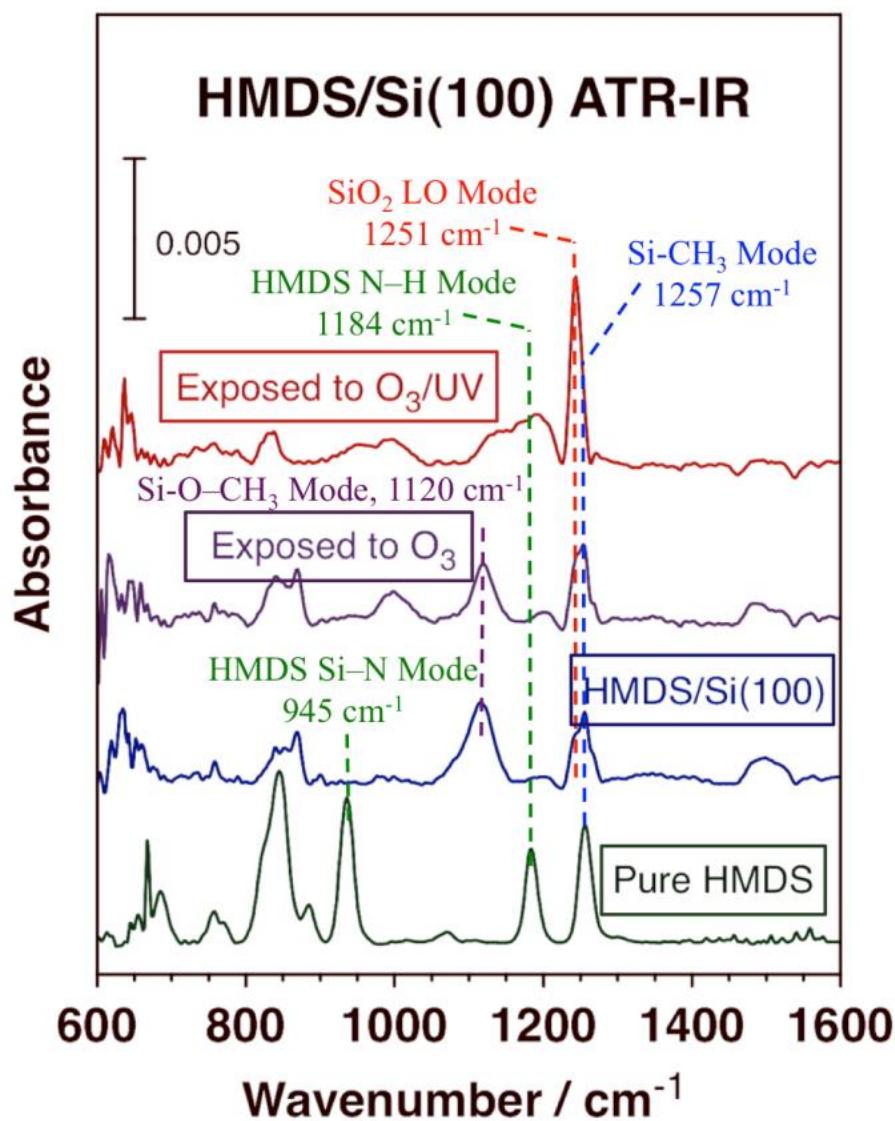


FIGURE 3.7 Attenuated total reflection infrared absorption (ATR-IR) spectra from Si(100) surfaces first silylated with hexamethyldisilazane (HMDS) and then treated with a combination of ozonolysis and UV radiation. The traces correspond to, from bottom to top: pure HMDS (green), provided for reference; the Si(100) surface right after HMDS silylation (blue); the half of the silylated surface exposed to ozone only, by keeping it covered during UV radiation (purple); and the half exposed to both UV radiation and O₃ (red). Silylation is evident by the peaks associated with methyl groups that develop at 1120 and 1257 cm⁻¹. Those are removed by the UV/O₃ treatment, but not by O₃ alone. (This figure is reproduced with permission from Ref. 68, Copyright 2014, Nanotechnology, IOPscience)

Silylation of silica surfaces blocks the -OH groups on their surface, and therefore makes them hydrophobic.[73-75] The contact angle measurement data show the progress of the hydrophobicity of Si(100) samples after each step of our cleaning and silylation treatments. Table 3.1 shows typical results, for HMDS and averaged over several measurements. The original, untreated, Si(100) surface exhibits intermediate hydrophobicity and mid values in terms of water contact angles (approximately 37°). Cleaning of the surface following a RCA procedure increases its hydrophilicity significantly, at which point the water contact angle decreases to ~12°. Silylation afterwards converts this hydrophilic substrate into a hydrophobic surface: after silylation with HMDS and ODTS, the water contact angles were measured to be ~91° and ~110°, respectively.⁶⁴ At last, an HF solution was used to treat the HMDS-silylated surface, after which the contact angle was reduced to a new value of ~76°. Given that this is the same value obtained upon direct HF treatment of the original Si(100) wafer (75°)[92], it is likely that the HF treatment strips the silylation layer from the surface and creates a new hydrogen-terminated silicon substrate. All these results are consistent with previous literature reports. [93, 94]

| Sample | Contact angle/° ($\pm 3^\circ$) |
|------------------------------|-----------------------------------|
| Si(100), As Is | 38 |
| Si(100), SC1 + SC2 | 13 |
| Si(100), SC1 + SC2, HMDS | 91 |
| Si(100), SC1 + SC2, HMDS, HF | 76 |
| Si(100), HF | 75 |

Table 3.1 Data from water contact angle measurements on the Si(100) surface after different cleaning and silylation steps. High values reflect the hydrophobic character of the surface, low values its hydrophilicity. After standard SC1 and SC2 RCA cleaning, the native SiO₂ layer exhibits high hydrophilicity due to the presence of hydroxo groups on the surface. However, those are blocked by methyl moieties upon silylation with HMDS, at which point the surface becomes hydrophobic. Treatment with HF removes both silylation and SiO₂ layers, and produces a hydrophobic hydrogen terminated surface. (This table is reproduced with permission from Ref. 68, Copyright 2014, Nanotechnology, IOPscience)

UV/ozonolysis treatments can restore the hydrophilicity of the silylated Si(100) wafers by removal of the organic surface layers. Figure 3.8 shows examples of the changes in contact angles induced by such treatment for HMDS- (left) and ODTS- (right) treated Si(100) surfaces as a function of time. Each picture shows two water droplets, one on the right half where the surface was exposed to the full UV/O₃ treatment, and a second on the left where the UV radiation was blocked by the Al mold and the surface only exposed to ozone. These images offer clear visual evidence for the need to add UV radiation to the ozonolysis treatment to modify the surface and regain the original hydrophilicity. It took approximately half an hour to reach full restoration of the hydrophilicity of the clean surface took under the conditions used in our experiments.

Contact Angle Measurements Versus UV/O₃ Treatment Time

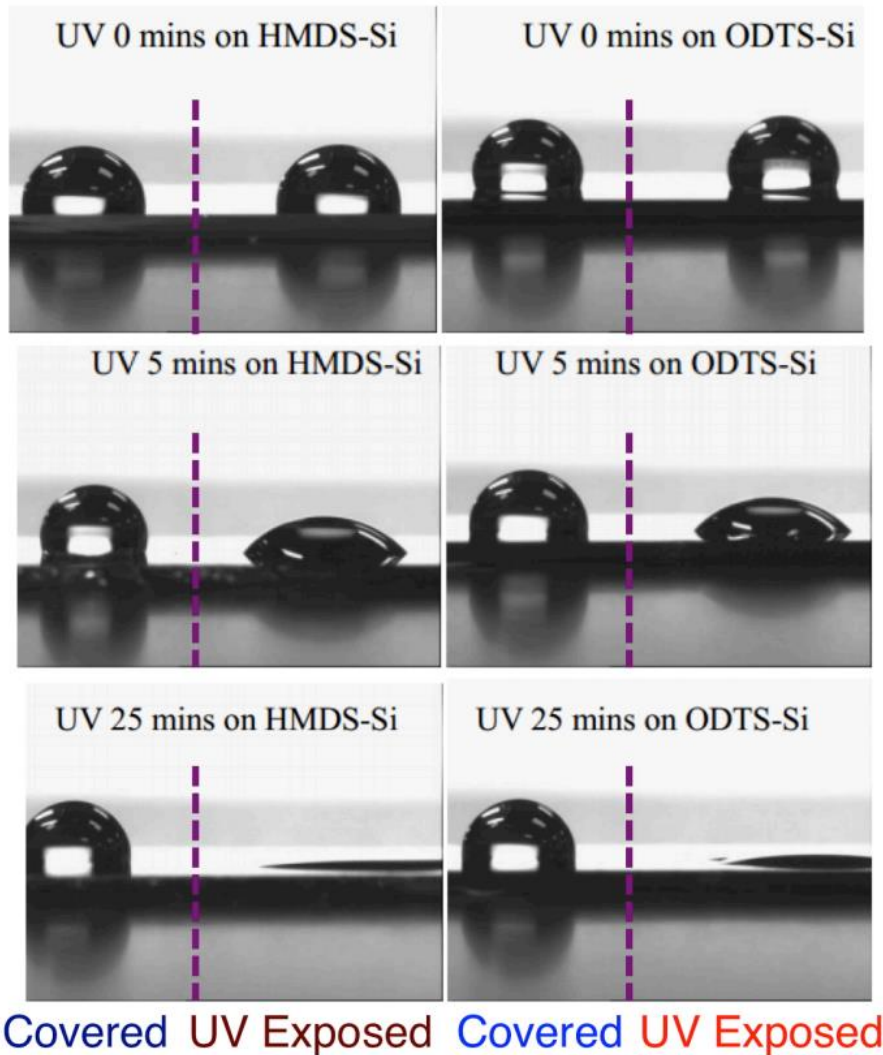


FIGURE 3.8 Pictures of water droplets on Si(100) surfaces silylated with either HMDS (left) or trichloro(octadecyl)silane (ODTS, right) as a function of time of exposure to our UV/O₃ treatment. The left half of these surfaces was covered to prevent direct exposure to the UV radiation. It can be seen that the initial silylated surfaces are quite hydrophobic, and also that their silylation layer can be removed in approximately 1/2 hour by treatment with a combination of UV and O₃ (but not by O₃ alone), a process that returns the hydrophilicity of the SiO₂ native film. (This figure is reproduced with permission from Ref. 68, Copyright 2014, Nanotechnology, IOPscience)

Figure 3.9 summarizes the kinetics of these procedures in the form of plots of contact angles versus time for surfaces exposed to either O₃ alone or UV/O₃ combinations. Data are provided for the untreated Si(100) surface as well as for surfaces silylated with HMDS, ODTS, and TMCS. Small differences are seen among the different silylation agents in terms of the initial contact angles and the rate at which the silylation layers are removed, but the general trends are similar in all cases. The ODTS does provide the best option (among the silylation agents tested here) for high initial hydrophobicity and higher resistance to the UV/O₃ treatment, but the differences with HMDS are not large. A more extensive study of the effect of the nature of the silylation compound as deactivating agent for ALD has been reported in the literature already;^[57] the important extension to the previously available data provided here is the behavior of those layer upon O₃ and UV/O₃ treatments.

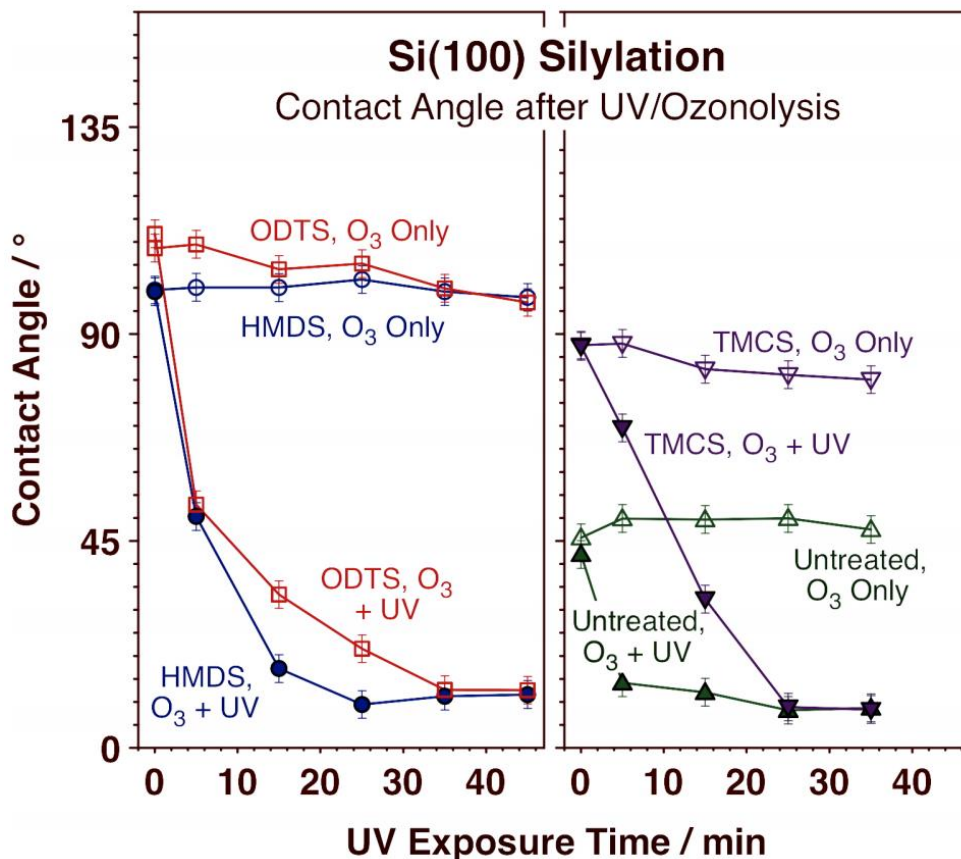


FIGURE 3.9 Summary of contact angle data obtained as a function of UV/O₃ exposure time for the original Si(100) substrate (right panel) and for Si(100) surfaces silylated with TMCS (trimethylchlorosilane, also right panel) and with HMDS and ODTS (left panel). Two sets of data are shown in each case, for surfaces exposed to O₃ alone and to the UV/O₃ combination, respectively. The trends observed are qualitatively similar with all the silylation agents tested in this work: the initial high hydrophobicity of the silylated surface, manifested by contact angles around 90 - 110°, is removed after ~ 30 min of UV/O₃ treatment, at which point the surface becomes highly hydrophilic (contact angles ~ 10 - 15°). In contrast, no changes in behavior were seen on the surfaces where the UV radiation was blocked. (This figure is reproduced with permission from Ref. 68, Copyright 2014, Nanotechnology, IOPscience)

The data in Figures 3.8 and 3.9 clearly indicate that UV radiation is required for our treatment to remove the silylation agent from the Si(100) surface and to increase its hydrophilicity. To assess the role of ozone, additional experiments were carried out. Figure 3.10 shows images of water droplets on HMDS-silylated Si(100) surfaces before

(left) and after (right) exposure to UV radiation of different wavelengths, namely, $\lambda = 254, 185,$ and $254 + 185$ nm. It has been established that of the two, only the $\lambda = 185$ nm produces ozone from activation of atmospheric oxygen. [79, 95] In fact, the $\lambda = 254$ nm not only does not produce ozone, but also decomposes any existing O_3 in the gas phase to produce reactive oxygen atoms. The images in Figure 3.10 show that the short wavelength ($\lambda = 185$ nm) radiation is required to activate the silylated Si(100) surfaces, which means that O_3 is needed for the removal of the organic surface layer. In addition, it was realized that although the process is feasible with $\lambda = 185$ nm alone, it is more efficient with the combination of both UV sources (the surface becomes more hydrophilic, compare the center versus bottom images on the right side of Figure 3.10), and not viable without any direct UV radiation (Figure 3.10). This means that UV radiation is essential for the process to work as well. The most likely scenario is one where the $\lambda = 185$ nm radiation produces gas-phase ozone and the $\lambda = 254$ nm decomposes that ozone to produce the atomic oxygen species that react with the organic layers on the Si(100) surfaces and/or activates those layers directly, as suggested in similar systems in the past.[80, 85, 96, 97] The requirement of direct UV exposure makes the UV/ O_3 treatment amenable to spatial patterning.

Contact Angle Measurements

Effect of Wavelength on UV/O₃

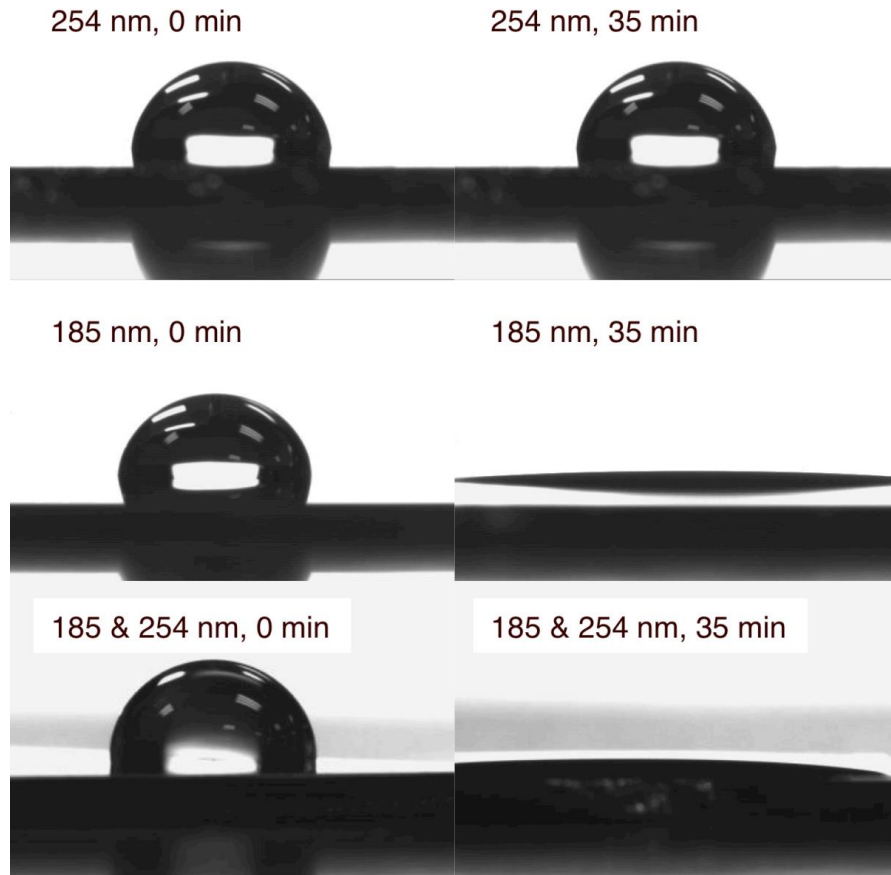


FIGURE 3.10 Pictures of water droplets on Si(100) surfaces silylated with HMDS before (left) and after (right) 35-min UV/O₃ treatments. Images are shown for experiments carried out by using ultraviolet light of different wavelengths, namely, 254 nm (top), 185 nm (center), and a combination of both (bottom). The data indicate that the 185 nm radiation is indispensable for the removal of the silylation layer from the surface, to regain its hydrophilicity, and that the combination of the two wavelengths enhances the removal of the organic layer. (This figure is reproduced with permission from Ref. 68, Copyright 2014, Nanotechnology, IOPscience)

One concern with patterning silicon surfaces by using chemical means is that such treatments can lead to surface etching and/or surface roughening. This is certainly the

case with aggressive treatments involving strong acids or bases. The changes in surface roughness induced by our silylation plus UV/ozonolysis procedure were followed by atomic force microscopy (AFM). Table 3.2 summarizes the key results obtained with ODTS, in the form RMS variations in surface height measured by AFM after each step of the surface treatment. It was found that the original, untreated, Si(100) wafers exhibit an AFM RMS roughness of approximately 1.4 Å, and that nanostripping of that surface (to clean it of spurious adsorbates) does not add much roughness, although the quality of the surface does deteriorate eventually if long exposure times are used (an AFM RMS roughness of ~2.4 Å was measured for surfaces nanostripped for 10 min). On the other hand, silylation of the nanostripped surfaces leads to clear increases in measured AFM RMS roughness: with ODTS, the AFM RMS roughness was seen to change from 1.1 to 5.1 Å on Si(100) surfaces exposed to 1 min of nanostripping, and from 2.4 to 3.7 Å in the case of 10 min nanostripping. However, it is known that silylation only builds up one monolayer of the silylation agent on the surface, and that the apparent increase in roughness is due to either disorder or "softness" within that organic layer; the increase in surface roughness seen here is in fact smaller than what has been reported before.[98] Moreover, the silylated surfaces regain their original degree of smoothness after removal of the organic layer with our UV/O₃ treatment: the 10 min-nanostripped Si(100) surface, which displayed AFM RMS roughness of 2.4 Å before ODTS silylation and 3.7 Å after ODTS silylation, returned to an AFM RMS roughness of 2.7 Å after UV/ozonolysis. We believe that our procedure is sufficiently mild to avoid significant etching of the underlying silicon substrate.

| Sample | Roughness, rms/ Å (± 0.1 Å) |
|--|-------------------------------------|
| Si(100) native | 1.4 |
| Si(100) nanostripper 1 min | 1.1 |
| Si(100) nanostripper 10 min | 2.4 |
| Si(100) nanostripper 1 min ODTS | 5.1 |
| Si(100) nanostripper 10 min ODTS | 3.7 |
| Si(100) nanostripper 10 min ODTS UV-O ₃ 30 min | 2.7 |

Table 3.2 Atomic force microscopy root-mean-square (AFM rms) roughness data from Si(100) surfaces after different cleaning, silylation, and UV/O₃ treatments. Nanostripping (NS) of the surface slowly increases its roughness, but limited exposures can still be used for cleaning without major alterations. The addition of an ODTS layer adds to the roughness, most likely because of the softness and disorder of the hydrocarbon chains, but the initial smoothness is regained upon its removal via a UV/O₃ treatment. (This table is reproduced with permission from Ref.68, Copyright 2014, Nanotechnology, IOPscience)

At last, the chemical selectivity of the silylation + UV/O₃ treated Si(100) surfaces toward ALD of HfO₂ thin films was tested. Figure 3.11 shows the selected Hf 4f XPS data acquired as a function of ALD cycles at 110° C for Si(100) surfaces silylated with HMDS. These surfaces were treated with the UV/O₃ procedure prior to the HfO₂ ALD, with one half covered to prevent its direct exposure to the UV radiation. The traces corresponding to the surface exposed to the UV/O₃ treatment show Hf 4f_{7/2} peaks centered at a binding energy of 17.5 eV, a value typical of HfO₂, and the doublets expected from Hf 4f spin splitting,[99] and their signal intensities grow with increasing number of ALD cycles, indicating Hf deposition. By contrast, no Hf deposition is seen on the covered side of the sample, the one not exposed to UV radiation during ozonolysis. As indicated before, this prevents the silylation layer from been removed

(the half exposed to the UV radiation is cleaned from all organic matter on the surface, and has the native SiO₂ surface re-exposed for reaction). The differences in ALD deposition seen between the two halves of the silicon substrate indicate that the HMDS-based layer is effective in inhibiting the deposition of the HfO₂ layer.

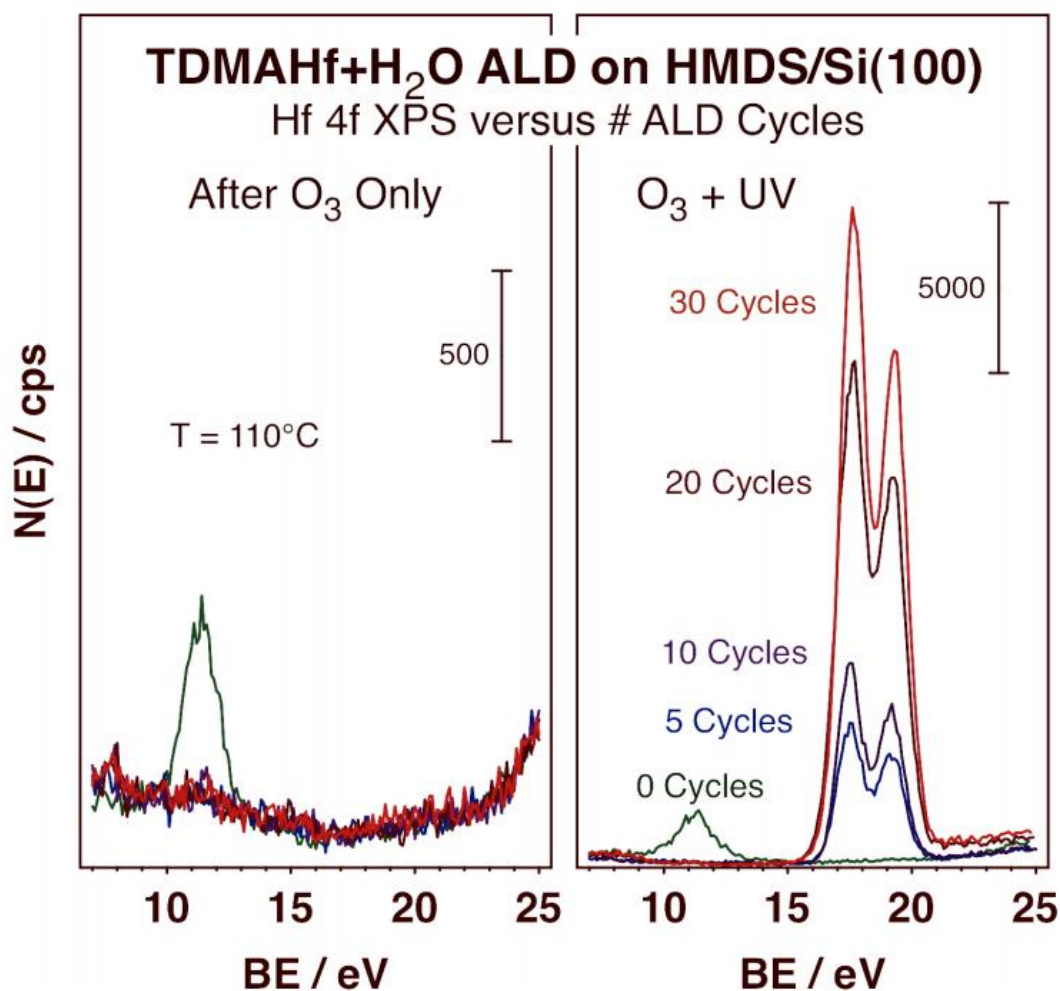


FIGURE 3.11 Hf 4f XPS from HMDS-silylated Si(100) surfaces after the growth of HfO₂ films via TDMAHf + H₂O ALD at 110 °C. Two sets of data are reported, from surfaces treated with O₃ alone (left), and with the UV/O₃ combination (right). The XPS peak positions indicate the formation of fully oxidized HfO₂ films, and the increase in signal intensities with increasing number of ALD cycles for the UV/O₃-treated surface point to the continuous growth of the oxide film. In contrast, no HfO₂ at all is deposited on the silylated surface not directly exposed to the UV radiation during ozonolysis. (This figure is reproduced with permission from Ref.68, Copyright 2014, Nanotechnology, IOPscience)

Figure 3.12 shows the selected Hf 4f XPS data acquired as a function of ALD cycles at 110° C for Si(100) surfaces silylated with ODTS. These surfaces were treated with the UV/O₃ procedure prior to the HfO₂ ALD, with one half covered to prevent its direct exposure to the UV radiation. The traces corresponding to the surface exposed to the UV/O₃ treatment show Hf 4f_{7/2} peaks centered at a binding energy of 17.5 eV, a value typical of HfO₂, and the doublets expected from Hf 4f spin splitting, and their signal intensities grow with increasing number of ALD cycles, indicating Hf deposition. By contrast, no Hf deposition is seen on the covered side of the sample, the one not exposed to UV radiation during ozonolysis. The ALD growth on half-half ODTS/Si(100) stays in agreement with the growth on half-half HMDS/Si(100).

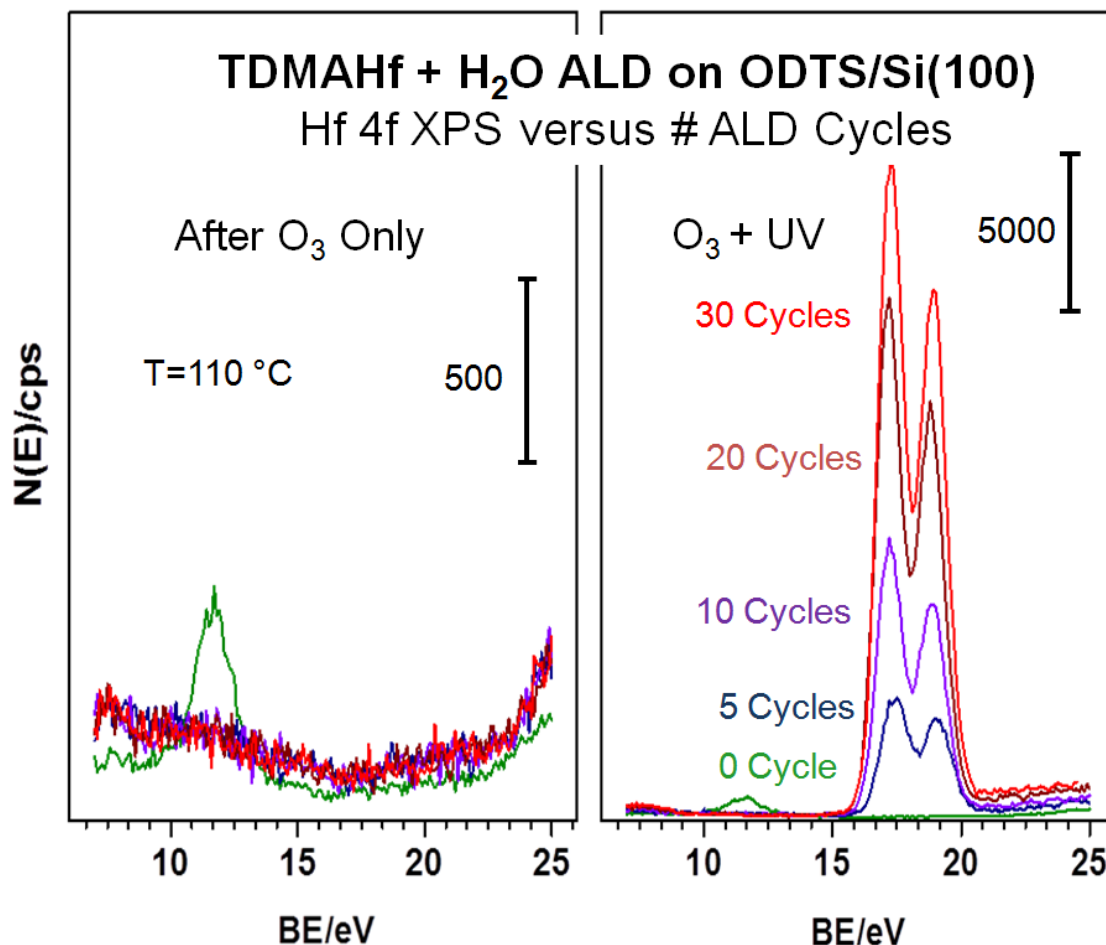


FIGURE 3.12 Hf 4f XPS from ODTs-silylated Si(100) surfaces after the growth of HfO₂ films via TDMAHf + H₂O ALD at 110 °C. Two sets of data are reported, from surfaces treated with O₃ alone (left), and with the UV/O₃ combination (right). The XPS peak positions indicate the formation of fully oxidized HfO₂ films, and the increase in signal intensities with increasing number of ALD cycles for the UV/O₃-treated surface point to the continuous growth of the oxide film. In contrast, no HfO₂ at all is deposited on the silylated surface not directly exposed to the UV radiation during ozonolysis.

The ALD growth rates on Si(100) surfaces silylated with HMDS and then treated with either O₃ alone (covered half) or UV/O₃ (exposed half), were quantified by processing the signal intensities from the Hf 4f and Si 2p XPS spectra. The film

thickness was estimated by assuming layer-by-layer growth and published electron inelastic mean free paths.[99, 100] The same quantitation was done on the Si(100) surfaces treated with ODTS. Figure 3.13 shows the resulting HfO₂ uptake curves for the two ALD temperatures tested, 110 and 250 °C. It is clearly seen that the surfaces cleaned with UV/O₃ display significantly faster rates of HfO₂ deposition than those exposed to O₃ alone, as mentioned above. This is true in both cases, with either HMDS or ODTS as the silylation agent. Indeed, both samples treated with UV/O₃ display comparable film growth rates, approximately 0.5 and 0.8 Å/ALD cycle at 110 and 250 °C, respectively, and the same, within experimental error, as those measured on the original oxide-covered silicon wafer (data not shown). By contrast, the surfaces exposed to O₃ only are totally passivated and show no HfO₂ deposition at all at 110 °C. The fact that ozonolysis alone does not affect the silylation layer was also checked directly by XPS. In particular, the C 1s and O 1s XPS traces recorded for the silylated Si(100) wafers before and after ozonolysis looked the same, within experimental error; no indication of partial oxidation of the organic layer was ever seen in those data (not shown).

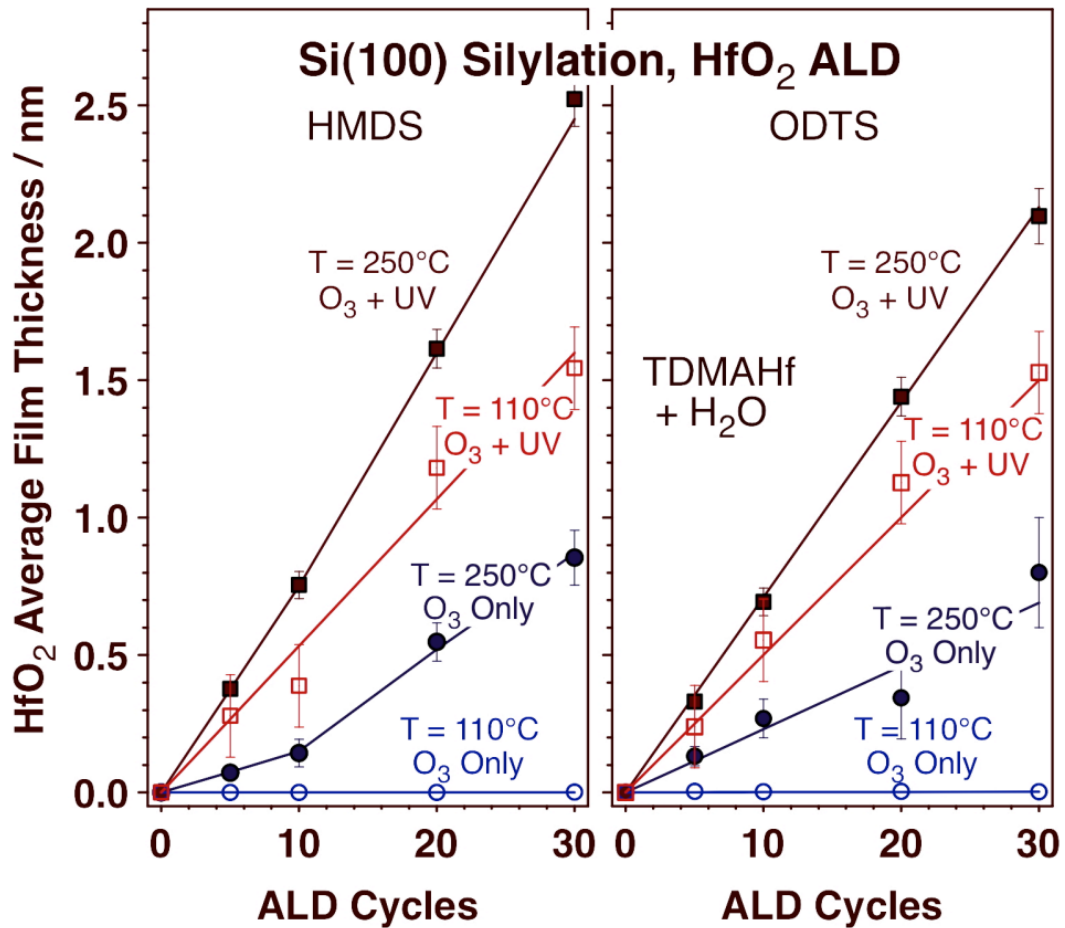
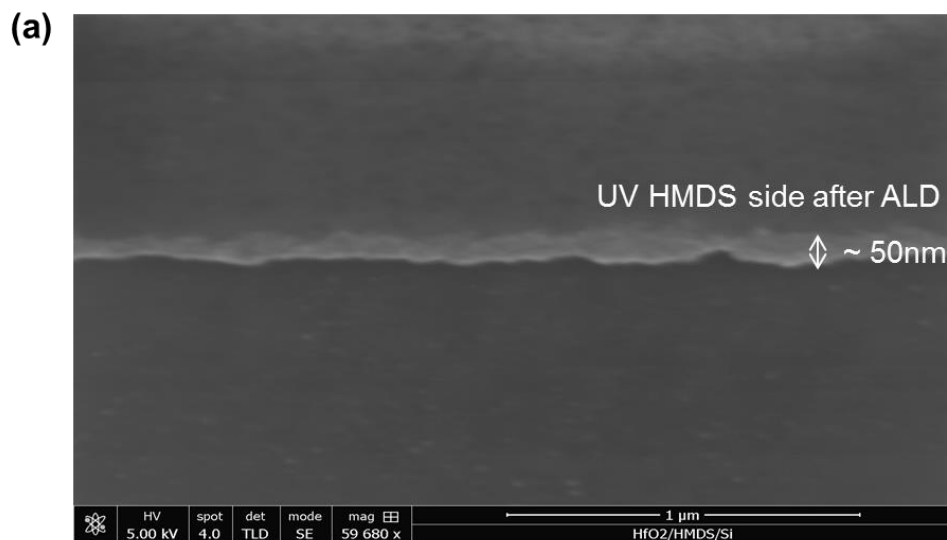


FIGURE 3.13 Average thickness of HfO₂ films grown on Si(100) via ALD as a function of the number of ALD cycles used, estimated from Hf 4f and Si 2p XPS data by assuming layer-by-layer growth and published electron inelastic mean free paths. Two surfaces were tested here, silylated with either HMDS (left panel) or ODTS (right), and two sets of data are shown for each case, for the two half-surfaces exposed to O₃ alone and to the UV/O₃ combination, respectively. In addition, HfO₂ uptakes are reported for ALD experiments carried out at two temperatures, 110 and 250 °C, in each case. Much faster film growth is seen on the surface treated with the full UV/O₃ procedure, and total inhibition is seen with the silylated surfaces for ALD at 110 °C. (This figure is reproduced with permission from Ref.68, Copyright 2014, Nanotechnology, IOPscience)

The boundary between the two areas (UV+O₃ vs. O₃ but no radiation) from a Si(100) surface silylated with HMDS, processed via the UV/O₃ or O₃-alone treatment, and exposed to 100 cycles of HfO₂ ALD, is shown by SEM in Figure 3.14(a). After 100

cycles, a smooth and conformal layer of HfO_2 is seen to have grown on the UV exposed HMDS/Si surface. The HfO_2 layer was around 50 nm thick (after 100 cycles), with a growth rate around 0.5 nm/cycle. This result is in accordance with the growth rate calculated from the XPS data. A EDX line-scan profile performed through the whole surface, as shown in Figure 3.14(b), shows that half surface layer was composed of Hf and O while the other half was not. This result is also consistent with the XPS data shown before.



(b) EDX Linescan (100 ALD cycles HfO₂/HMDS/Si)

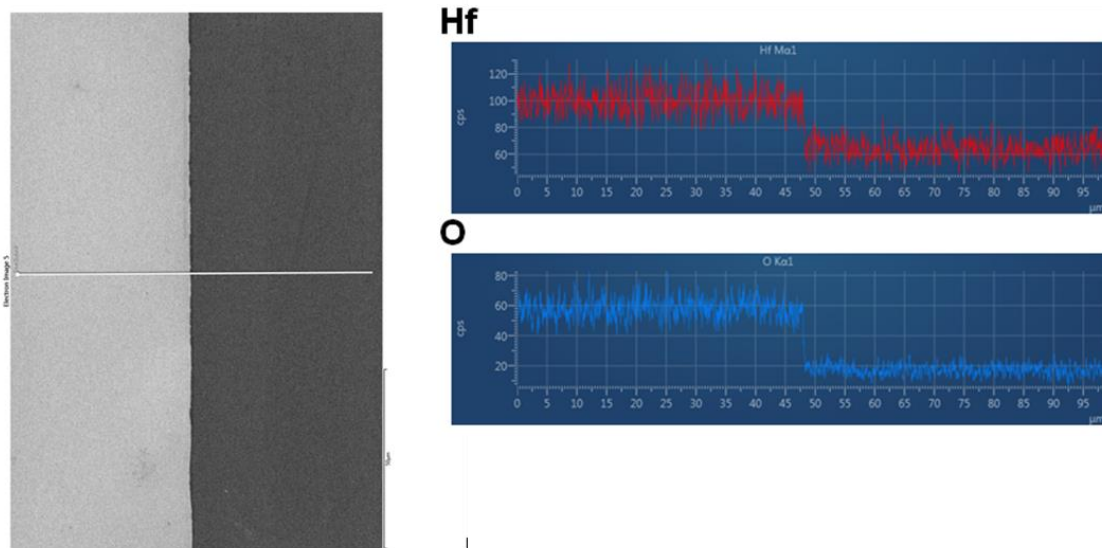


FIGURE 3.14 (a) Scanning electron microscopy image (SEM, top) and (b) energy dispersive X-ray microanalysis data (EDX, bottom) line-scan profile from a Si(100) surface silylated with HMDS, processed using the UV/O₃ treatment, and exposed to 100 cycles of HfO₂ ALD. The boundary between the two areas (UV+O₃ vs. O₃ but no radiation) is evidenced by the SEM image. The pulse sequence used in the ALD in the sample this image was: TDMAHf/N₂/H₂O/N₂=0.25s/25s/0.025s/25s, at 110 °C.

It is interesting to note that there is some HfO_2 deposition on the silylated surface at the ALD temperature of 250 °C. The final HfO_2 layers on the covered side of the wafer after 30 ALD cycles at 250 °C are approximately 8 Å thick on average (as opposed to ~25 Å on the surfaces cleaned by UV/O₃). Also, there seem to be an induction period before deposition starts in the early ALD cycles in those cases. It would appear that the silylation layer is not fully stable at such high ALD temperatures, and may partially decompose and open up nucleation sites for ALD growth. Scanning electron microscopy (SEM) images indicate that this is indeed the case. An example is presented in Figure 3.15, for a HMDS-silylated Si(100) surface first treated with our UV/O₃ procedure and then exposed to 30 HfO_2 ALD cycles. The bottom image, which corresponds to a SEM image of the surface, shows the formation of small (2 - 3 nm) nanoparticles on the surface, whereas the data on the top, from an EDX analysis of the nanoparticles (left) and of the rest of the surface (right), indicate that those nanoparticles are composed of HfO_2 . Only a few dispersed nanoparticles were detected on the surfaces not exposed to the UV radiation. Thick and contiguous HfO_2 films are obtained at both 110 and 250 °C after extensive ALD growth (~30 cycles), after which no signal from the silicon substrate could be detected in the Si 2p XPS data.

HMDS/Si(100) + UV/O₃, 30 cycles TDMAHf+H₂O ALD

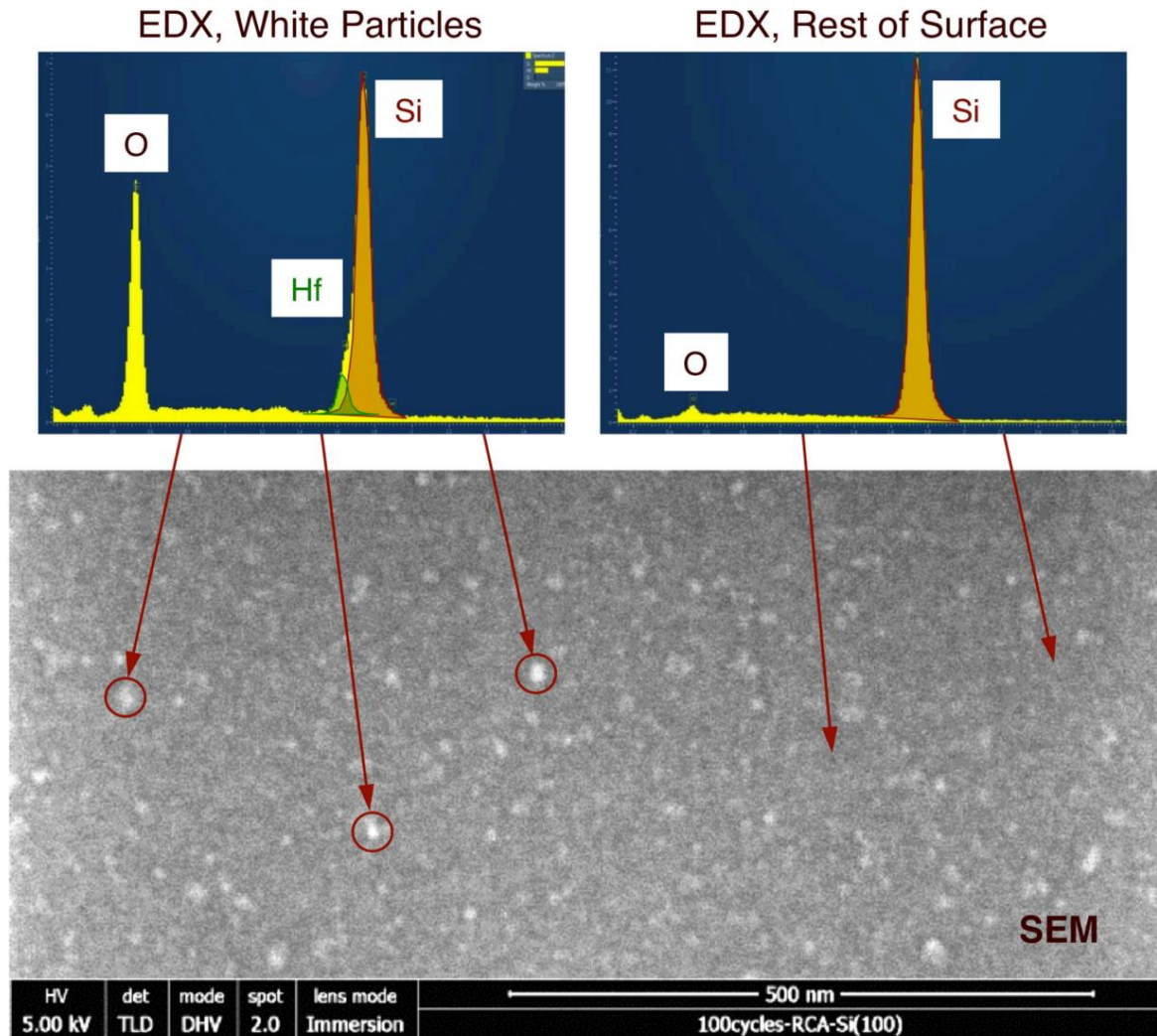


FIGURE 3.15 SEM (bottom) and EDX (top) from a Si(100) surface silylated with HMDS, processed using a UV/O₃ treatment, and exposed to 30 cycles of HfO₂ ALD. The initiation of the ALD process at surface nucleation sites is evidenced by the detection of small HfO₂ nanoparticles, the identity of which were corroborated by the detection of Hf and O in the EDX data on the left image (from the particles) but not on the right panel (from the flat surface). (This figure is reproduced with permission from Ref.68, Copyright 2014, Nanotechnology, IOPscience)

Table 3.3 summarizes additional ellipsometry data in the case of HMDS as the silylation agent. These data are estimates of film thicknesses after each step, namely, after silylation, UV/ozonolysis (or ozonolysis without UV radiation), and 30-cycle HfO₂ ALD. The amplitude and phase difference of the complex reflectance ratio as a function of photon energy were in the range between 1.5 and 4.2 eV. They were fit to a model consisting of SiO₂/HMDS/HfO₂ stacked layers. The resulting data are summarized in Table 3.3. The native SiO₂ layer in the initial Si(100) sample was estimated to be approximately 18.1 ± 0.1 Å in thickness, consistent with Si 2p and O 1s XPS data acquired for the initial substrates (not shown). The organic layer grown upon HMDS silylation was estimated to add another 6.9 ± 0.1 Å. As can be seen in Table 3.3, the side of the silylated sample that was kept covered during the UV/ozonolysis process was not affected by any of the subsequent steps of our treatment, retaining both SiO₂ and HMDS-based layers basically intact, and showing virtually no HfO₂ uptake during the ALD step (a HfO₂ film thickness of 0.1 ± 0.1 Å was calculated in this case). On the other hand, the other half of the HMDS-treated Si(100) substrate, the one exposed to the full UV+O₃ treatment, was fully cleaned of the HMDS based layer, and show a small increase in the thickness of the SiO₂ layer (to a value of 22.0 ± 0.1 Å). ALD on those surfaces resulted in the deposition of a 8.9 ± 0.1 Å thick HfO₂ film after 30 cycles, a value somewhat smaller but in qualitative agreement with the XPS data.

| Thickness in Å ($\pm 0.1\text{Å}$) | Covered, after | | | Exposed to UV/O ₃ , after | | |
|--------------------------------------|----------------|------|-------------------|--------------------------------------|------|-------------------|
| | Layer | HMDS | UV/O ₃ | ALD | HMDS | UV/O ₃ |
| SiO ₂ | 18.1 | 16.8 | 18.2 | 18.1 | 22.0 | 21.0 |
| HMDS | 6.9 | 7.4 | 6.6 | 6.9 | 0.0 | 0.0 |
| HfO ₂ | | | 0.1 | | | 8.9 |

Table 3.3 Average film thicknesses in Å, estimated from ellipsometry measurements, for Si(100) surfaces right after silylation with HMDS, UV/O₃ treatment, and a 20 cycle HfO₂ ALD. Two sets of data are provided, for the halves of the substrate covered and exposed to the UV radiation during UV/ozonolysis, respectively. The raw data were fitted to a model consisting of three flat and smooth layers, reported in the different rows of the table: the underlying SiO₂ substrate, the HMDS-based silylation layer, and the ALD-grown HfO₂. The behavior here qualitatively matches that extracted from the XPS studies. (This figure is adapted with permission from Ref.68, Copyright 2014, Nanotechnology, IOPscience)

The same behavior was observed with the ODTS silylated Si samples, as indicated by the data shown in Table 3.4.

| Thickness in Å $\pm 0.1\text{Å}$ | Covered, after | | | Exposed to UV/O ₃ , after | | |
|----------------------------------|----------------|------|-------------------|--------------------------------------|------|-------------------|
| | Layer | ODTS | UV/O ₃ | ALD | ODTS | UV/O ₃ |
| SiO ₂ | 19.8 | 20.1 | 20.1 | 19.8 | 24.7 | 19.6 |
| ODTS | 20.2 | 19.9 | 19.9 | 20.2 | 0.0 | 0.0 |
| HfO ₂ | | | 0.1 | | | 9.1 |

Table 3.4 Average film thicknesses in Å, estimated from ellipsometry measurements, for Si(100) surfaces right after silylation with ODTS, UV/O₃ treatment, and a 20 cycle HfO₂ ALD. Two sets of data are provided, for the halves of the substrate covered and exposed to the UV radiation during UV/ozonolysis, respectively. The raw data were fitted to a model consisting of three flat and smooth layers, reported in the different rows of the table: the underlying SiO₂ substrate, the ODTS-based silylation layer, and the ALD-grown HfO₂. The behavior here qualitatively matches that extracted from the XPS studies.

Finally, a photomask was used to check if our selective ALD method is useful for more complex patterning. A photomask instead of the Al mold was used during the UV/Ozone step. The photomask was placed above the Si sample in the UV/Ozone instrument. All other experiment parameters were kept the same. In order to see the pattern clearly enough, a thick HfO_2 film was grown in this sample by using 200 ALD cycles. Figure 3.16 shows the SEM image of a Hall bar pattern from the photomask after the 200 cycles of ALD. The length of the side of each of the squares is 200 μm , the width of the wider bar is 20 μm , and the narrow one is 10 μm . The lighter grey area is the place where the HMDS was removed from the Si surface by UV light. The rest, dark grey area was the part protected by photomask, so there was still a HMDS silylated layer on the Si surface which prevented the ALD growth. From the SEM image, the Hall Bar pattern can be repeated, with borders that were very sharp and clear.

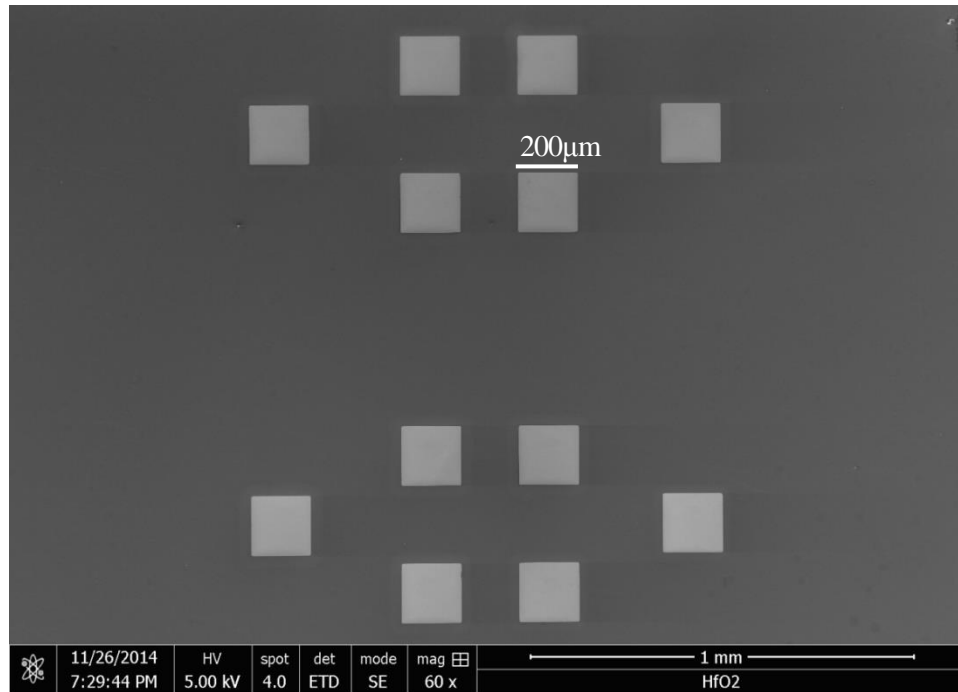


FIGURE 3.16 SEM image from a Si(100) surface silylated with HMDS, processed using our UV/O₃ treatment, and exposed to 200 cycles of HfO₂ ALD.

Two different types of “Hall Bar” patterns were used in the photomask. Figure 3.17 shows a different pattern from the same photomask (the pattern in Figure 3.16 is also from this photomask). The squares are the same size as mentioned in the previous figure, 200 by 200 μm, but there are extra bars connecting each pair of squares. The surface layer composition was further confirmed by EDX. Figure 3.17(c) shows the EDX data taken on the light grey square area, and indicates that this area is composed of Si, Hf and O, confirming that the surface layer is covered with HfO₂. Figure 3.17(d) displays the EDX data taken at the remaining dark grey area, and shows a strong Si peak and decreased oxygen peak intensity because of the absence of HfO₂. Figure 3.18 shows an EDX line-profile across the bar, and indicates that only the bar area is composed of HfO₂ while the rest is composed mostly of silicon (and some oxygen). Both SEM and EDX

data further confirm that our selective ALD process is suitable for high-resolution patterning on Si related substrates.

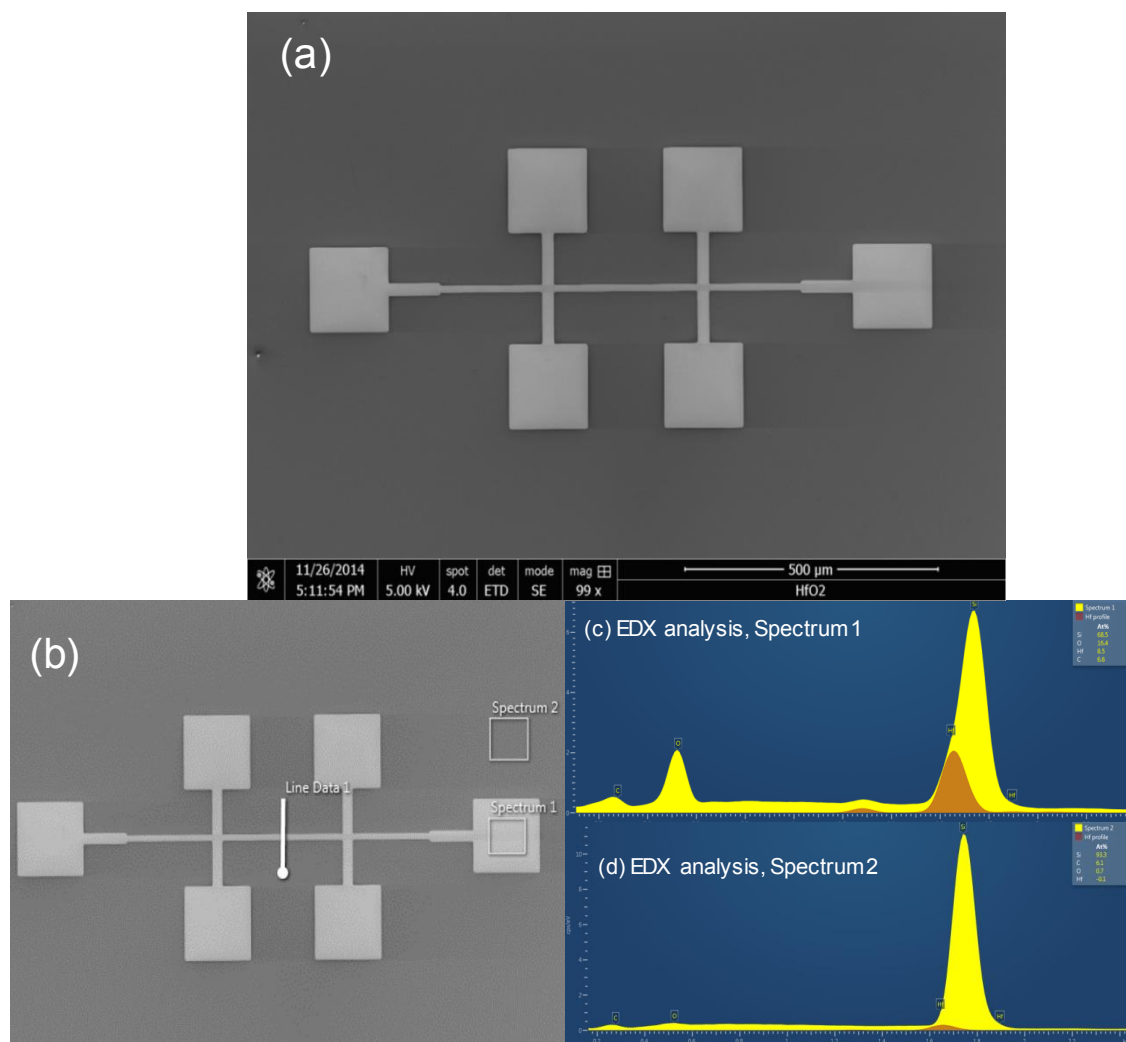
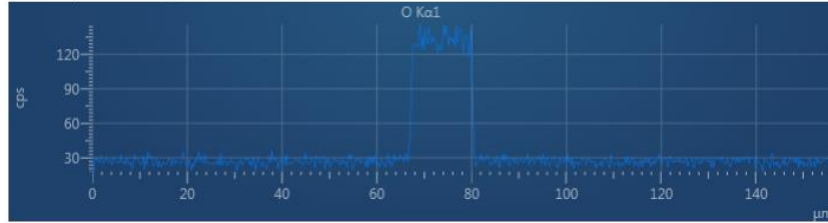


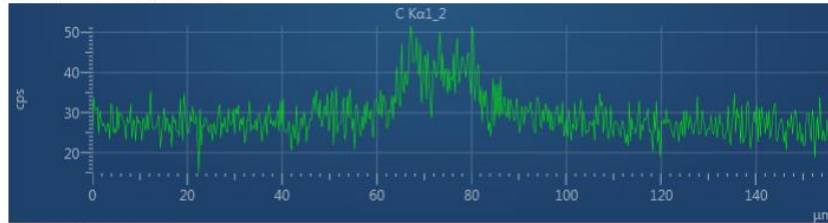
FIGURE 3.17 SEM image (a) and energy dispersive X-ray microanalysis data (b, c and d) from a Si(100) surface silylated with HMDS, patterned using our UV/O₃ treatment and a mask, and exposed to 200 cycles of HfO₂ ALD.

EDX analysis, Line Data 1

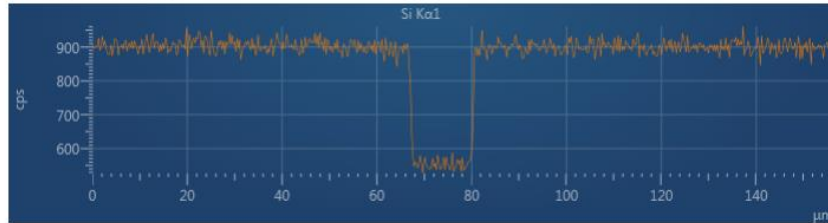
O K α 1 (O Ka1.csv)



C K α 1_2 (C Ka1_2.csv)



Si K α 1 (Si Ka1.csv)



Hf M α 1 (Hf Ma1.csv)

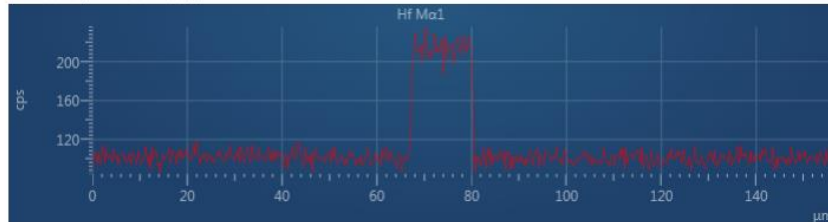


FIGURE 3.18 EDX line-profile from the photomask.

3.6 Conclusions

A simple approach (Figure 3.19) has been developed and tested to modify the chemistry of silicon surfaces. Emphasis has been placed on the surface reactivity toward the metalorganic precursors that are used in the chemical deposition of thin solid films. A thin native silicon oxide film is always present on silicon wafers, normally around 1-2 nm thick, because of their handling under atmospheric environments. Starting from this

substrate, the hydroxo groups on those surfaces are capable of covalently reacting with a number of metalorganic compounds, facilitating their dissociative adsorption and initiating chemically based film deposition processes. These native oxide also increase the hydrophilicity of the Si(100) surface, a property that was evaluated here by measuring the contact angle between the surface and a droplet of water deposited on top.

Our research corroborated known behavior of these surfaces in terms of standard cleaning and surface processing procedures. First, surface hydrophilicity may be enhanced by using reported RCA cleaning steps. RCA cleaning is a treatment that presumably increases the surface concentration of hydroxo moieties. Conversely, hydrophobicity can be introduced by silylation using any of many viable silanes, including HMDS, ODTS, and TMCS, (the ones tested here). Due to the blocking of the OH groups by alkyl fragments, the contact angle increases after silylation, as corroborated in our infrared absorption spectroscopy study with HMDS. The organic layer was next shown to be removable by using a combination of ozonolysis and UV radiation. Both O₃ and 185 nm-wavelength UV radiation were shown to be required for this process. In addition, the combination of 185 and 254 nm radiation was proven to help enhance the removal of the silylation layer. Also, because of the "softness" of the organic layer, the surface roughness was determined to increase somewhat after silylation, but the original smoothness was restored once that layer is removed via UV/ozonolysis.

The UV/O₃ treatment of the silylated Si(100) wafers regains back their original hydrophilicity, and may even produce more hydrophilic surfaces than the original native oxide. This was tested by evaluating the rate of growth of HfO₂ films via atomic layer deposition (ALD) using TDMAHf and water. It was found that the silylated layer does completely block the film growth at lower temperatures, especially in the early cycles of ALD. However, there is still some HfO₂ deposition detected on the silylated side if ALD is carried out at high temperatures, because of the partial decomposition of the silylation layer and the formation of nucleation sites on the surface, as suggested by SEM. Overall, the sequence of silylation and UV/ozonolysis treatments described in this chapter provides an easy way to process silicon surfaces with spatial resolution for the selective deposition of solid films.

It should be said that the initial test used for the effectiveness of our procedure to achieve selective ALD, the growth of HfO₂ films on SiO₂/Si(100) surfaces, may not be a good choice for microelectronic applications. Future work will be directed to test the deposition of metals such as Cu for interconnects, a case for which selectivity in deposition may be simpler to achieve, and of high k dielectrics such as HfO₂ on H-terminated silicon substrates, for which hydrosilylation may be required.

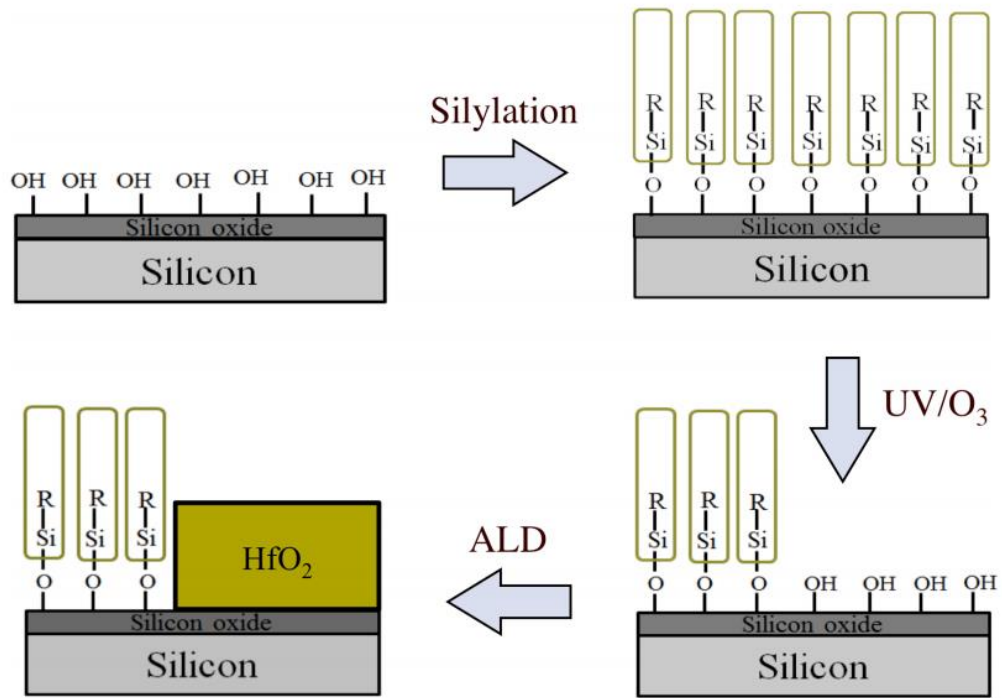


FIGURE 3.19 Schematic of our selective ALD process (This figure is reproduced with permission from Ref.68, Copyright 2014, Nanotechnology, IOPscience)

Selective ALD on IBM wafers by combining silylation and UV/Ozonolysis

4.1 Introduction

The wafers used in the experiments in this chapter were provided by IBM. The motivation for this work regarding the application of our selective ALD process on IBM wafers is to test if our method is effective for industrial applications, for deposition on ultra-low K dielectrics.

The information about the characteristics of the four wafers is listed in Table 4.1.

| Name | Wafer ID | Surface modification | ThK (Å) | RI | GOF | Std (%) |
|-------|--------------|----------------------------------|---------|--------|--------|---------|
| IBM-1 | 46AK6071MMA2 | Blanket Control | 2003 | 1.4193 | 0.9926 | 1.9015 |
| IBM-2 | 46AK6070MMD3 | Chemical Mechanical Polish (CMP) | 1819 | 1.4189 | 0.9922 | 2.9917 |
| IBM-3 | 462A0S8ASEB0 | Blanket Control | 2037 | 1.3796 | 0.9934 | 1.2611 |
| IBM-4 | 462A0S89SED7 | Chemical Mechanical Polish (CMP) | 1697 | 1.385 | 0.9927 | 2.4381 |

Table 4.1 Information on the characteristics of the wafers offered by IBM.

From tests of the four types of wafers by contact angle measurement, it was found that the IBM-1 and IBM-3 samples were hydrophobic, while IBM-2 and IBM-4 were hydrophilic. We had only limited information on the compositions of these four types of wafers, but know that they are representative of the ultralow dielectric constants (ulk) pSiCOH films, composed of Si, C, O, and H atoms, developed by IBM, which are typically prepared by plasma-assisted chemical vapor deposition (PECVD).

4.2 Experiment details

4.2.1 Sample preparation

The IBM wafers (IBM) were cut into $1 \times 1 \text{ cm}^2$ pieces. Then, the IBM 2 and IBM 4 samples were soaked in different silylation solutions. For instance, for hexamethyldisilazane (HMDS, Sigma-Aldrich, 99.9% purity) silylation, the samples were immersed in pure HMDS, in a dry N_2 environment, at $T = 112 \text{ }^\circ\text{C}$ for 24 hours;

UV/Ozonolysis: This is the step to make a half-half pattern of the silane on the Si surface. The instrument used for the UV radiation is a Spectrolinker XL-1500 UV crosslinker equipped with both its original λ (wavelength) = 254 nm lamp and an additional $\lambda = 185 \text{ nm}$. UV power was set to $10,000 \mu\text{W}/\text{cm}^2$, and UV/ O_3 exposures for 1500 s were used for both HMDS and ODTS silylated samples. Since the thickness of the IBM wafer was larger than the Si(100) wafers, another Al mold was made to cover the IBM wafers. The mold was placed close to the wafer surface without touching it, as with the other samples. The UV radiation could be blocked by this mold; however the ozone produced could still disperse into the space between the mold and covered substrate wafer.

HfO₂ ALD: Atomic layer depositions (ALD) of HfO₂ thin films were carried out by using a commercial Savannah, Ultratech/Cambridge Nanotech instrument. The ALD cycles were set for sequential exposures to the TDMAHf (TDMAHf, $[(\text{CH}_3)_2\text{N}]_4\text{Hf}$, Sigma- Aldrich, 99%) and water precursors, with dry N_2 purging in between. The time sequence of the exposure and gas purging used was:

TDMAHf/N₂/H₂O/N₂=0.25s/45s/0.025s/35s. The chamber temperature was set to 110 °C. The TDMAHf precursor was kept at 75 °C and delivered using a bubbler (the gas lines were kept at 115 °C to avoid condensation), and N₂ was used as a continuous carrier gas, at a rate of 20 sccm. The sample was loaded in the center of the chamber.

4.2.2 Characterization

ATR-IR Absorption Spectroscopy: Attenuated total reflection (ATR) infrared absorption spectra were acquired by using a Tensor 27 Bruker FTIR spectrometer with a deuterated triglycine sulfate (DTGS) detector and a commercial Harrick Scientific horizontal reflection Ge attenuated total reflection semispherical accessory (GATR, 65 ° incidence angle). All spectra were taken by averaging 1024 scans taken at 4 cm⁻¹. The spectra of the treated all IBM samples were reference to air background.

Water Contact Angles: A Kruss Easy Drop instrument was used to measure the contact angle of the water droplets on the top of the surface of the samples. The hydrophobicity or hydrophilicity of the surfaces was evaluated using the contact angle data. Contact angles were calculated with an accuracy of 0.1 ° by the instrument's software. However, an overall measurement error of ± 3 ° was estimated by averaging six to twelve measurements with different samples. All samples were prepared starting with the original IBM 1 to 4 wafers to include any errors introduced in the preparation procedures.

AFM: Surface roughness was estimated by using atomic force microscopy (AFM). A Nanoscope IIIa Digital Instrument was employed for these measurements. They were carried out in tapping mode, using n-type silicon tips. Scanning was carried out at a rate of 1.0 Hz, typically over an area of $1 \times 1 \mu\text{m}^2$. Surface roughness was estimated by calculating the root-mean-square (RMS) variation in height over the entire area scanned.

XPS: X-ray photoelectron spectroscopy (XPS) was used to monitor the deposition of HfO_2 . A Kratos analytical AXIS instrument equipped with a 165-mm mean radius semihemispherical electron energy analyzer and a 120-element delay line detector was used. A monochromatized Al-anode X-ray gun was used as the excitation source. An electron flood source was used as needed to compensate for sample charging. The Hf 4f and Si 2p data were acquired using spectrometer constant pass energy of 20 eV, 0.1 eV energy steps, and a 200 ms dwell time. Film thicknesses were estimated by using a homogeneous layer model and exponential signal decay versus film thickness, using reported electron inelastic mean free paths[101].

4.3 Results and data analysis

ATR was used to characterize the four IBM samples, since no information was disclosed by IBM on how the wafers were made or what was the composition of the surface layers of each wafer. IBM 1 was the blanket control of IBM 2, since IBM 2 was obtained from IBM 1 after CMP. The same applies for IBM 3 and 4; IBM 3 is the blanket control of

IBM 4. In our data analysis, IBM 1 and 2 were placed together as one set, and IBM 3 and 4 as the second set.

The ATR results, shown in Figure 4.1, show no difference between each set. The ATR of IBM 1 and 2 look exactly the same. The adsorption peak at $\sim 798\text{cm}^{-1}$ indicates Si-C bonding on the wafer surface, the adsorption peak at $\sim 1029\text{cm}^{-1}$ is assigned to the vibrational stretch of C-C bonds, and the small peak at 1270cm^{-1} indicates the presence of CH_3 groups. There is no big difference between the ATR spectra of the native IBM 1 and 2 samples. Further, comparison of the ATR data from HMDS-silylated IBM 2 with the native IBM 2 indicated no differences. UV/ozonolysis treatment of the IBM 1 sample also lead to no changes. No further information about the nature of these surfaces could be extracted from the ATR traces. ATR data for the native IBM 3 and 4 samples led to a similar lack of insight as with IBM 1 and 2.

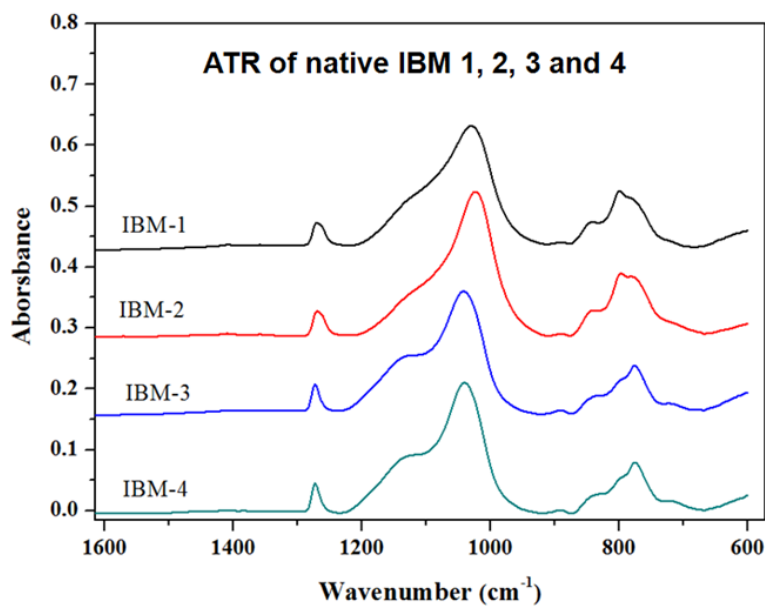


FIGURE 4.1 ATR traces for native IBM 1, 2 3 and 4 wafers

Additional separate studies were done on each set of the four wafers. It was found that the native IBM 1 is hydrophobic, and that silylation of IBM 2 with HMDS makes the surface hydrophobic. UV/Ozonolysis treatments can restore the hydrophilicity of the surface hydrophobic. UV/Ozonolysis treatments can restore the hydrophilicity of the silylated IBM 2 wafers by removal of the organic surface layers. UV/ozonolysis can also remove the surface layer of the native IBM 1 and change its surface to hydrophilic for ALD deposition. Figure 4.2 shows examples of the changes in contact angles induced by such treatment for the native IBM 1 (left) and the HMDS-IBM 2 (right) surfaces as a function of time. Each picture shows two water droplets: one on the right for the surface exposed to the full UV/O₃ treatment, and a second on the left where the UV radiation was blocked by the Al mold and the surface was only exposed to ozone. These images offer clear visual evidence for the need to add UV radiation to the ozonolysis treatment to modify the surface and reach hydrophilicity. It took approximately half an hour to reach full restoration of the hydrophilicity of the clean surface took under the conditions used in our experiments.

Contact Angle Measurements Versus UV/O₃ Treatment Time

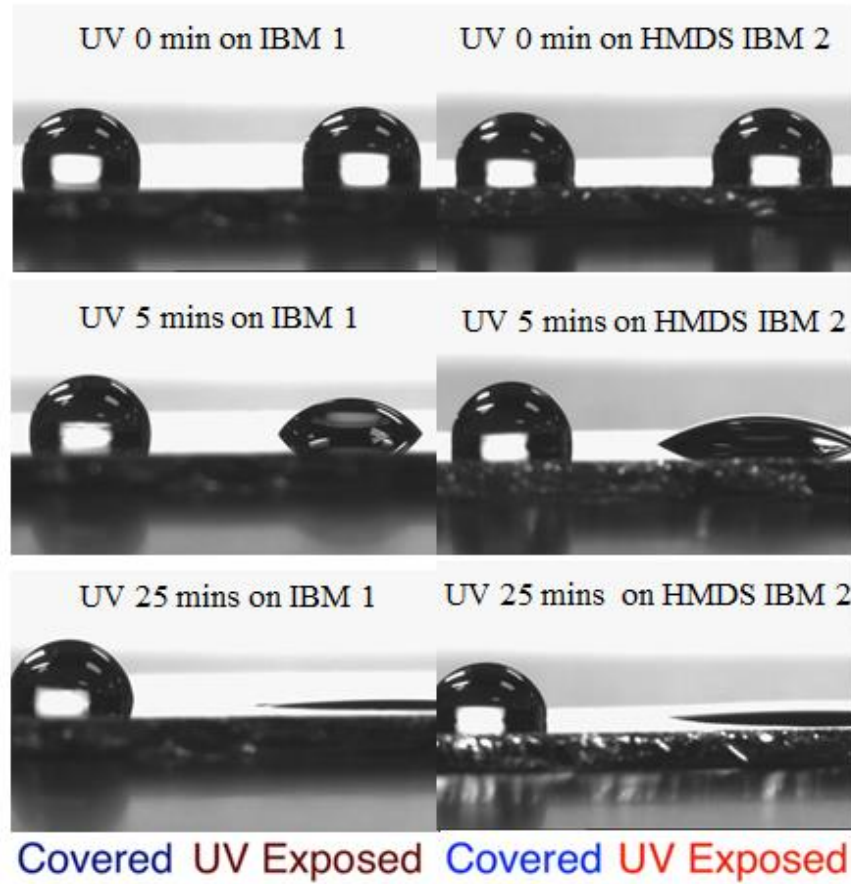


FIGURE 4.2 Pictures of water droplets on the surfaces of the native IBM 1(left) and HMDS silylated IBM 2 (right) wafers as a function of time of exposure to our UV/O₃ treatment. The left half of these surfaces was covered to prevent direct exposure to the UV radiation. It can be seen that the initial silylated surfaces are quite hydrophobic, and also that their native hydrophobic layer or silylation layer can be removed in approximately 1/2 hour by treatment with a combination of UV and O₃ (but not by O₃ alone), a process that induces hydrophilicity in the films.

Figure 4.3 shows the AFM image of the IBM 1 surface before and after UV/Ozone treatment and the native IBM 2 and HMDS/IBM 2 before and after UV/Ozone. Figures 4.3(a) and (d) show the surface image of the native IBM 1 before and after UV/Ozone. There is almost no difference between these two images, even if the contact angles

decreased significantly after 35 minutes of UV/ozone exposure. Figure 4.3(b) shows the AFM image of the native IBM 2 surface, and shows that it is smoother compared to native IBM 1. This is because native IBM 2 is the result of IBM 1 after CMP. After silylating IBM 2 with HMDS, the surface became rougher (Figure 4.3(c)), but after UV/ozonolysis treatment, it turned smooth again. However, the other half of the HMDS/IBM 2 sample, which was covered by the Al mold during UV/ozone exposure, retains the same roughness as before (Figure 3.4(f)). Both the contact angle and AFM figures indicate that our selective ALD method may be used to make clear patterns without sacrificing on substrate surface roughness.

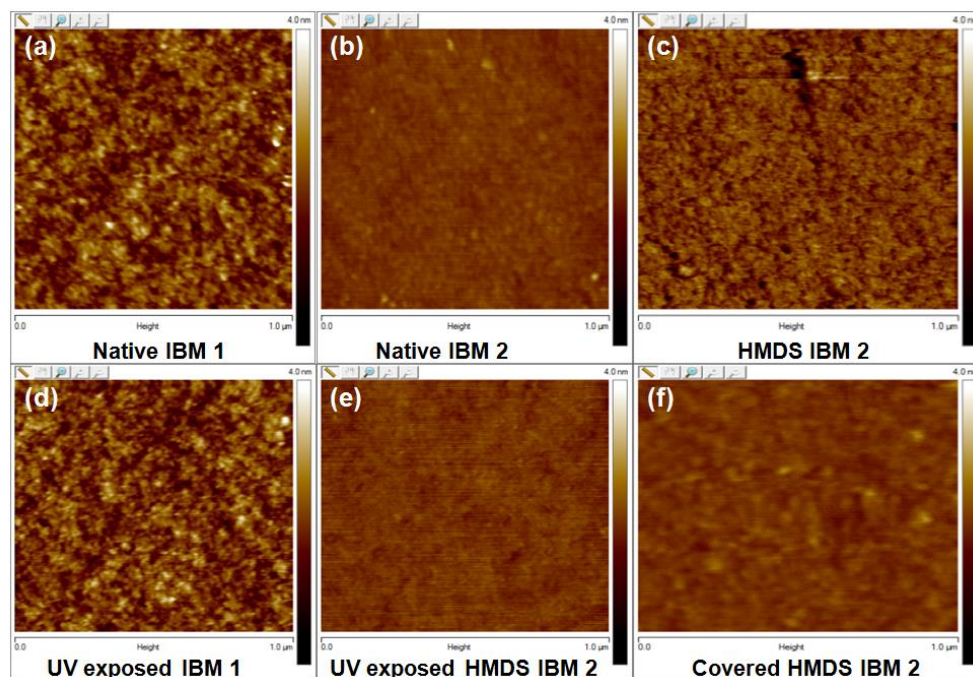


FIGURE 4.3 AFM images from (a) native IBM 1, (b) native IBM 2, (c) HMDS/IBM 2, (d) UV-exposed IBM 1, (e) UV-exposed HMDS/IBM2, (f) Covered HMDS/IBM 2.

Similarly, native IBM 3 is hydrophobic, but silylation of IBM 4 with HMDS makes the surface turns hydrophobic. UV/ozonolysis treatments can restore the hydrophilicity of the silylated IBM 4 wafers by removal of the organic surface layers. UV/ozonolysis can also remove the surface layer of native IBM 3 and make its surface hydrophilic. Figure 4.4 shows examples of the changes in contact angles induced by such treatment for native IBM 3 (left) and HMDS-IBM 4 (right) surfaces as a function of time. Each picture shows two water droplets, one on the right half, exposed to the full UV/O₃ treatment, and the second on the left where the UV radiation was blocked by the Al mold and the surface only exposed to ozone. These images offer clear visual evidence for the need to add UV radiation to the ozonolysis treatment to modify the surface and reach hydrophilicity. It took approximately 35 mins to reach full restoration of the hydrophilicity of the clean surface took under the conditions used in our experiments.

Contact Angle Measurements Versus UV/O₃ Treatment Time

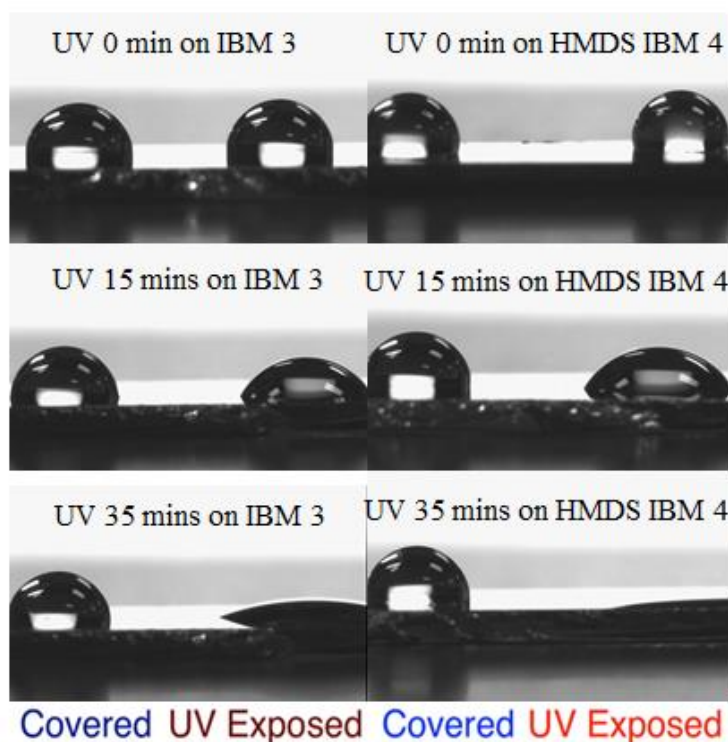


FIGURE 4.4 Pictures of water droplets on native IBM 3(left) and HMDS silylated IBM 4 (right) as a function of time of exposure to our UV/O₃ treatment. The left half of these surfaces was covered to prevent direct exposure to the UV radiation. It can be seen that the initial silylated surfaces are quite hydrophobic, and also that their native hydrophobic layer or silylation layer can be removed in approximately 35 minutes by treatment with a combination of UV and O₃ (but not by O₃ alone).

Figure 4.5 provides the AFM images of the IBM 3 surface before and after UV/ozonolysis, and of native IBM 4 and HMDS/IBM 4 before and after UV/ozonolysis.

Figures 4.5(a) and (d) show the surface image of native IBM 3 before and after

UV/ozonolysis. There is almost no difference between these two images, even if the contact angles decreased after 35 minutes of UV/O₃ exposure. Figure 4.5(b) shows the AFM image of the native IBM 4 surface, and indicates that it is smoother than native 1. After silylating IBM 4 with HMDS, the surface became rougher (Figure 4.5(c)), but after UV/O₃ treatment, the surface of HMDS/IBM 4 turned smooth again. However the other half HMDS/IBM 4, which was covered under the Al mold during the UV/Ozone exposure, remained the same as before (Figure 4.5(f)).

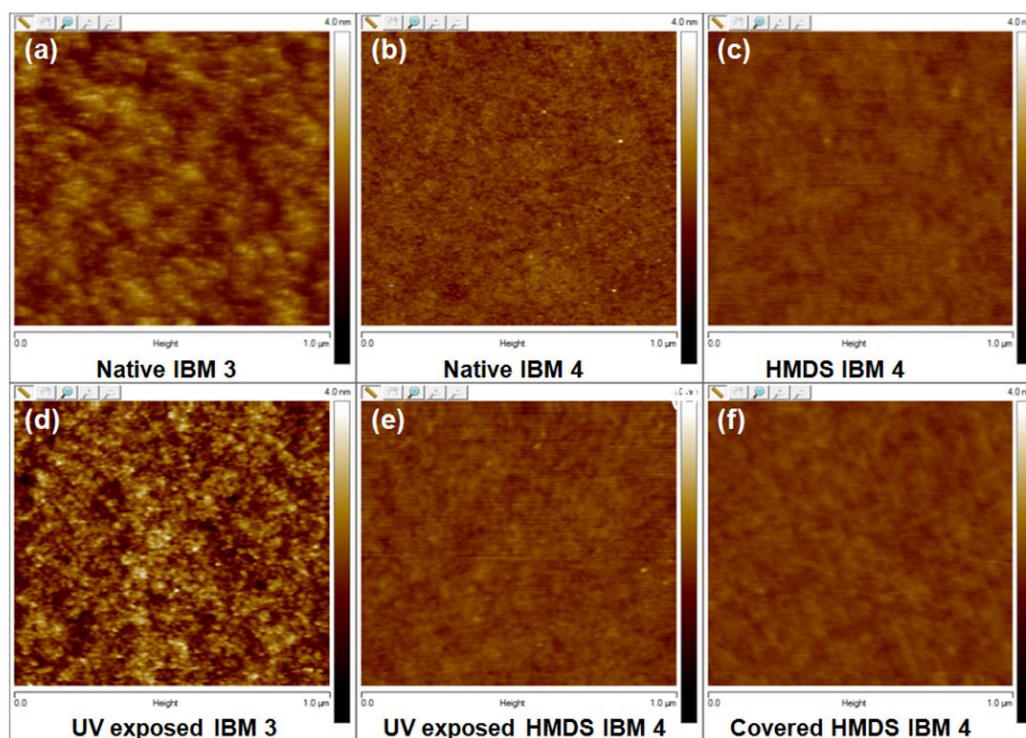


FIGURE 4.5 AFM images of (a) native IBM 3, (b) native IBM 4, (c) HMD /IBM 4, (d) UV-exposed IBM 3, (e) UV-exposed HMDS/IBM4, (f) Covered HMDS/IBM 4 surfaces.

Figure 4.6 summarizes the kinetics of the modification of the hydrophobicity of the surfaces in the form of plots of contact angles versus time of exposure to either O₃ alone or UV/O₃ combinations. Data are provided for the native IBM 1 and 3 surfaces as well

as for IBM 2 and 4 surfaces silylated with HMDS. Small differences are seen among each different sample in terms of the initial contact angles and the rate at which the silylation layers are removed, but the general trends are similar in all cases. 30 minutes UV radiation is enough to returns the hydrophilicity of IBM 1 and HMDS/IBM 2 surfaces. For the set of IBM 3 and HMDS/IBM 4 wafers, it took almost 35 minutes to restore the hydrophilicity.

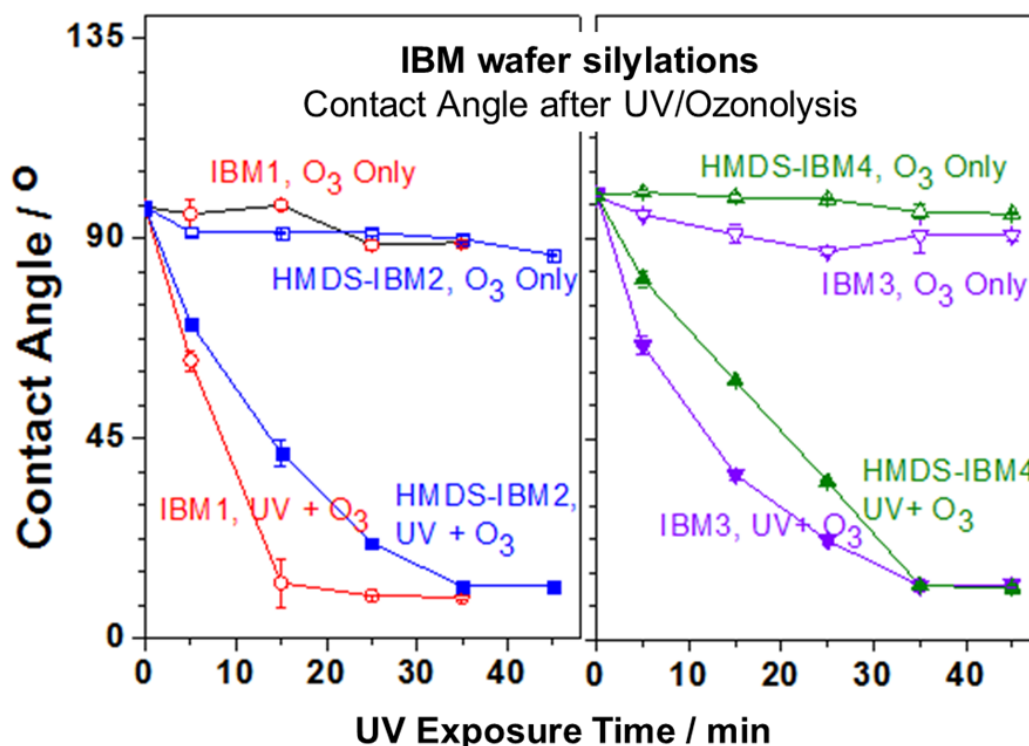


FIGURE 4.6 Summary of contact angle data obtained as a function of UV/O₃ exposure time for the original native IBM 1 (left panel) and 3(right panel) substrates and for IBM 2(left panel) and 4(right panel) surfaces silylated with HMDS. Two sets of data are shown in each case, for surfaces exposed to O₃ alone and to the UV/O₃ combination, respectively. The trends observed are qualitatively similar with all the silylation agents tested in this work: the initial high hydrophobicity of the silylated surface, manifested by contact angles around 90 -

110°, is removed after ~ 30 min of UV/O₃ treatment, at which point the surfaces become highly hydrophilic (contact angles ~ 10 - 12°). In contrast, no changes in behavior were seen on the surfaces where the UV radiation was blocked.

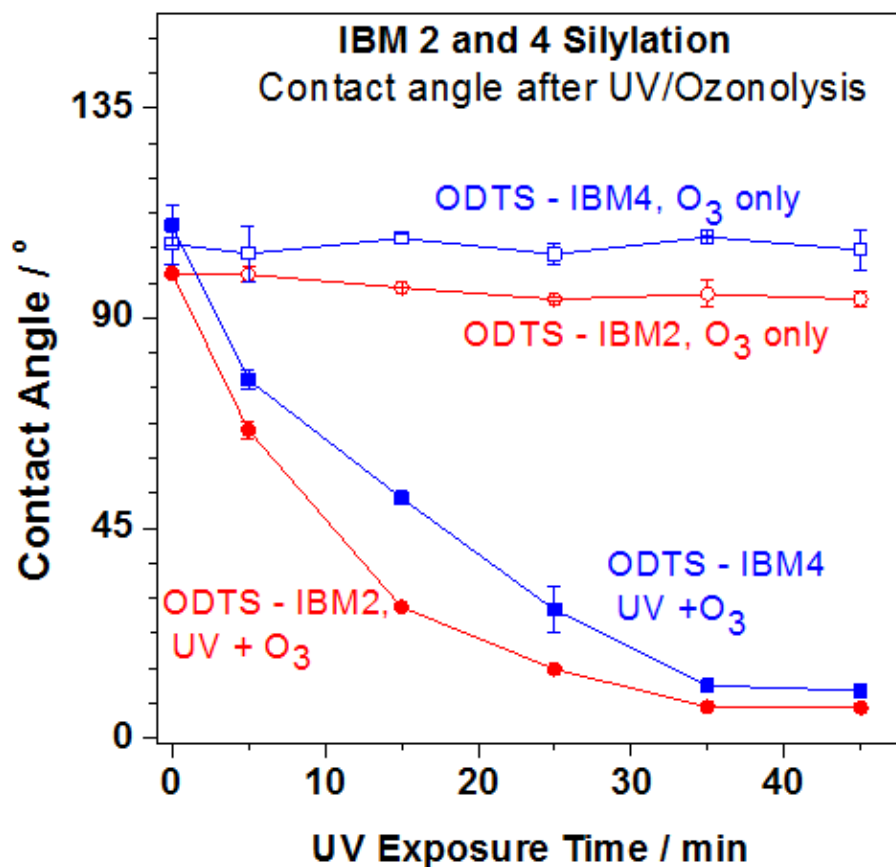


FIGURE 4.7 Summary of contact angle data obtained as a function of UV/O₃ exposure time for the IBM 2 and 4 surfaces silylated with ODTS. Two sets of data are shown in each case, for surfaces exposed to O₃ alone and to the UV/O₃ combination, respectively. The trends observed are qualitatively similar with all the silylation agents tested in this work: the initial high hydrophobicity of the silylated surface, manifested by contact angles around 95 - 110°, is removed after ~ 30 min of UV/O₃ treatment, at which point the surfaces become highly hydrophilic (contact angles ~ 10 - 15°). In contrast, no changes in behavior were seen on the surfaces where the UV radiation was blocked.

Figure 4.8 shows that after the UV/Ozone exposure, the ODTS silylated Si IBM 2 and 4 surfaces can regain their smooth texture.

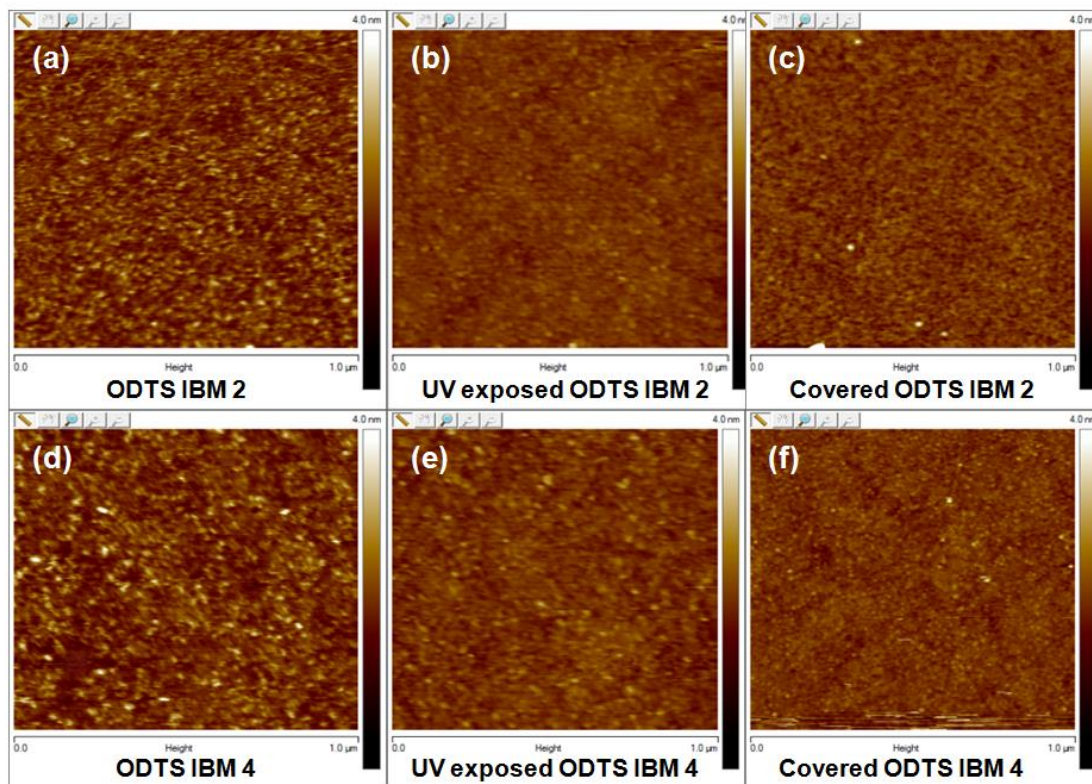


FIGURE 4.8 AFM images of (a) ODTs IBM 2, (b) UV-exposed ODTs IBM 2, (c) Covered ODTs IBM 2, (d) ODTs IBM 4, (e) UV-exposed ODTs/IBM4, (f) Covered ODTs/IBM 4 surfaces.

From Table 4.2, it is clear that the surface roughness of IBM 2 and 4 decreases significantly, to 0.11 and 0.15 Å, respectively, after chemical mechanical polishing, comparing to that of the blanket controls of native IBM 1 (0.38 Å) and native IBM 3 (0.35 Å). The UV/ozone treatment can return the smooth character of the HMDS or ODTs silylated surfaces. The AFM data confirms again that our selective ALD method should be able to achieve successful patterning without sacrificing the surface roughness.

| | IBM1 | IBM2 | | IBM-3 | IBM-4 | |
|------------------|------|------|------|-------|-------|------|
| | | HMDS | ODTS | --- | HMDS | ODTS |
| Native | 0.38 | 0.11 | --- | 0.35 | 0.15 | --- |
| UV/Ozone | 0.34 | --- | --- | 0.31 | --- | --- |
| Silane | --- | 0.3 | 0.31 | --- | 0.21 | 0.29 |
| UV-Silane/IBM | --- | 0.13 | 0.15 | --- | 0.13 | 0.19 |
| Covered under UV | 0.37 | 0.29 | --- | 0.19 | 0.33 | 0.27 |

Table 4.2 Surface roughness, in nm, of the IBM 1 and 3 samples before and after silane, and UV/Ozone treatments, respectively. Also reported are the surface roughness of IBM 2 and 4 before and after HMDS or ODTS silylation and UV/Ozone, respectively.

Lastly, the chemical selectivity of the UV/O₃-treated IBM 1 surface toward ALD of HfO₂ thin films was tested. Figure 4.9 shows selected Hf 4f XPS data acquired as a function of ALD cycles at 110° C for the IBM 1 sample. These surfaces were treated with the UV/O₃ procedure prior to the HfO₂ ALD, with one half covered to prevent its direct exposure to the UV radiation. The traces corresponding to the surface exposed to the UV/O₃ treatment show Hf 4f_{7/2} peaks centered at a binding energy of 17.5 eV, a value typical for HfO₂, and the doublets expected from Hf 4f spin splitting,[99] and their signal intensities grow with increasing number of ALD cycles, indicating Hf deposition. By contrast, no Hf deposition is seen on the covered side of the sample, the one not exposed to UV radiation during ozonolysis. As indicated before, this prevents the surface layer from being removed (the half exposed to the UV radiation is cleaned from all organic matter on the surface, and has the hydrophilic surface exposed for reaction). The differences in ALD deposition seen between the two halves of the IBM 1 substrate indicate that the hydrophobic half layer is effective in inhibiting the deposition of the HfO₂ layer.

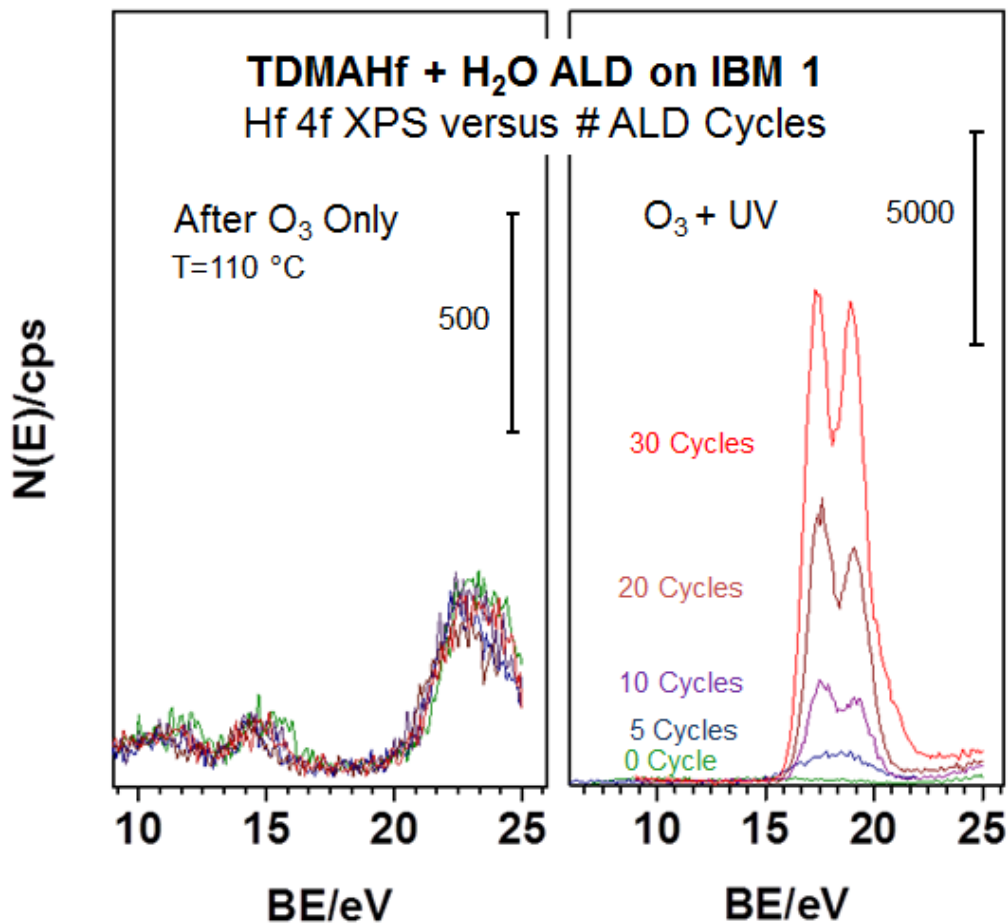


FIGURE 4.9 Hf 4f XPS from IBM 1 surfaces after the growth of HfO₂ films via TDMAHf + H₂O ALD at 110 °C. Two sets of data are reported, from surfaces treated with O₃ alone (left), and with the UV/O₃ combination (right). The XPS peak positions indicate the formation of fully oxidized HfO₂ films, and the increase in signal intensities with increasing number of ALD cycles for the UV/O₃-treated surface point to the continuous growth of the oxide film. In contrast, no HfO₂ at all is deposited on the original IBM 1 surface not directly exposed to the UV radiation during ozonolysis.

The chemical selectivity of the UV/O₃ treated HMDS/IBM 2 surfaces toward ALD of HfO₂ thin films was tested next. Figure 4.10 shows selected Hf 4f XPS data acquired as a function of ALD cycles at 110° C for HMDS silylated IBM 2 surfaces. These surfaces were treated with the UV/O₃ procedure prior to the HfO₂ ALD, with one half covered to prevent its direct exposure to the UV radiation. The traces corresponding to the surface exposed to the UV/O₃ treatment show Hf 4f_{7/2} peaks centered at a binding energy of 17.5 eV, a value typical of HfO₂, and the doublets expected from Hf 4f spin splitting,[99] and their signal intensities grow with increasing number of ALD cycles, indicating Hf deposition. By contrast, no Hf deposition is seen on the covered side of the sample, the one not exposed to UV radiation during ozonolysis. As indicated before, this prevents the surface layer from been removed (the half exposed to the UV radiation is cleaned from all organic matter on the surface, and the hydrophilic surface re-exposed for reaction). The differences in ALD deposition seen between the two halves of the IBM 2 substrate indicate that the HMDS-based layer is effective in inhibiting the deposition of the HfO₂ layer.

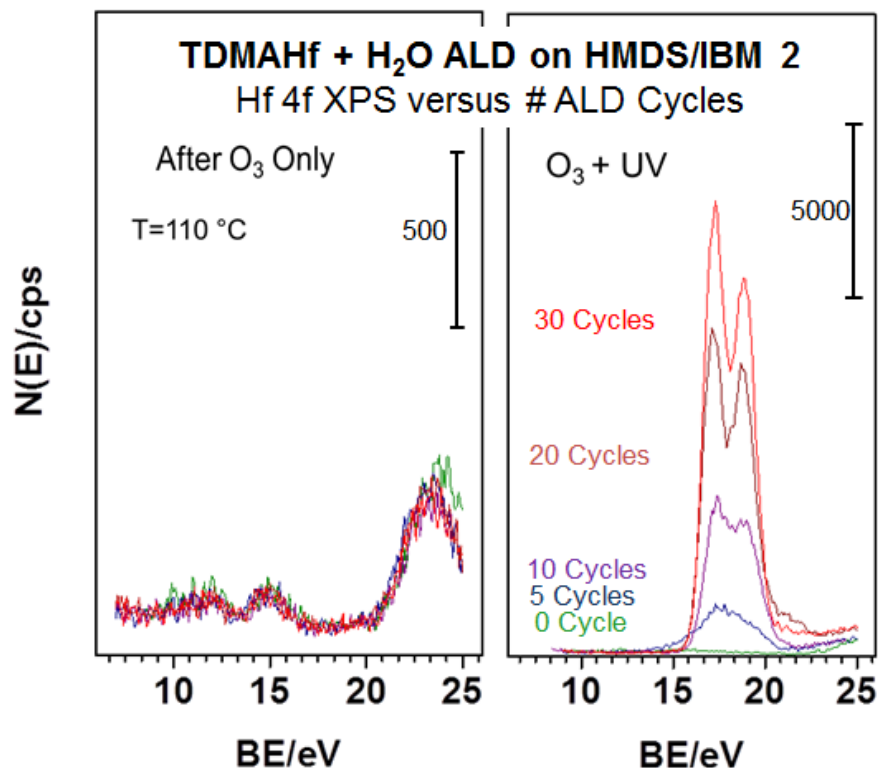


FIGURE 4.10 Hf 4f XPS from HMDS/IBM 2 surfaces after the growth of HfO₂ films via TDMAHf + H₂O ALD at 110 °C. Two sets of data are reported, from surfaces treated with O₃ alone (left), and with the UV/O₃ combination (right). The XPS peak positions indicate the formation of fully oxidized HfO₂ films, and the increase in signal intensities with increasing number of ALD cycles for the UV/O₃-treated surface point to the continuous growth of the oxide film. In contrast, no HfO₂ at all is deposited on the silylated IBM 2 surface not directly exposed to the UV radiation during ozonolysis.

The chemical selectivity of UV/O₃ treated IBM 3 surfaces toward ALD of HfO₂ thin films was tested. Figure 4.11 shows selected Hf 4f XPS data acquired as a function of ALD cycles at 110° C for IBM 3 surfaces. These surfaces were treated with the UV/O₃ procedure prior to the HfO₂ ALD, with one half covered to prevent its direct exposure to the UV radiation. The traces corresponding to the surface exposed to the UV/O₃ treatment show Hf 4f_{7/2} peaks centered at a binding energy of 17.5 eV, a value typical of

HfO₂, and the doublets expected from Hf 4f spin splitting,[99] and their signal intensities grow with increasing number of ALD cycles, indicating Hf deposition. By contrast, no Hf deposition is seen on the covered side of the sample, the one not exposed to UV radiation during ozonolysis. As indicated before, this prevents the surface layer from being removed (the half exposed to the UV radiation is cleaned from all organic matter on the surface, and has the hydrophilic surface exposed for reaction). The differences in ALD deposition seen between the two halves of the IBM 3 substrate indicate that the hydrophobic half layer is effective in inhibiting the deposition of the HfO₂ layer.

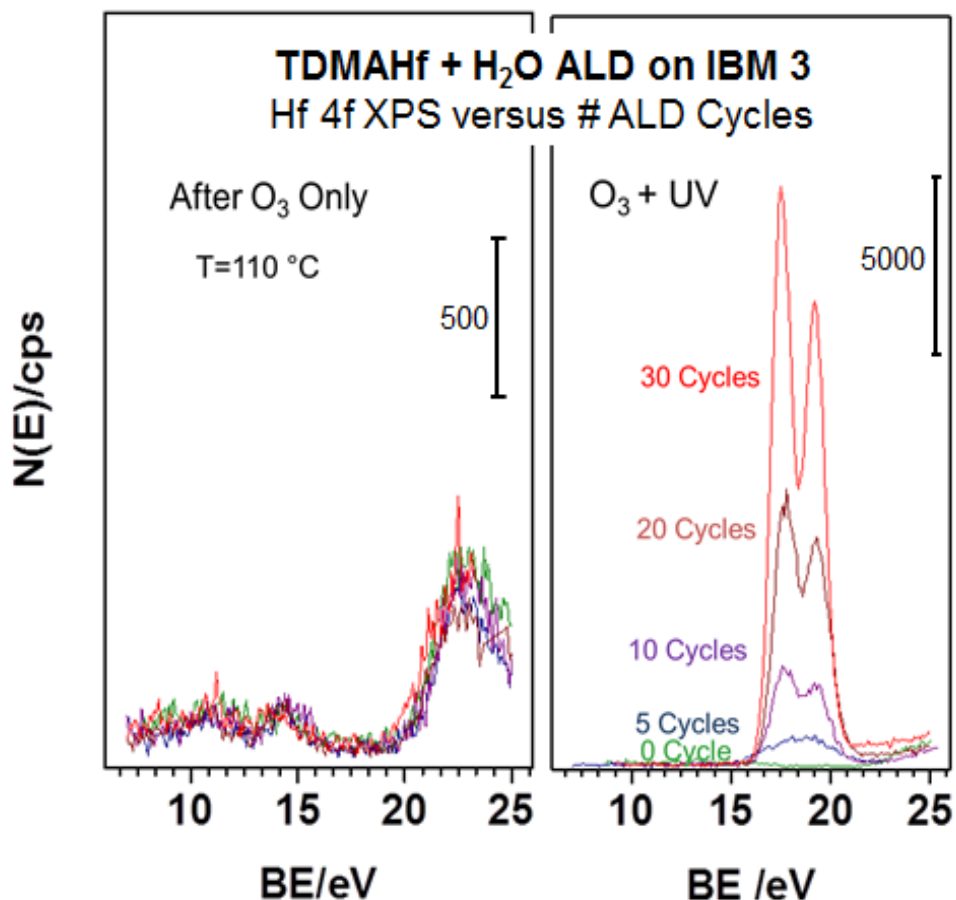


FIGURE 4.11 Hf 4f XPS from IBM 3 surfaces after the growth of HfO₂ films via TDMAHf + H₂O ALD at 110 °C. Two sets of data are reported, from surfaces treated with O₃ alone (left), and with the UV/O₃ combination (right). The XPS peak positions indicate the formation of fully oxidized HfO₂ films, and the increase in signal intensities with increasing number of ALD cycles for the UV/O₃-treated surface point to the continuous growth of the oxide film. In contrast, no HfO₂ at all is deposited on the native IBM 3 surface not directly exposed to the UV radiation during ozonolysis.

The chemical selectivity of UV/O₃ treated HMDS/IBM 4 surfaces toward ALD of HfO₂ thin films was tested. Figure 4.12 shows selected Hf 4f XPS data acquired as a function of ALD cycles at 110° C for HMDS silylated IBM 4 surfaces. These surfaces were treated with the UV/O₃ procedure prior to the HfO₂ ALD, with one half covered to prevent its direct exposure to the UV radiation. The traces corresponding to the surface

exposed to the UV/O₃ treatment show Hf 4f_{7/2} peaks centered at a binding energy of 17.5 eV, a value typical of HfO₂, and the doublets expected from Hf 4f spin splitting, [99] and their signal intensities grow with increasing number of ALD cycles, indicating Hf deposition. By contrast, no Hf deposition is seen on the covered side of the sample, the one not exposed to UV radiation during ozonolysis. As indicated before, this prevents the surface layer from been removed (the half exposed to the UV radiation is cleaned from all organic matter on the surface, and the hydrophilic surface re-exposed for reaction). The differences in ALD deposition seen between the two halves of the IBM 4 substrate indicate that the HMDS-based layer is effective in inhibiting the deposition of the HfO₂ layer.

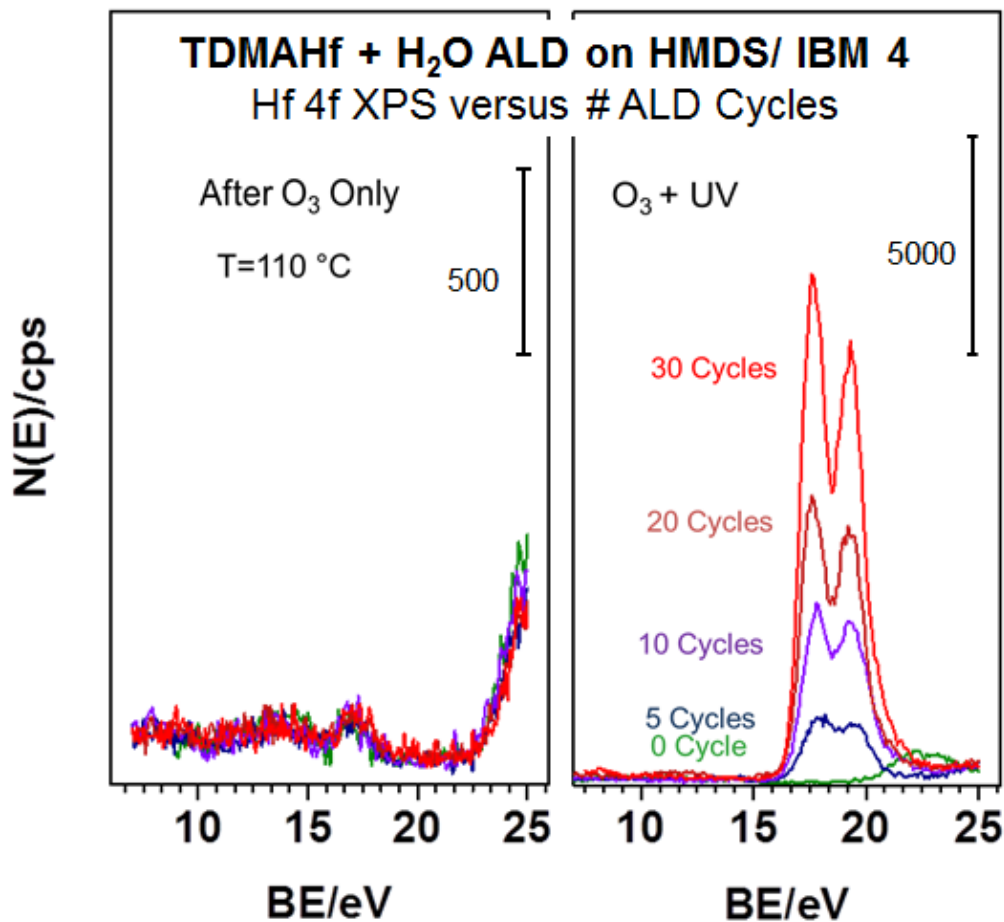


FIGURE 4.12 Hf 4f XPS from HMDS silylated IBM 4 surfaces after the growth of HfO₂ films via TDMAHf + H₂O ALD at 110 °C. Two sets of data are reported, from surfaces treated with O₃ alone (left), and with the UV/O₃ combination (right). The XPS peak positions indicate the formation of fully oxidized HfO₂ films, and the increase in signal intensities with increasing number of ALD cycles for the UV/O₃-treated surface point to the continuous growth of the oxide film. In contrast, no HfO₂ at all is deposited on the native IBM 4 surface not directly exposed to the UV radiation during ozonolysis.

The ALD growth rates on the IBM 1 and 3 surfaces and IBM 2 and 4 silylated with HMDS and then treated with either O₃ alone (covered half) or UV/O₃ (exposed half), were quantified by processing the signal intensities from the Hf 4f and Si 2p XPS spectra. Figure 4.13 shows the resulting HfO₂ uptake curves reported at 110 °C. Clearly,

the surfaces cleaned with UV/O₃ display significantly faster rates of HfO₂ deposition than those exposed to O₃ alone, as mentioned above. This is true in both cases (IBM 2 and 4), with HMDS as the silylation agent. Indeed, the UV/ozone-exposed half of IBM 1 shows the fastest growth rate, around 0.8 Å/ALD cycle at 110 °C. By contrast, the surfaces exposed to O₃ only are totally passivated and show no HfO₂ deposition at all at 110 °C. However, the growth rate on the UV/ozone-exposed half of HMDS/IBM 2 is 0.6 Å/cycle; no HfO₂ deposition is observed on the HMDS blocking side.

The HfO₂ growth rate on the UV/ozone-exposed half of IBM 3 is around 0.6 Å/cycle; while there is no deposition on the surface exposed to ozone only. The HfO₂ growth rate on the UV/ozone-exposed half of HMDS/IBM 4 is around 0.5 Å/cycle, and no deposition occurs on the surface exposed to ozone only. The growth rate on the different substrates is different, since ALD is a surface sensitive deposition technique. The different substrate surface properties will influence the growth rate of HfO₂ ALD. All these data confirm that our selective ALD process has good applications on ultra-low K dielectrics for patterning.

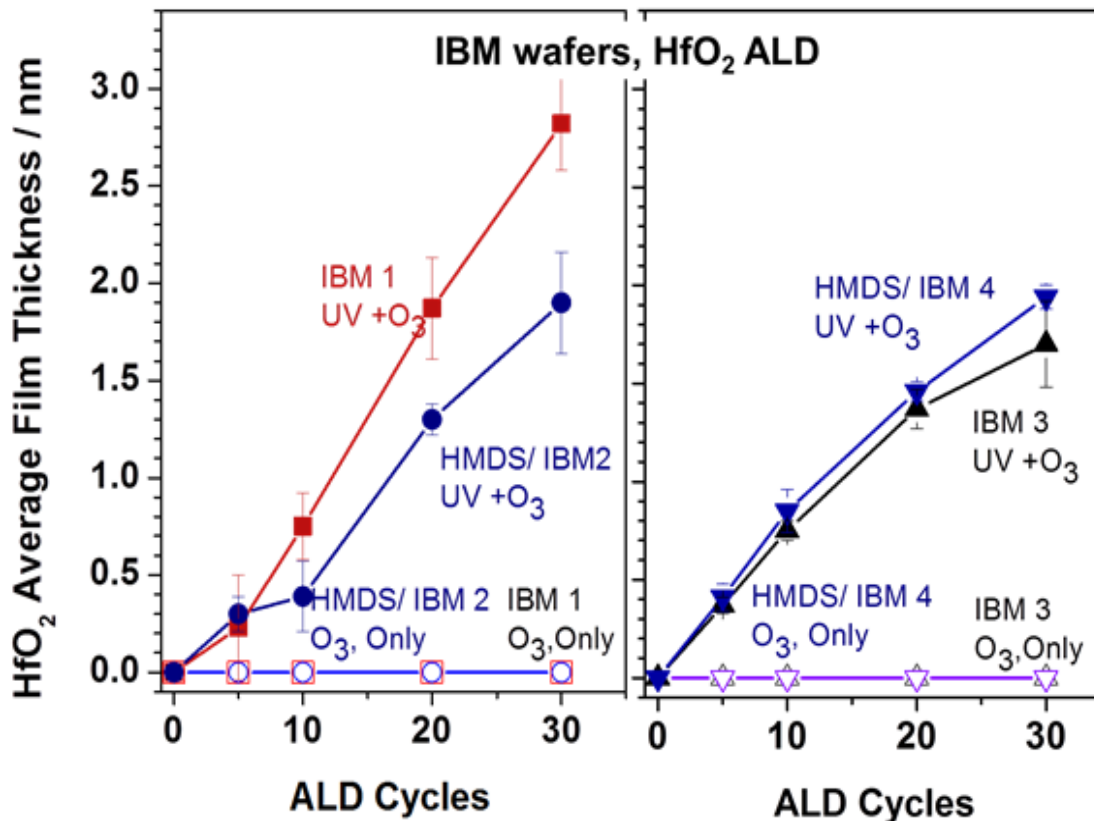


FIGURE 4.13 Average thickness of HfO₂ films grown on the IBM 1 to 4 series of wafers via ALD as a function of the number of cycles used, estimated from Hf 4f and Si 2p XPS data by assuming layer-by-layer growth and published electron inelastic mean free paths. Four surfaces were tested here; IBM 1 and HMDS/IBM 2 (Left), IBM 3 and HMDS/IBM 4 (Right). Two sets of data are shown for each case, for the two half-surfaces exposed to O₃ alone and to the UV/O₃ combination, respectively. In addition, HfO₂ uptakes are reported for ALD experiments carried out at 110 °C, in each case. Much faster film growth is seen on the surface treated with the full UV/O₃ procedure, and total inhibition is seen with the silylated surfaces for ALD at 110 °C

4.4 Conclusions

Our selective ALD approach has been tested on the IBM 1 to 4 series of wafer surfaces, which are ultra-low dielectrics for industrial applications. Emphasis has been placed on the surface reactivity toward the metalorganic precursors which are used in the chemical deposition of thin solid films. Native IBM 2 and 4 are hydrophilic; starting from this substrate, the hydroxo groups on the surface are capable of covalently reacting with a number of metalorganic compounds, facilitating their dissociative adsorption and initiating chemically based film deposition processes. IBM 1 and 3 are natively hydrophobic; hence UV/ozonolysis can restore the hydrophilicity of those surfaces, so ALD growth can be carried out. These hydrophobic and hydrophilic properties were evaluated here by means of contact angle measurements between the surface and a droplet of water deposited on top.

The UV/O₃ treatment of the silylated IBM 2 and 4 wafers returns their original hydrophilicity. This was tested by evaluating the rate of growth of HfO₂ films via ALD using TDMAHf and water. Overall, the sequence of silylation and UV/ozonolysis treatments described here for selective ALD process indicates good performance on industrial wafers.

It should be said that this selective ALD process is a good way to achieve patterning for microelectronics industry applications. It can achieve selective ALD without sacrificing surface roughness.

Reference

1. Leskela, M. and M. Ritala, *Atomic layer deposition (ALD): from precursors to thin film structures*. Thin Solid Films, 2002. **409**(1): p. 138-146.
2. Leskela, M. and M. Ritala, *ALD precursor chemistry: Evolution and future challenges*. Journal De Physique Iv, 1999. **9**(P8): p. 837-852.
3. Kolanek, K., et al., *Atomic layer deposition reactor for fabrication of metal oxides*. Physica Status Solidi C: Current Topics in Solid State Physics, Vol 8, No 4, 2011. **8**(4).
4. Longrie, D., D. Deduytsche, and C. Detavernier, *Reactor concepts for atomic layer deposition on agitated particles: A review*. Journal of Vacuum Science & Technology A, 2014. **32**(1).
5. van Delft, J.A., D. Garcia-Alonso, and W.M.M. Kessels, *Atomic layer deposition for photovoltaics: applications and prospects for solar cell manufacturing*. Semiconductor Science and Technology, 2012. **27**(7).
6. Ponraj, J.S., G. Attolini, and M. Bosi, *Review on Atomic Layer Deposition and Applications of Oxide Thin Films*. Critical Reviews in Solid State and Materials Sciences, 2013. **38**(3): p. 203-233.
7. Johnson, R.W., A. Hultqvist, and S.F. Bent, *A brief review of atomic layer deposition: from fundamentals to applications*. Materials Today, 2014. **17**(5): p. 236-246.
8. Zhu, W.J., J.P. Han, and T.P. Ma, *Mobility measurement and degradation mechanisms of MOSFETs made with ultrathin high-k dielectrics*. Ieee Transactions on Electron Devices, 2004. **51**(1): p. 98-105.
9. Kang, L.G., et al., *MOSFET devices with polysilicon on single-layer HfO₂ high-k dielectrics*. International Electron Devices Meeting 2000, Technical Digest, 2000: p. 35-38.
10. Choi, K.J., et al., *Metal/ferroelectric/insulator/semiconductor structure of Pt/SrBi₂Ta₂O₉/YMnO₃/Si using YMnO₃ as the buffer layer*. Applied Physics Letters, 1999. **75**(5): p. 722-724.

11. Lee, W.J., et al., *Electrical properties of SrBi₂Ta₂O₉/insulator/Si structures with various insulators*. Japanese Journal of Applied Physics Part 1-Regular Papers Short Notes & Review Papers, 1999. **38**(4A): p. 2039-2043.
12. Zhai, J.W., et al., *Dielectric and ferroelectric properties of highly oriented (Pb, Nb) (Zr, Sn, Ti)O₃ thin films grown by a sol-gel process*. Applied Physics Letters, 2002. **81**(19): p. 3621-3623.
13. Fujisaki, Y., T. Kijima, and H. Ishiwara, *High-performance metal-ferroelectric-insulator-semiconductor structures with a damage-free and hydrogen-free silicon-nitride buffer layer*. Applied Physics Letters, 2001. **78**(9): p. 1285-1287.
14. Lee, S. and K. Kim, *Current development status and future challenges of ferroelectric random access memory technologies*. Japanese Journal of Applied Physics Part 1-Regular Papers Brief Communications & Review Papers, 2006. **45**(4B): p. 3189-3193.
15. Kim, Y.K., et al., *Novel capacitor technology for high density stand-alone and embedded DRAMs*. International Electron Devices Meeting 2000, Technical Digest, 2000: p. 369-372.
16. Rossnagel, S.M., A. Sherman, and F. Turner, *Plasma-enhanced atomic layer deposition of Ta and Ti for interconnect diffusion barriers*. Journal of Vacuum Science & Technology B, 2000. **18**(4): p. 2016-2020.
17. Moon, D.Y., et al., *Atomic Layer Deposition of Copper Seed Layers from a (hfac)Cu(VTMOs) Precursor*. Journal of the Korean Physical Society, 2009. **54**(3): p. 1330-1333.
18. Solanki, R. and B. Pathangey, *Atomic layer deposition of copper seed layers*. Electrochemical and Solid State Letters, 2000. **3**(10): p. 479-480.
19. Kim, S.H., et al., *A comparative study of the atomic-layer-deposited tungsten thin films as nucleation layers for W-plug deposition*. Journal of the Electrochemical Society, 2006. **153**(10): p. G887-G893.

20. Chen, Y.T., et al., *ALD TiN Barrier Metal for pMOS Devices With a Chemical Oxide Interfacial Layer for 20-nm Technology Node*. Ieee Electron Device Letters, 2014. **35**(3): p. 306-308.
21. Lo, W.H., et al., *Charge trapping induced drain-induced-barrier-lowering in HfO₂/TiN p-channel metal-oxide-semiconductor-field-effect-transistors under hot carrier stress*. Applied Physics Letters, 2012. **100**(15).
22. Dingemans, G., M.C.M. van de Sanden, and W.M.M. Kessels, *Influence of the Deposition Temperature on the c-Si Surface Passivation by Al₂O₃ Films Synthesized by ALD and PECVD*. Electrochemical and Solid State Letters, 2010. **13**(3): p. H76-H79.
23. Torndahl, T., et al., *Atomic layer deposition of Zn_{1-x}Mg_xO buffer layers for Cu(In,Ga)Se-2 solar cells*. Progress in Photovoltaics, 2007. **15**(3): p. 225-235.
24. Hegedus, S., et al., *ENCAPSULATION OF Cu(InGa)Se-2 SOLAR CELLS WITH ALD Al₂O₃ FLEXIBLE THIN-FILM MOISTURE BARRIER: STABILITY UNDER 1000 HOUR DAMP HEAT AND UV EXPOSURE*. 35th IEEE Photovoltaic Specialists Conference, 2010: p. 1178-1183.
25. Carcia, P.F., R.S. McLean, and S. Hegedus, *Encapsulation of Cu(InGa)Se-2 solar cell with Al₂O₃ thin-film moisture barrier grown by atomic layer deposition*. Solar Energy Materials and Solar Cells, 2010. **94**(12): p. 2375-2378.
26. Klahr, B.M. and T.W. Hamann, *Performance Enhancement and Limitations of Cobalt Bipyridyl Redox Shuttles in Dye-Sensitized Solar Cells*. Journal of Physical Chemistry C, 2009. **113**(31): p. 14040-14045.
27. Tien, T.C., et al., *Coverage Analysis for the Core/Shell Electrode of Dye-Sensitized Solar Cells*. Journal of Physical Chemistry C, 2010. **114**(21): p. 10048-10053.
28. Ganapathy, V., B. Karunagaran, and S.W. Rhee, *Improved performance of dye-sensitized solar cells with TiO₂/alumina core-shell formation using atomic layer deposition*. Journal of Power Sources, 2010. **195**(15): p. 5138-5143.

29. Shanmugam, M., M.F. Baroughi, and D. Galipeau, *Effect of atomic layer deposited ultra-thin HfO₂ and Al₂O₃ interfacial layers on the performance of dye sensitized solar cells*. Thin Solid Films, 2010. **518**(10): p. 2678-2682.
30. Martinson, A.B.F., et al., *ZnO nanotube based dye-sensitized solar cells*. Nano Letters, 2007. **7**(8): p. 2183-2187.
31. Martinson, A.B.F., et al., *Electron Transport in Dye-Sensitized Solar Cells Based on ZnO Nanotubes: Evidence for Highly Efficient Charge Collection and Exceptionally Rapid Dynamics*. Journal of Physical Chemistry A, 2009. **113**(16): p. 4015-4021.
32. Pang, C., C. Lee, and K.Y. Suh, *Recent advances in flexible sensors for wearable and implantable devices*. Journal of Applied Polymer Science, 2013. **130**(3): p. 1429-1441.
33. Purniawan, A., et al., *TiO₂ ALD Nanolayer as Evanescent Waveguide for Biomedical Sensor Applications*. Eurosensors Xxiv Conference, 2010. **5**: p. 1131-1135.
34. Adiga, S.P., et al., *Nanoporous materials for biomedical devices*. Jom, 2008. **60**(3): p. 26-32.
35. DiBenedetto, S. A., Facchetti, A., Ratner, M.A. and Marks, T.J., *Molecular Self-Assembled Monolayers and Multilayers for Organic and Unconventional Inorganic Thin-Film Transistor Applications*. Adv. Mater., 2009, **21**, 1407-1433.
36. Lee, S., et al., *Self-assembled monolayers on Pt(111): Molecular packing structure and strain effects observed by scanning tunneling microscopy*. Journal of the American Chemical Society, 2006. **128**(17): p. 5745-5750.
37. Vericat, C., et al., *Surface characterization of sulfur and alkanethiol self-assembled monolayers on Au(111)*. Journal of Physics-Condensed Matter, 2006. **18**(48): p. R867-R900.
38. Noh, J., et al., *Surface structure and interface dynamics of alkanethiol self-assembled monolayers on Au(111)*. Journal of Physical Chemistry B, 2006. **110**(6): p. 2793-2797.

39. Jennings, G.K., et al., *Structural effects on the barrier properties of self-assembled monolayers formed from long-chain omega-alkoxy-n-alkanethiols on copper*. Journal of the American Chemical Society, 2003. **125**(10): p. 2950-2957.
40. Vollmer, S., G. Witte, and C. Woll, *Determination of site specific adsorption energies of CO on copper*. Catalysis Letters, 2001. **77**(1-3): p. 97-101.
41. Schreiber, F., et al., *Adsorption mechanisms, structures, and growth regimes of an archetypal self-assembling system: Decanethiol on Au(111)*. Physical Review B, 1998. **57**(19): p. 12476-12481.
42. Han, Y. and K. Uosaki, *Effects of concentration and temperature on the formation process of decanethiol self-assembled monolayer on Au(111) followed by electrochemical reductive desorption*. Electrochimica Acta, 2008. **53**(21): p. 6196-6201.
43. Zhang, J.D., Q.J. Chi, and J. Ulstrup, *Assembly dynamics and detailed structure of 1-propanethiol monolayers on Au(111) surfaces observed real time by in situ STM*. Langmuir, 2006. **22**(14): p. 6203-6213.
44. Patrone, L., et al., *Direct comparison of the electronic coupling efficiency of sulfur and selenium anchoring groups for molecules adsorbed onto gold electrodes*. Chemical Physics, 2002. **281**(2-3): p. 325-332.
45. James, D.K. and J.M. Tour, *Molecular wires*. Molecular Wires: From Design to Properties, 2005. **257**: p. 33-62.
46. Svedberg, F., et al., *Raman spectroscopic studies of terthiophenes for molecular electronics*. Journal of Physical Chemistry B, 2006. **110**(51): p. 25671-25677.
47. Chabynyc, M.L., et al., *Molecular rectification in a metal-insulator-metal junction based on self-assembled monolayers*. Journal of the American Chemical Society, 2002. **124**(39): p. 11730-11736.
48. Yu, B.C., Y. Shirai, and J.M. Tour, *Syntheses of new functionalized azobenzenes for potential molecular electronic devices*. Tetrahedron, 2006. **62**(44): p. 10303-10310.

49. Henzl, J., T. Bredow, and K. Morgenstern, *Irreversible isomerization of the azobenzene derivate Methyl Orange on Au(111)*. Chemical Physics Letters, 2007. **435**(4-6):p. 278-282.
50. MCGovern, M.E., K.M.R. Kallury, and M. Thompson, *Role of Solvent on the Silanization of Glass with Octadecyltrichlorosilane*. Langmuir, 1994. **10**(10): p. 3607-3614.
51. Spori, D.M., et al., *Influence of alkyl chain length on phosphate self-assembled monolayers*. Langmuir, 2007. **23**(15): p. 8053-8060.
51. Carey, R.I., J.P. Folkers, and G.M. Whitesides, *Self-Assembled Monolayers Containing Omega-Mercaptoalkylboronic Acids Adsorbed onto Gold Form a Highly Cross-Linked, Thermally Stable Borate Glass-Surface*. Langmuir, 1994. **10**(7): p. 2228-2234.
52. Kluth, G.J., M.M. Sung, and R. Maboudian, *Interaction of H(D) atoms with octadecylsiloxane self-assembled monolayers on the Si(100) surface*. Langmuir, 1997. **13**(24): p. 6491-6496.
53. Kluth, G.J., M.M. Sung, and R. Maboudian, *Thermal behavior of alkylsiloxane self-assembled monolayers on the oxidized Si(100) surface*. Langmuir, 1997. **13**(14): p. 3775-3780.
54. Kluth, G.J., M.M. Sung, and R. Maboudian, *Thermal behavior of butylsiloxane self-assembled monolayers on Si(100)*. Abstracts of Papers of the American Chemical Society, 1997. **213**: p. 162-COLL.
55. Bunker, B.C., et al., *The impact of solution agglomeration on the deposition of self-assembled monolayers*. Langmuir, 2000. **16**(20): p. 7742-7751.
56. Chen, R., et al., *Investigation of self-assembled monolayer resists for hafnium dioxide atomic layer deposition*. Chemistry of Materials, 2005. **17**(3): p. 536-544.
57. Ulman, A., *Formation and structure of self-assembled monolayers*. Chemical Reviews, 1996. **96**(4):p. 1533-1554.
58. Ulman, A., *Wetting studies of molecularly engineered surfaces*. Thin Solid Films, 1996. **273**(1-2):p. 48-53.

59. Allara, D.L., A.N. Parikh, and F. Rondelez, *Evidence for a Unique Chain Organization in Long-Chain Silane Monolayers Deposited on 2 Widely Different Solid Substrates*. Langmuir, 1995. **11**(7): p. 2357-2360.
60. Hong, J., et al., *ALD resist formed by vapor-deposited self-assembled monolayers*. Langmuir, 2007. **23**(3): p. 1160-1165.
61. Kobrin, B., et al., *Molecular Vapor Deposition (MVD) for improved SAM coatings*. Reliability, Packaging, Testing, and Characterization of MEMS/MOEMS IV, 2005. **5716**: p. 151-157.
62. Ashurst, W.R., et al., *Alkene based monolayer films as anti-stiction coatings for polysilicon MEMS*. Sensors and Actuators a-Physical, 2001. **91**(3): p. 239-248.
63. Ashurst, W.R., C. Carraro, and R. Maboudian, *Vapor phase anti-stiction coatings for MEMS*. Ieee Transactions on Device and Materials Reliability, 2003. **3**(4): p. 173-178.
64. Chen, R., et al., *Achieving area-selective atomic layer deposition on patterned substrates by selective surface modification*. Applied Physics Letters, 2005. **86**(19).
65. Crespo-Quesada, M., et al., *UV-Ozone Cleaning of Supported Poly(vinylpyrrolidone)-Stabilized Palladium Nanocubes: Effect of Stabilizer Removal on Morphology and Catalytic Behavior*. Langmuir, 2011. **27**(12): p. 7909-7916.
66. Ramanathan, S., et al., *Ultraviolet-ozone oxidation of metal films*. Journal of the Electrochemical Society, 2003. **150**(5): p. F110-F115.
67. Guo, L. and Zaera, F., *Spatial Resolution in Thin Film Deposition on Silicon Surfaces by Combining Silylation and UV/Ozonolysis*, Nanotechnology, 2014. **25**(50).
68. Farm, E., et al., *Self-assembled octadecyltrimethoxysilane monolayers enabling selective-area atomic layer deposition of iridium*. Chemical Vapor Deposition, 2006. **12**(7): p. 415-+.

69. Sinha, A., D.W. Hess, and C.L. Henderson, *Area-selective ALD of titanium dioxide using lithographically defined poly (methyl methacrylate) films*. Journal of the Electrochemical Society, 2006. **153**(5):p. G465-G469.
70. Liu, J.R., et al., *Generation of Oxide Nanopatterns by Combining Self-Assembly of S-Layer Proteins and Area-Selective Atomic Layer Deposition*. Journal of the American Chemical Society, 2008. **130**(50):p. 16908-16913.
71. Jiang, X.R. and S.F. Bent, *Area-Selective ALD with Soft Lithographic Methods: Using Self-Assembled Monolayers to Direct Film Deposition*. Journal of Physical Chemistry C, 2009. **113**(41):p. 17613-17625.
72. Deyhimi, F. and J.A. Coles, *Rapid Silylation of a Glass-Surface - Choice of Reagent and Effect of Experimental Parameters on Hydrophobicity*. Helvetica Chimica Acta, 1982. **65**(6):p. 1752-1759.
73. Flinn, D.H., D.A. Guzonas, and R.H. Yoon, *Characterization of Silica Surfaces Hydrophobized by Octadecyltrichlorosilane*. Colloids and Surfaces a-Physicochemical and Engineering Aspects, 1994. **87**(3):p. 163-176.
74. Schmohl, A., A. Khan, and P. Hess, *Functionalization of oxidized silicon surfaces with methyl groups and their characterization*. Superlattices and Microstructures, 2004. **36**(1-3): p. 113-121.
75. Hong, J.H. and F. Zaera, *Interference of the Surface of the Solid on the Performance of Tethered Molecular Catalysts*. Journal of the American Chemical Society, 2012. **134**(31):p. 13056-13065.
76. Uosaki, K., et al., *Decomposition processes of an organic monolayer formed on Si(111) via a silicon-carbon bond induced by exposure to UV irradiation or ozone*. Langmuir, 2004. **20**(4):p. 1207-1212.
77. McIntire, T.M., O. Ryder, and B.J. Finlayson-Pitts, *Secondary Ozonide Formation from the Ozone Oxidation of Unsaturated Self-Assembled Monolayers on Zinc Selenide Attenuated Total Reflectance Crystals*. Journal of Physical Chemistry C, 2009. **113**(25): p. 11060-11065.
78. Vig, J.R., *UV-Ozone Cleaning of Surfaces*. Journal of Vacuum Science & Technology a-Vacuum Surfaces and Films, 1985. **3**(3): p. 1027-1034.

79. Chen, S.F., C.Y. Chang, and Y.C. Ku, *Resist residue removal using UV ozone treatment*. Advances in Resist Materials and Processing Technology Xxvii, Pts 1 and 2, 2010. **7639**.
80. Hook, D.A., et al., *Evaluation of Oxygen Plasma and UV Ozone Methods for Cleaning of Occluded Areas in MEMS Devices*. Journal of Microelectromechanical Systems, 2010. **19**(6):p. 1292-1298.
81. Al Alam, E., et al., *Effect of surface preparation and interfacial layer on the quality of SiO₂/GaN interfaces*. Journal of Applied Physics, 2011. **109**(8).
82. Ouyang, M., et al., *Conversion of some siloxane polymers to silicon oxide by UV/ozone photochemical processes*. Chemistry of Materials, 2000. **12**(6):p. 1591-1596.
83. Egitto, F.D. and L.J. Matienzo, *Transformation of Poly(dimethylsiloxane) into thin surface films of SiO_x by UV/Ozone treatment. Part I: Factors affecting modification*. Journal of Materials Science, 2006. **41**(19): p. 6362-6373.
84. Nakamura, K., et al., *Photochemical reaction of ozone and 1, 1, 1, 3, 3, 3-hexamethyldisilazane: Analysis of the gas reaction between precursors in a photochemical vapor deposition process*. Japanese Journal of Applied Physics, 2008. **47**(9): p. 7349-7355.
85. Hollinger, G., et al., *Evidence for a New Passivating Indium Rich Phosphate Prepared by Ultraviolet Ozone Oxidation of Inp*. Applied Physics Letters, 1991. **59**(13): p. 1617-1619.
86. Matero, R., et al., *Effect of water dose on the atomic layer deposition rate of oxide thin films*. Thin Solid Films, 2000. **368**(1):p. 1-7.
87. Kelly, M.J., et al., *In-situ infrared spectroscopy and density functional theory modeling of hafnium alkylamine adsorption on Si-OH and Si-H surfaces*. Chemistry of Materials, 2005. **17**(21): p. 5305-5314.
88. Zaera, F., *Mechanisms of surface reactions in thin solid film chemical deposition processes*. Coordination Chemistry Reviews, 2013. **257**(23-24): p. 3177-3191.

89. Kern, W., *The Evolution of Silicon-Wafer Cleaning Technology*. Journal of the Electrochemical Society, 1990. **137**(6):p. 1887-1892.
90. Queeney, K.T., et al., *Infrared spectroscopic analysis of an ordered Si/SiO₂ interface*. Applied Physics Letters, 2004. **84**(4): p. 493-495.
91. Maccarini, M., et al., *Characterization and stability of hydrophobic surfaces in water*. Applied Surface Science, 2005. **252**(5):p. 1941-1946.
92. Franssila, S. and S. Tuomikoski, *MEMS Lithography*. Handbook of Silicon Based Mems Materials and Technologies, 2010: p. 333-348.
93. Niskanen, A.J., et al., *Atomic layer deposition of tin dioxide sensing film in microhotplate gas sensors*. Sensors and Actuators B-Chemical, 2010. **148**(1): p. 227-232.
94. Morganro. We and J.G. Calvert, *Photolysis of 1,1'-Azo-N-Butane Vapor . Reactions of N-Butyl Free Radical*. Journal of the American Chemical Society, 1966. **88**(23): p. 5387-&.
95. Clark, T., et al., *A new application of UV-ozone treatment in the preparation of substrate-supported, mesoporous thin films*. Chemistry of Materials, 2000. **12**(12): p. 3879-3884.
96. Chou, M.S. and K.L. Chang, *UV/ozone degradation of gaseous hexamethyldisilazane (HMDS)*. Chemosphere, 2007. **69**(5):p. 697-704.
97. Pillai, S. and R.K. Pai, *Controlled growth and formation of SAMs investigated by atomic force microscopy*. Ultramicroscopy, 2009. **109**(2):p. 161-166.
98. Renault, O., et al., *HfO₂/SiO₂ interface chemistry studied by synchrotron radiation x-ray photoelectron spectroscopy*. Applied Physics Letters, 2002. **81**(19):p. 3627-3629.

99. Seah, M.P. and W.A. Dench, *Smoothing and the Signal-to-Noise Ratio of Peaks in Electron-Spectroscopy*. Journal of Electron Spectroscopy and Related Phenomena, 1989. **48**(1-2): p. 43-54.
100. Seah, M.P., et al., *Towards a Single Recommended Optimal Convolutional Smoothing Algorithm for Electron and Other Spectroscopies*. Journal of Physics E-Scientific Instruments, 1988. **21**(4): p. 351-363.